MICROCOPY RESOLUTION TEST CHART

NATIONAL BUREAU OF STANDARDS-1963-A

①

| REPORT DOCUMENTATION PAGE | | READ INSTRUCTIONS BEFORE COMPLETING FORM |
|---|---|---|
| **1. REPORT NUMBER** <br> AFIT/CI/NR 85-111D | **2. GOVT ACCESSION NO.** | **3. RECIPIENT'S CATALOG NUMBER** |
| **4. TITLE (and Subtitle)** <br> Equivalent Continuum Finite Element Modelling of Plate-like Space Lattice Structures | | **5. TYPE OF REPORT & PERIOD COVERED** <br> THESIS/DISSERTATION |
| | | **6. PERFORMING ORG. REPORT NUMBER** |
| **7. AUTHOR(s)** <br> Steven Edward Lamberson | | **8. CONTRACT OR GRANT NUMBER(s)** |
| **9. PERFORMING ORGANIZATION NAME AND ADDRESS** <br> AFIT STUDENT AT: Purdue University | | **10. PROGRAM ELEMENT, PROJECT, TASK AREA & WORK UNIT NUMBERS** |
| **11. CONTROLLING OFFICE NAME AND ADDRESS** <br> AFIT/NR <br> WPAFB OH 45433 - 6583 | | **12. REPORT DATE** <br> August 1985 |
| | | **13. NUMBER OF PAGES** <br> 126 |
| **14. MONITORING AGENCY NAME & ADDRESS(If different from Controlling Office)** | | **15. SECURITY CLASS. (of this report)** <br> UNCLASS |
| | | **15a. DECLASSIFICATION/DOWNGRADING SCHEDULE** |

AD-A160 879

**16. DISTRIBUTION STATEMENT (of this Report)**

APPROVED FOR PUBLIC RELEASE; DISTRIBUTION UNLIMITED

DTIC
ELECTE
OCT 30 1985

B

**17. DISTRIBUTION STATEMENT (of the abstract entered in Block 20, if different from Report)**

**18. SUPPLEMENTARY NOTES**

APPROVED FOR PUBLIC RELEASE: IAW AFR 190-1

LYNN E. WOLAVER        3 of 85
Dean for Research and
        Professional Development
AFIT, Wright-Patterson AFB O

**19. KEY WORDS (Continue on reverse side if necessary and identify by block number)**

**20. ABSTRACT (Continue on reverse side if necessary and identify by block number)**

ATTACHED

DD ₁ FORM JAN 73 **1473**    EDITION OF 1 NOV 65 IS OBSOLETE

UNCLASS

## ABSTRACT

Lamberson, Steven Edward.  Ph.D., Purdue University, August 1985.
Equivalent Continuum Finite Element Modelling of Plate-like Space
Lattice Structures.  Major Professor:  Henry Yang.

A variety of research projects are being pursued involving the
dynamics and control of large plate-like space platforms made up
of repetitive lattice-type truss structures.  A method involving
finite element modelling of an equivalent continuum formulation
based on matching the strain energy and kinetic energy is developed
for truss type lattices with pinned joints.  The method is shown to
give modal results consistent with those obtained using detailed
finite element modelling of the pin jointed space lattice structure,
even for structures with fairly small numbers of repetitions of an
identical unit cell.  Feedback controllers designed using reduced
system models derived from these modal results using Modal Cost
Analysis are shown to perform as well as controllers designed using
the detailed analysis results.

The efficiency of this method for coupled structure, control
system design is demonstrated with a parametric study.  Lattice plate
finite elements are used to examine the effect of variation of
several fundamental structural parameters on the natural frequencies
and mode shapes of the structure.  Feedback control systems are
designed and the resulting system performance evaluated by

examining the steady state regulation cost of the structure as a function of the structural design parameters.

A micropolar plate continuum model of large plate-like repetitive space lattice structures with rigid joints is derived. A plate finite element is derived based on this continuum model with micropolar rotations and transverse shear deformations included as nodal degrees of freedom (d.o.f.'s). The natural frequencies and mode shapes are calculated using this element for a free floating hexahedral plate-like space lattice structure. These natural frequencies and mode shapes are compared to those calculated using a detailed finite element model (with every structural member modelled by a beam-column element) for several sets of frame member cross sectional properties. The static deflections of a centrally loaded and corner supported rectangular plate-like space lattice structure are also obtained and compared using these two types of structural models.

DTIC
COPY
INSPECTED
1

A-1

## AFIT RESEARCH ASSESSMENT

The purpose of this questionnaire is to ascertain the value and/or contribution of research accomplished by students or faculty of the Air Force Institute of Technology (AU). It would be greatly appreciated if you would complete the following questionnaire and return it to:

AFIT/NR
Wright-Patterson AFB OH 45433

RESEARCH TITLE: Equivalend Continuum Finite Element Modelling of Plate-like Space Lattice Structures

AUTHOR: Steven Edward Lamberson

RESEARCH ASSESSMENT QUESTIONS:

1. Did this research contribute to a current Air Force project?

( ) a. YES                              ( ) b. NO

2. Do you believe this research topic is significant enough that it would have been researched (or contracted) by your organization or another agency if AFIT had not?

( ) a. YES                              ( ) b. NO

3. The benefits of AFIT research can often be expressed by the equivalent value that your agency achieved/received by virtue of AFIT performing the research. Can you estimate what this research would have cost if it had been accomplished under contract or if it had been done in-house in terms of manpower and/or dollars?

( ) a. MAN-YEARS _____        ( ) b. $_____

4. Often it is not possible to attach equivalent dollar values to research, although the results of the research may, in fact, be important. Whether or not you were able to establish an equivalent value for this research (3. above), what is your estimate of its significance?

( ) a. HIGHLY        ( ) b. SIGNIFICANT        ( ) c. SLIGHTLY        ( ) d. OF NO
        SIGNIFICANT                                       SIGNIFICANT        SIGNIFICANCE

5. AFIT welcomes any further comments you may have on the above questions, or any additional details concerning the current application, future potential, or other value of this research. Please use the bottom part of this questionnaire for your statement(s).

_____
NAME                              GRADE                          POSITION

_____
ORGANIZATION                      LOCATION

STATEMENT(s):

EQUIVALENT CONTINUUM FINITE ELEMENT

MODELLING OF PLATE-LIKE SPACE

LATTICE STRUCTURES


A Thesis

Submitted to the Faculty

of

Purdue University

by

Steven Edward Lamberson


In Partial Fulfillment of the

Requirements for the Degree

of

Doctor of Philosophy


August 1985

To Mada,

Annah, Steven Jr., and Eileen

ACKNOWLEDGMENTS

# TABLE OF CONTENTS

# LIST OF TABLES

LIST OF FIGURES

# CHAPTER I - INTRODUCTION

## Problem Statement

Now that the shuttle has made access to space more economical, many projects are being proposed which involve large space platforms made up of lattice-type truss structures. These structures are generally too flexible to meet the mission requirements and automated control systems must be used both to maintain the structures' orientation and to reduce vibrations of the structure. Often, these large space structures are made up of a simple cell of truss bars repeated a large number of times in one or two directions. The resulting structure resembles a beam or a plate when viewed from a distance. Detailed finite element models of such truss structures have a large number of degrees of freedom (d.o.f.'s), which are cumbersome and expensive to use in modal analysis even when dynamic substructuring and reduction methods are used extensively. An alternative method is to derive a plate finite element model based on an equivalent continuum formulation which is used to perform the modal analysis. In either case the modal model generated must be reduced to an evaluation model of a size which can be used to evaluate the effectiveness of various control systems. The modal model must also be reduced further to a series of design models which are used to design feedback control systems. For large lattice-type space truss

structures the order of the detailed finite element model, the order
of the solvable eigenvalue problem, the order of the solvable control
system evaluation model, and the order of the controller which can
be implemented usually from a rapidly decreasing monotonic sequence.
The object of this research is to develop equivalent plate finite
elements based on equivalent continuum representations of large
plate-like space lattices. The resulting equivalent plate finite
elements are shown to be accurate, flexible, and efficient. They
are also demonstrated to be useful in designing and evaluating the
closed loop system performance of large repetitive plate-like space
lattices with reduced order controllers.

## Structural Modelling Methods

### Background

There have been many studies examining finite element modelling
methods of various types of structures which will yield accurate
modal results. There have also been a variety of methods developed
to allow progressively larger finite element models to be used for
modal analysis. In general, this is done using some means of model
reduction. Several methods have been developed to allow large finite
element models (which are discrete representations) to be reduced to
smaller mathematical models (which are also discrete representations).
These methods range from heuristic techniques such as Guyan
reduction[1] which rely heavily on the user's experience for accuracy,
to iterative techniques such as generalized dynamic reduction[2], which
effectively eliminate the need for an experienced user at the expense

of substantially increasing the computational cost.  Other techniques
involve breaking the structure up into substructures which are
analyzed dynamically using a system modelling technique such as
Component Modal Synthesis.[3]  Basically, this involves developing
a modal model of each of the subcomponents, then combining these
individual modal models into a system model whose only physical
d.o.f.'s are the boundaries connecting the various substructures.
The remaining d.o.f.'s are those representing the modal coordinates
of the individual substructures.  The principle problem with this
method is that it is often difficult to determine which modes of a
substructure will contribute to the modes of the entire structure
which are within the desired frequency bandwidth.  Therefore, while
the available techniques have increased the order of finite element
models of structures that can be utilized to perform structural
vibration analysis, there are sufficient difficulties associated
with each reduction method to require that the original finite
element model of the system be generated using the minimum number of
d.o.f.'s consistent with generating an accurate solution[4].

Since many of the large flexible space structures being
considered are built on a platform which is a space lattice
consisting of truss type members connected together in a repetitive
manner, several methods have been developed to allow the repetitive
space lattice to be modelled as an equivalent continuum.  The first
of these applies static loads to a model of a unit cell of the
repetitive space lattice in such a way that the displacement
calculated can be used to determine one or more of the "equivalent"

properties.[5] Another method is to calculate the equivalent properties based on the number of truss elements within the unit cell aligned in each direction.[6] A third method matches the strain energy of the unit cell in terms of a Taylor's series expansion of the midplane displacements with the strain energy of the unit cell in terms of a Taylor's series based on the midplane strains.[7] The existing work has focused on predicting the vibration modes of simply supported truss lattices with pinned joints. There has been some work with simply supported "beam-like" lattices with the frame members connected by rigid joints which makes use of the higher order micropolar beam continuum formulation.[8]

## Detailed Models

For this research the baseline against which the performance of the equivalent continuum models is evaluated are calculated values of the free vibration natural frequencies and mode shapes. For repetitive plate-like space lattices with pinned joints the detailed finite element model is made with each truss member modelled using a single axial force type truss element. Chapter II contains a discussion of the detailed finite element modelling method, a description of the detailed finite element model of a specific space lattice, and a comparison of the resulting natural frequencies and mode shapes with those obtained with an equivalent transverse shear plate finite element. Repetitive plate-like space lattices with rigid joints are modelled using a detailed finite element model with each frame member modelled as a beam-column type finite element.

Chapter IV contains a description of the detailed finite element model of a specific space lattice, and a comparison of the resulting natural frequencies and mode shapes with those obtained with an equivalent micropolar plate finite element. In both cases, Guyan reduction is used to reduce the order of the eigenvalue problem.

### Equivalent Modelling of Space Lattices with Pinned Joints

The equivalent plate finite element for repetitive space lattices with pinned joints is derived using an existing equivalent continuum representation.[7] The strain energy expression derived in the reference in terms of the in-plane, bending, and transverse shear strains is used as a constitutive law to develop a transverse shear type plate finite element. This element assumes a linear displacement functions for the two inplane displacement and two transverse shear deformation d.o.f.'s at each node, and a bicubic Hermite polynomial displacement function for the transverse displacement. This element allows considerable simplicity and flexibility in handling various geometries, boundary conditions, attachments, and other structural complexities. Chapter II contains a discussion of the existing equivalent continuum representation, a derivation of the equivalent plate finite element, a description of the equivalent plate finite element model for a specific space lattice, and a comparison of the resulting natural frequencies and mode shapes with those obtained using a detailed finite element model. Chapter III contains a parametric study examining the effect on the natural frequencies and mode shapes of varying the geometric properties of the unit cell building block of a specific repetitive space lattice.

Equivalent Modelling of Space Lattices with Rigid Joints

An equivalent continuum representation is available for beam-like repetitive space lattices with rigid joints.[8] This method is extended to allow plate-like repetitive space lattices with rigid joints to be represented by a micropolar plate continuum. The strain energy expression derived for this continuum representation in terms of the in-plane, bending, transverse shear, and micropolar strains is used as a constitutive law to develop a micropolar type plate finite element. This element assumes linear displacement functions for the two in-plane displacement, two transverse shear deformation, and two micropolar rotation d.o.f.'s at each node, and a bicubic Hermite polynomial displacement function for the transverse displacement. Chapter IV contains a derivation of the micropolar equivalent continuum and micropolar type plate finite element of repetitive space lattices with rigid joints. Chapter IV also contains a description of the micropolar plate finite element model for a specific space lattice and a comparison of the resulting natural frequencies and mode shapes for several sets of cross sectional areas with those obtained using detailed finite element models.

It should be pointed out that by using the equivalent continuum representations as bridges between the discrete space lattice structures and the discrete equivalent plate finite element models, the number and location of node points in the equivalent plate models is determined based on the number of modes which are desired to be accurately calculated, not by the geometry of the structure. Specifically, there is no requirement that (or advantage to) having

the internal nodal points of the equivalent plate finite element
models coincide with joint locations or unit cell boundaries. For
large structures, the number of nodal d.o.f.'s used in the equivalent
plate finite element model will generally be much smaller than the
number of nodal d.o.f.'s required to represent the structure as a
detailed finite element model.

## Control System Design Method

Even though the order of the eigenvalue problem describing the
repetitive plate-like space lattice structure has been reduced
significantly using Guyan reduction for the detailed finite element
models and the inherent reduction associated with using the equivalent
plate finite elements, there will still, in general, be many more
natural frequencies and mode shapes extracted than can be readily
used to evaluate control system performance. In addition, the higher
natural frequencies and mode shapes, particularly when Guyan reduction
is used are known to contain considerable error.[9] Therefore, the
higher natural frequencies and mode shapes are truncated and those
retained are used as a modal model of the structure for evaluation
purposes. In order to evaluate the performance of the closed loop
system containing this modal model of the structure and a feedback
controller a cost function is defined as the integral over all time
of the weighted norm of a vector of system d.o.f.'s of interest. The
optimum structure, feedback controller combination is defined to be
that system which minimizes this quadratic cost function.[10] In
general, the order of the controller to be used is much smaller

than the order of the modal model needed to represent the dynamic properties of the structure. Therefore, the modal evaluation model must be further reduced to obtain the modal model for which the optimal control system will be designed. While this could also be done by truncating the higher modes, an alternative method called Modal Cost Analysis (MCA) is used instead.[11] In this method the open loop cost of each mode is used to rank the modes in terms of their effect on system performance. Those modes which make the largest contribution to the open loop system cost are retained. Once the reduced order control system design modal model has been obtained the standard Linear Quadratic Gaussian (LQG) theory[10] is used to design a feedback controller which is optimal for the reduced order system. This system performance is then calculated using the reduced order controller to drive the evaluation modal model. It is important that the evaluation modal model be of substantially higher order than the reduced order design model to determine the effect of control system spillover on the modes which were not retained in the reduce order model. Chapter II contains a description of the feedback control system design and closed loop system performance evaluation methods used. This chapter also contains a description of the application of these methods for modal models of a specific lattice structure generated with both a detailed finite element model and an equivalent plate finite element model, and a comparison of the resulting closed loop system performance costs for several different orders of reduced order controller. Chapter III describes the application of these control system design and evaluation methods to

a series of modal models generated using equivalent plate finite
element models with various member properties in the form of a
parametric study.  The resulting system performance costs are
used to determine the best set of member properties.

# CHAPTER II - EQUIVALENT MODELLING OF
## TRUSSES WITH PINNED JOINTS

Many large space structures are being designed which are made up of a simple cell of truss bars repeated a large number of times in two directions. Such a plate-like space lattice has been represented as an equivalent plate continuum with transverse shear deformation included.[7] This representation is used to derive an equivalent plate finite element.[12] As a benchmark to compare the resulting natural frequencies and mode shapes of the structure to, a detailed finite element model is also developed in which each member of the truss is modelled as a simple axial force type truss element. A specific plate-like space lattice structure is used to demonstrate the accuracy of the simplified equivalent plate finite element model. The eight by eight repeating cell structure chosen is large enough to allow the continuum modelling to be acceptable. However, most structures would have many more repetitions than this example. This would, of course, increase the cost and cumbersomeness of the detailed finite element model relative to the continuum model. This would also improve the basic assumptions inherent in the continuum model development. The results shown that even with as few as eight repeating cells in each direction, the control system designs based on the simplified finite element continuum models are effective as reduced order controllers for the detailed finite element model.

## Detailed Finite Element Model

A large finite element model of the lattice-type truss structure is developed using standard axial force truss bar elements.[13] This model treats each member of the structure as a pinned-pinned axial force member with a constant strain. In order to calculate the frequencies and modes of the detailed finite element model, the model must be reduced to a manageable order using some form of dynamic reduction. Guyan reduction[1] is used in this study to reduce the detailed finite element model to a dynamic analysis model retaining d.o.f.'s specified by the user. They are normally chosen to adequately represent the mass distribution within the structure and the anticipated frequencies and mode shapes.

$$[M]\{\ddot{q}\} + [K]\{q\} = 0 \qquad \qquad (II.1)$$

where:

$\{q\}$ = vector of the d.o.f.'s of the complex model;

$[M]$ = mass matrix of the complex model;  and

$[K]$ = stiffness matrix of the complex model.

The mass and stiffness matrices are partitioned into submatrices associated with the d.o.f.'s to be retained and those to be removed.

$$[M] = \begin{bmatrix} M_{aa} & M_{ao} \\ M_{ao}^T & M_{oo} \end{bmatrix} \quad \{q\} = \begin{Bmatrix} q_a \\ q_o \end{Bmatrix} \quad [K] = \begin{bmatrix} K_{aa} & K_{ao} \\ K_{ao}^T & K_{oo} \end{bmatrix} \qquad (II.2)$$

$$\begin{bmatrix} K_{aa} & | & K_{ao} \\ \hline K_{ao}^T & | & K_{oo} \end{bmatrix} \begin{Bmatrix} q_a \\ \hline q_o \end{Bmatrix} = \begin{Bmatrix} F \\ 0 \end{Bmatrix} \qquad (II.3)$$

where:

$\{q_a\}$ = vector of the d.o.f.'s to be retained;

$\{q_o\}$ = vector of the d.o.f.'s to be removed; and

$\{F\}$ = force vector.

The static problem can be reduced exactly by using the lower partition of Equation (II.3) as a constraint equation.

$$[K_a]\{q_a\} = \{[K_{aa}] - [K_{ao}][K_{oo}]^{-1}[K_{ao}]^T\}\{q_a\} = \{F\} \qquad (II.4)$$

Guyan reduction assumes that this same transformation can be applied to the mass matrix.

$$[M_a] = [M_{aa}] - [M_{ao}][K_{oo}]^{-1}[K_{ao}]^T - [K_{ao}][K_{oo}]^{-1}[M_{ao}]^T$$
$$+ [K_{ao}][K_{oo}]^{-1}[M_{oo}][K_{oo}]^{-1}[K_{ao}]^T \qquad (II.5)$$

In general this reduction is not exact. However, it is widely used and gives good results if a suitable set of d.o.f.'s is chosen to be retained.

In order to perform free vibration analysis of a lattice plate structure with all edges free, the rigid body motion of the structure, which renders the stiffness matrix singular, must be accounted for. In this study, the procedures used in the NASA Structural Analysis code (NASTRAN) will be used. This procedure is given in detail in

the NASTRAN theoretical manual[14] and is briefly described here. The reduced dynamic system is solved for the eigenvalues and eigenvectors.

$$\{[K_a] - \lambda[M_a]\} \quad \{q_a(\lambda)\} = \{0\} \tag{II.6}$$

where:

$\lambda_i$ = the ith eigenvalue of the reduced dynamic system;

$\{q_{ai}\} = \{q_a(\lambda_i)\}$ = the ith eigenvector of the reduced

dynamic system; and

$[Q_a] = [q_{a1}, q_{a2}, \ldots]$ = the reduced dynamic system modal

matrix.

However, for the free floating or unsupported plate the stiffness matrix is singular to order six. The first six eigenvalues are not precisely zero due to numerical error in the eigenvalue extraction process. Consequently, the eigenvectors calculated are not precisely the rigid body modes. Therefore a procedure is implemented to replace these six eigenvalues and eigenvectors with six rigid body modes.

The stiffness and mass matrices which have already been reduced using Guyan reduction are further partitioned based on a set of d.o.f.'s specified by the user as necessary to specify the rigid body motions of the structure $\{q_r\}$. The remaining d.o.f.'s are placed in a set $\{q_f\}$.

$$[M] = \begin{bmatrix} M_{ff} & M_{fr} \\ \hline M_{fr}^T & M_{rr} \end{bmatrix} \quad \{q_a\} = \begin{Bmatrix} q_f \\ \hline q_r \end{Bmatrix} \quad [K_a] = \begin{bmatrix} K_{ff} & K_{fr} \\ \hline K_{fr}^T & K_{rr} \end{bmatrix} \tag{II.7}$$

where:

$\{q_f\}$ = the d.o.f.'s in the flexible set; and

$\{q_r\}$ = the d.o.f.'s used to define the rigid body
motion of the structure.

For a rigid body mode the equations of motion can be reduced to a
constraint equation relating the flexible d.o.f.'s to the rigid body
motion d.o.f.'s.

$$\{[K_a] - \omega^2[M_a]\} \{q_a\} = \{0\} \tag{II.8}$$

For rigid body modes, $\omega = 0$, thus Eq. (II.8) reduces to

$$[K_{ff}]\{q_f\} + [K_{fr}]\{q_r\} = \{0\} \tag{II.9}$$

$$\{q_f\} = [D]\{q_r\} \tag{II.10}$$

where

$$[D] = - [K_{ff}]^{-1}[K_{fr}]; \text{ and}$$

$\omega$ = natural frequency of the mode.

By matching the kinetic energy of the structure in the rigid body
mode and using the constraint Eq. (II.10) to eliminate $\{q_f\}$ the
rigid body mass matrix is defined.

$$M_r = \frac{1}{2} \begin{Bmatrix} \dot{q}_f \\ \dot{q}_r \end{Bmatrix}^T \begin{bmatrix} M_{ff} & M_{fr} \\ M_{fr}^T & M_{rr} \end{bmatrix} \begin{Bmatrix} \dot{q}_f \\ \dot{q}_r \end{Bmatrix} = \frac{1}{2} \{\dot{q}_r\}^T [M_r]\{\dot{q}_r\} \tag{II.11}$$

Substituting Eq. (II.10) for $\{q_f\}$ in (II.11) and multiplying out
Eq. (II.11) gives

$$\{\dot{q}_r\}^T[M_r]\{\dot{q}_r\} = \{\dot{q}_r\}^T[D]^T[M_{ff}][D]\{\dot{q}_r\} + \{\dot{q}_r\}^T[D]^T[M_{fr}]\{\dot{q}_r\}$$

$$+ \{\dot{q}_r\}^T[M_{fr}]^T[D]\{\dot{q}_r\} + \{\dot{q}_r\}^T[M_{rr}]\{\dot{q}_r\}$$

where the rigid body mass matrix

$$[M_r] = [D]^T[M_{ff}][D] + [D]^T[M_{fr}] + [M_{fr}]^T[D] + [M_{rr}] . \qquad (II.12)$$

A set of rigid body modes is generated such that they form an orthogonal, normalized set with respect to the rigid body mass matrix.

$$[Q_{ro}]^T[M_r][Q_{ro}] = [I] \qquad (II.13)$$

The rigid body eigenvectors are calculated for the flexible d.o.f.'s and augmented to the rigid body modes to give the rigid body mode shapes of the entire set of d.o.f.'s.

$$[Q_{ao}] = \begin{bmatrix} [D][Q_{ro}] \\ ------- \\ [Q_{ro}] \end{bmatrix} \qquad (II.14)$$

The original modal matrix calculated using Eq. (II.6) is partitioned into the approximate eigenvectors and accurate flexible eigenvectors.

$$[Q_a] = [[Q_{ar}] \mid [Q_{af}]] \qquad [Q] = [[Q_{ao}] \mid [Q_{af}]] \qquad (II.15)$$

The rigid body partitioned matrix $[Q_{ar}]$ is discarded and replaced by the more accurate rigid body mode shapes calculated using Eq. (II.13). The resulting modal matrix is orthogonalized and normalized to give the system modal matrix.

$$[Q]^T[M_a][Q] = [I] \qquad (II.16)$$

## Equivalent Continuum Representation

The method developed in Reference 7 is used to generate strain energy and kinetic energy expressions for the structure in terms of strain components of the plate at the midplane. Briefly, the displacements are assumed to vary linearly through the thickness of the plate (Fig. 1).

$$u(x,y,z) = u^\circ(x,y) + z\phi_x(x,y)$$

$$v(x,y,z) = v^\circ(x,y) + z\phi_y(x,y) \qquad (II.17)$$

$$w(x,y,z) = w^\circ(x,y) + z\varepsilon_3^\circ(x,y)$$

where

$(x,y,z)$ are the coordinates of a point within the plate;

$(u,v,w)$ are the displacements along $(x,y,z)$;

$(\phi_x,\phi_y)$ are the rotations about the $(-y,x)$ axes at the midplane $(z = 0)$;

$(u^\circ,v^\circ,w^\circ)$ are the displacements along $(x,y,z)$ at the midplane; and

$\varepsilon_3^\circ = \dfrac{dw}{dz}$ at the midplane.

The axial strain in the truss members of a typical unit cell is expressed in terms of strain components.

$$\varepsilon^k = \sum_{i=1}^{3} \sum_{j=1}^{3} \varepsilon_{ij}^k \ell_i^k \ell_j^k \qquad (II.18)$$

JOINT TRANSLATIONS:

MIDPLANE TRANSLATIONS
AND ROTATIONS
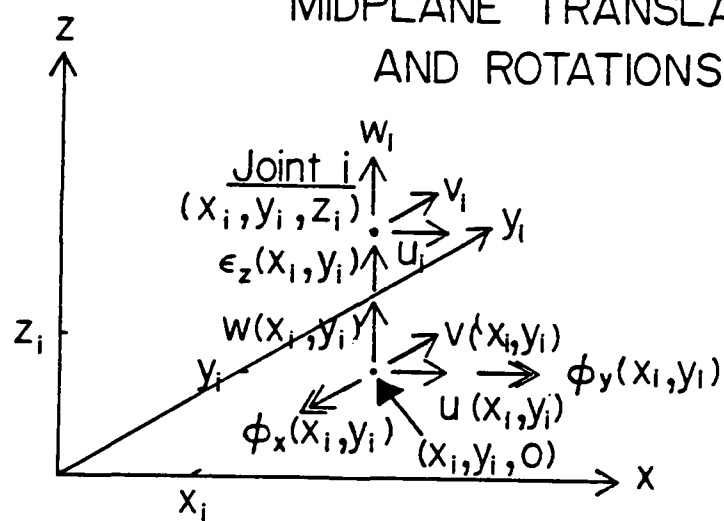


Figure 1. Plate Displacement Components

where:

$\varepsilon^k$ = axial strain in the k'th truss bar;

$\varepsilon_{ij}{}^k$ = strain component of $\varepsilon^k$; and

$\ell_i{}^k$ = direction cosines of the member.

These are then expanded using a Taylor's series in terms of the strain components and their derivatives about some arbitrary origin within the unit cell. The fact that the forces associated with certain of the strain components and derivatives are zeros is used to reduce the strain energy expression to an expression in terms of eight strain components at the plate midplane. The truss cell geometry used in this study is one of those analyzed in the reference.

$$U_{cell} = \frac{1}{2} a_{cell} \{\varepsilon_\ell\}^T [W_{eq}]\{\varepsilon_\ell\} \tag{II.19}$$

where

$U_{cell}$ = strain energy of a unit cell;

$a_{cell}$ = cross sectional area of a unit cell;

$[W_{eq}]$ = equivalent constitutive matrix;

$\{\varepsilon_\ell\} = [\varepsilon_{11}^0, \ \varepsilon_{22}^0, \ \varepsilon_{12}^0, \ \kappa_{11}^0, \ \kappa_{22}^0, \ \kappa_{12}^0, \ \varepsilon_{13}^0, \ \varepsilon_{23}^0]^T$;

$\varepsilon_{ij}^0 = \frac{1}{2} (\frac{\partial u}{\partial y} + \frac{\partial v}{\partial x})$;

$\kappa_{ij} = \frac{1}{2} (\frac{\partial \phi x}{\partial y} + \frac{\partial \phi y}{\partial x})$; and

$\varepsilon_{i3} = \frac{1}{2} (\frac{\partial w}{\partial x_i} + \phi_{x_i})$ .

## Equivalent Finite Element Model

The 16 d.o.f. rectangular plate element[15] is modified to include transverse shear terms and in-plane terms yielding a 32 d.o.f. element (Fig. 2). The interpolation functions are assumed as linear except for the out-of-plane displacement which is assumed as a bi-cubic Hermite polynomial.

$$u = a_1 + a_2x + a_3y + a_4xy$$

$$v = a_5 + a_6x + a_7y + a_8xy$$

$$w = a_9 + a_{10}x + a_{11}y + a_{12}x^2 + a_{13}xy + a_{14}y^2 + a_{15}x^3 + a_{16}x^2y$$
$$+ a_{17}xy^2 + a_{18}y^3 + a_{19}x^3y + a_{20}x^2y^2 + a_{21}xy^3 \quad (II.20)$$
$$+ a_{22}x^3y^2 + a_{23}x^2y^3 + a_{24}x^3y^3$$

$$\varepsilon_{13}^0 = a_{25} + a_{26}x + a_{27}y + a_{28}xy$$

$$\varepsilon_{23}^0 = a_{29} + a_{30}x + a_{31}y + a_{32}xy$$

Substituting Eq. (II.20) into Eq. (II.19) gives the strain energy expression for the element.

$$U_{el} = \frac{1}{2a_{cell}} \int_{AREA}\int \{a\}^T[B]^T[W_{eq}][B]\{a\}dydx \quad (II.21)$$

where

$$\{\varepsilon_\ell\} = [B] \{a\}; \quad \{a\} = [a_1, a_2, \ldots a_{32}]^T; \quad (II.21)$$

# NODAL DEGREES OF FREEDOM:

$$u; \quad v; \quad w; \quad W_{,x}; \quad W_{,y}; \quad W_{,xy}; \quad \epsilon^o_{12}; \quad \epsilon^o_{13}$$
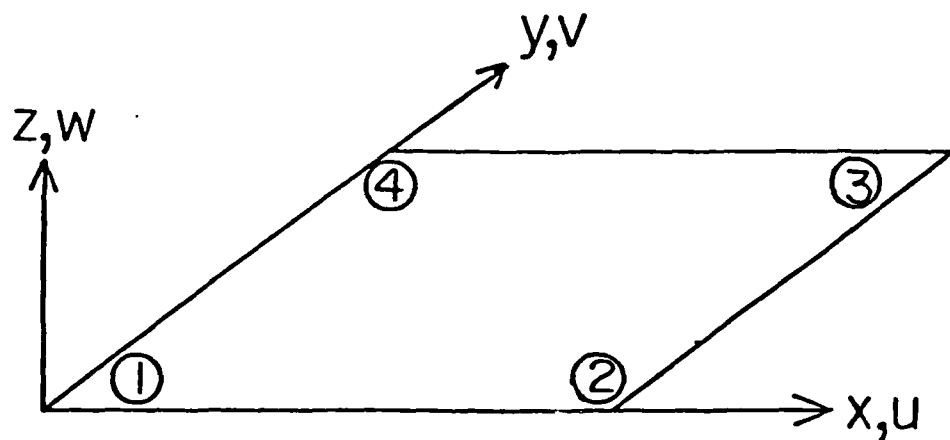


Figure 2. The 32 Degree of Freedom Equivalent
Lattice Plate Finite Element.

$$[B] = \begin{bmatrix} B_1 & 0 & 0 & 0 \\ 0 & B_2 & B_3 & B_4 \\ 0 & 0 & 0 & B_5 \end{bmatrix} \quad ;$$

$$[B_1] = \begin{bmatrix} 0 & 1 & 0 & y & 0 & 0 & 0 & 0 \\ 0 & 0 & 0 & 0 & 0 & 0 & 1 & x \\ 0 & 0 & 0.5 & 0.5x & 0 & 0.5 & 0 & 0.5x \end{bmatrix} \quad ;$$

$$[B_2] = \begin{bmatrix} 0 & 0 & 0 & -2 & 0 & 0 & -6x & -2y & 0 & 0 & -6xy \\ 0 & 0 & 0 & 0 & 0 & -2 & 0 & 0 & -2x & -6y & 0 \\ 0 & 0 & 0 & 0 & -1 & 0 & 0 & -2y & -2y & 0 & -3x^2 \end{bmatrix} \quad ;$$

$$[B_3] = \begin{bmatrix} -2y^2 & 0 & -6xy^2 & -2y^3 & -6xy^3 \\ -2x^2 & -6xy & -2x^3 & -6x^2y & -6x^3y \\ -4x & -3y^2 & -6x^2y & -6xy^2 & -9x^2y^2 \end{bmatrix} \quad ;$$

$$[B_4] = \begin{bmatrix} 0 & 1 & 1 & y & 0 & 0 & 0 & 0 \\ 0 & 0 & 0 & 0 & 0 & 0 & 1 & x \\ 0 & 0 & 0.5 & 0.5x & 0 & 0.5 & 0 & 0.5y \end{bmatrix} \quad ; \quad \text{and}$$

$$[B_5] = \begin{bmatrix} 1 & x & y & xy & 0 & 0 & 0 & 0 \\ 0 & 0 & 0 & 0 & 1 & x & y & xy \end{bmatrix} \quad .$$

Relating the 32 displacement function coefficients to the 32 d.o.f.'s
of the element the strain energy of the element is transformed in
terms of the element d.o.f.'s.

$$U_{el} = \frac{1}{2a_{cell}} \{g\}^T \int_{AREA} \int [T]^T[B]^T[W_{eq}][B][T]dydx\{g\} \qquad (II.22)$$

where:

$$\{a\} = [T]\{g\} \; ;$$

$$\{g\} = [\{g_1\}^T, \{g_2\}^T, \{g_3\}^T, \{g_4\}^T]^T; \; \text{and AREA is the area}$$

of the rectangular plate finite element.

This defines the stiffness matrix of the element.

$$[K_{el}] = \frac{1}{a_{cell}} \int_{AREA} \int [T]^T[B]^T[W_{eq}][B][T]dydx \qquad (II.23)$$

The kinetic energy expression derived in Ref. 7 is used to generate the lumped mass matrix of the element.

$$K.E. = \frac{1}{2} a_{cell} \begin{Bmatrix} \dot{u} \\ \dot{v} \\ \dot{w} \\ \dot{\phi}_x \\ \dot{\phi}_y \end{Bmatrix}^T \begin{bmatrix} m_0 & 0 & 0 & m_1 & 0 \\ 0 & m_0 & 0 & 0 & m_1 \\ 0 & 0 & m_0 & 0 & 0 \\ m_1 & 0 & 0 & m_2 & 0 \\ 0 & m_1 & 0 & 0 & m_2 \end{bmatrix} \begin{Bmatrix} \dot{u} \\ \dot{v} \\ \dot{w} \\ \dot{\phi}_x \\ \dot{\phi}_y \end{Bmatrix} \qquad (II.24)$$

where $m_0$, $m_1$, and $m_2$ are equivalent lumped masses of the space truss defined in the reference.

$$[M_{el}] = \begin{bmatrix} M_1 & 0 & 0 & 0 \\ 0 & M_2 & 0 & 0 \\ 0 & 0 & M_3 & 0 \\ 0 & 0 & 0 & M_4 \end{bmatrix} \qquad (II.25)$$

where

$$[M_i] = \frac{AREA}{a_{cell}} \begin{bmatrix} m_0 \\ 0 & m_0 \\ 0 & 0 & m_0 & & & \text{SYMMETRY} \\ m_1 & 0 & 0 & m_2 \\ 0 & m_1 & 0 & 0 & m_2 \\ 0 & 0 & 0 & 0 & 0 & 0 \\ 0 & 0 & 0 & 0 & 0 & 0 & 0 \end{bmatrix}$$

## Control System Design Method

The detailed finite element model is reduced to an evaluation modal model which can be readily analyzed to determine the effectiveness of the various control designs. The modes retained in the evaluation model are arbitrarily selected to be the lowest frequency modes of the complex model that are both controllable and observable. The evaluation model is used in the real modal form.[15]

$$\begin{Bmatrix} \dot{Q}_1 \\ \dot{Q}_2 \\ \dot{Q}_3 \\ \vdots \\ \dot{Q}_n \end{Bmatrix} = \begin{bmatrix} W_1 & 0 & 0 \ldots 0 \\ 0 & W_2 & 0 \ldots 0 \\ 0 & 0 & W_3 \ldots 0 \\ \vdots & \vdots & \ddots \\ 0 & 0 & & W_n \end{bmatrix} \begin{Bmatrix} Q_1 \\ Q_2 \\ Q_3 \\ \vdots \\ Q_n \end{Bmatrix} + \begin{bmatrix} B_1 \\ B_2 \\ \vdots \\ B_n \end{bmatrix} u + \begin{bmatrix} D_1 \\ D_2 \\ \vdots \\ D_n \end{bmatrix}$$

$$\{y\} = [C_1, C_2, \ldots C_n] \begin{Bmatrix} Q_1 \\ Q_2 \\ \vdots \\ Q_n \end{Bmatrix} \qquad \{z\} = [M_1, M_2, \ldots M_n] \begin{Bmatrix} Q_1 \\ Q_2 \\ \vdots \\ Q_n \end{Bmatrix} + \{v\}$$

$$(II.26)$$

where

        $\{u\}$ is the input force vector to the system;

        $\{w\}$ is the input disturbance vector to the system;

        $\{v\}$ is the measurement disturbance vector of the system;

        $\{z\}$ is the measurement vector of the system;

        $\{y\}$ is the output vector of the system;

$$\{Q_i\} = \left\{\begin{array}{c} q_i \\ \dot{q}_i \end{array}\right\} \text{ with } q_i = \text{ the modal coordinate associated with mode } i;$$

$$[B_i] = \left\{\begin{array}{c} 0 \\ b_i{}^T \end{array}\right\} \text{ with } \{b_i\}^T = \text{ the modal coefficients of the applied force for mode } i;$$

$$[D_i] = \left\{\begin{array}{c} 0 \\ d_i{}^T \end{array}\right\} \text{ with } \{d_i\}^T = \text{ the modal coefficient of the applied disturbance vector for mode } i;$$

$$[C_i] = [c_i \; 0] \text{ with } \{c_i\} = \text{ the modal coefficients of the output vector for mode } i;$$

$$[M_i] = [m_i \; 0] \text{ with } \{m_i\} = \text{ the modal coefficients of the measurement vector for mode } i;$$

$$[W_i] = \begin{bmatrix} 0 & 1 \\ -\omega_i^2 & -2\zeta\omega_i \end{bmatrix} \text{ with } \omega_i = \text{ the natural frequency of the mode } i; \text{ and}$$

$$\zeta = \text{ the modal damping coefficient.}$$

The full models available from either the complex model or the equivalent plate finite element models usually generate too many

modes to be used directly as control design models. Therefore, some means of model reduction is required. Several dynamic reduction schemes have been developed to al'ow the control problem to influence the model reduction; of these Modal Cost Analysis (MCA) is the most straightforward to use.[17] In order to use MCA, the relative importance of a set of outputs, each of which is a linear combination of d.o.f.'s of the structure is used to build a positive definite output weighting matrix $[Q]$. The cost which is to be minimized by the control system is then defined as the sum of a weighted norm of the output vector plus a weighted norm of the measurement vector.

$$V = V_y + \rho V_z \qquad (II.27)$$

where

$$V_y = \lim_{T \to \infty} E \int_0^T \{y\}^T [Q]\{y\} dt \; ;$$

$$V_z = \lim_{T \to \infty} E \int_0^T \{z\}^T [Z]^{-1}\{z\} dt \; ;$$

$E$ = expected value; and

$\rho$ = measurement weight.

The weighting matrix used for measurements is the inverse of the covariance matrix of the measurement errors.

$$[Z] = E[\{v\}\{v\}^T] \qquad (II.28)$$

For small values of modal damping this can be reduced to an uncoupled set of equations as derived in Ref. 17.

$$V_i = \frac{1}{4\zeta\omega_i^3} (\{c_i\}^T [Q]\{c_i\} + \{m_i\}^T [Z]^{-1}\{m_i\})(\{b_i\}^T \{b_i\}) \quad (II.29)$$

Control design models of order n are derived from the detailed finite element and the equivalent plate model by retaining the n/2 modes having the largest modal costs. Since rigid body modes have infinite modal cost, they must always be retained in the reduced models if they are controllable and observable.

Each control design model is used to design a standard LQG controller.[10]

$$\{\dot{q}\} = [A]\{q\} + [B]\{u\} + [D]\{w\}$$

$$\{y\} = [C]\{q\}$$

$$\{z\} = [M]\{q\} + v \quad (II.30)$$

where

$$E\{w\} = E\{v\} = 0;$$

$$E[\{w(\tau)\}\{w(t)\}^T] = [W]\delta(t-\tau);$$

$$E[\{v(\tau)\}\{v(t)\}^T] = [V]\delta(t-\tau);$$

$$E[\{w(t)\}\{q(0)\}^T] = E[\{v(t)\}\{q(0)\}^T] = 0; \text{ and}$$

$$E[\{v(t)\}\{w(\tau)\}^T] = 0 .$$

Starting with a reduced system in the form of Eq. (II.26) a state estimator is designed to allow a feedback controller to be designed.

$$\{\dot{\hat{q}}\} = [A]\{\hat{q}\} + [B]\{u\} + [F][\{z\} - [M]\{\hat{q}\}]$$ (II.31)

Where the filter matrix is defined as a Riccati equation.

$$[F] = [P][M]^T[V]^{-1}$$

$$[0] = [P][A]^T + [A][P] - [P][M]^T[V]^{-1}[M][P] + [D][W][D]^T$$ (II.32)

Once the estimate of the state is available a state feedback controller is designed.

$$\{u\} = [G]\{\hat{q}\}$$ (II.33)

Where the feedback gain matrix [G] is defined as a Riccati equation.

$$[G] = -\frac{1}{\rho} [R]^{-1}[B]^T[K]$$

$$[0] = [K][A] + [A]^T[K] - \frac{1}{\rho} [K][B][R]^{-1}[B]^T[K] + [C]^T[Q][C]$$ (II.34)

### Closed Loop System Performance

The full order controller based on the evaluation model can be evaluated directly, as in Ref. 10.

$$V = V_y + \rho V_u$$

$$V_y = \lim_{T \to \infty} \frac{1}{T} \int_0^T \{y\}^T[Q]\{y\}dt = tr[C]^T[Q][C] [[X] + [P]]$$ (II.35)

$$V_u = \lim_{T \to \infty} \frac{1}{T} \int_0^T \{u\}^T [R]\{u\} dt = tr[G]^T[R][G][X]$$

where

$$[0] = [X]\{[A] + [B][G]\}^T + \{[A] + [B][G]\}[X] + [F][V][F]^T$$

$$(II.36)$$

In order to evaluate the full evaluation model driven by a reduced order controller, the evaluation model must be augmented with the controller model as in Ref. 16.

For the evaluation model,

$$\{\dot{q}_e\} = [A_e]\{q_e\} + [B_e]\{u\} + [D_e]\{w\}$$

$$\{y\} = [C_e]\{q_e\}$$

$$\{z\} = [M_e]\{q_e\} + \{v\} \qquad (II.37)$$

For the controller model,

$$\{\dot{\hat{q}}\} = [A_C]\{\hat{q}\} + [F_R]\{z\}$$

$$\{u\} = [G_R]\{\hat{q}\} \qquad (II.38)$$

where

$$[A_C] = [A_R] + [B_R][G_R] - [F_R][M_R]$$

This forms an augmented system.

$$\begin{Bmatrix} \dot{q}_e \\ \dot{\hat{q}} \end{Bmatrix} = \begin{bmatrix} A_e & B_e G_R \\ F_R M_e & A_c \end{bmatrix} \begin{Bmatrix} q_e \\ \hat{q} \end{Bmatrix} + \begin{bmatrix} D_e & 0 \\ 0 & F_R \end{bmatrix} \quad \text{or}$$

$$\{\dot{\hat{q}}_a\} = [A_a]\{q_a\} + [D_q]\{w_a\} \tag{II.39}$$

$$\begin{Bmatrix} y \\ u \end{Bmatrix} = \begin{bmatrix} C & 0 \\ 0 & G_R \end{bmatrix} \begin{Bmatrix} q_e \\ \hat{q} \end{Bmatrix} = [C_a]\{q_a\} \quad [W_a] = \begin{bmatrix} W & 0 \\ 0 & V \end{bmatrix}$$

from which

$$V_y = tr[C_e]^T[Q][C_e][X_e]; \quad \text{and}$$

$$V_u = tr[G_R]^T[R][G_R][X_R]$$

where

$$[X_a] = \begin{bmatrix} X_e & X_c \\ X_c & X_R \end{bmatrix} \quad ; \quad \text{and}$$

$$[0] = [X_a][A_a]^T + [A_a][X_a] + [D_a][W_a][D_a]^T .$$

## Results

### Detailed Finite Element Model

A unit cell of the lattice-type space structure to be analyzed in this study is shown in Fig. 3. The dimensions of the unit cell are those from Ref. 7. It is 15 meters square by 7.5 meters deep. Structural members on the upper surface have an area of 80 $mm^2$. The bottom surface members have an area of 50 $mm^2$. Elements connecting the two surfaces have an area of 10 $mm^2$. The material has a Young's Modulus of $71.7 \times 10^9$ $Nt/m^2$ and a density of 2768 $kg/m^3$. The structure to be analyzed consists of identical cells repeated eight times in

ORIGINAL
VALUES

——— UPPER SURFACE MEMBERS    $A_1 = 80\,mm^2$
—·—·— LOWER SURFACE MEMBERS    $A_2 = 50\,mm^2$
— — — VERTICAL MEMBERS    $A_v = 10\,mm^2$
------- DIAGONAL MEMBERS    $A_d = 10\,mm^2$
    $L = h = 7.5\,m$
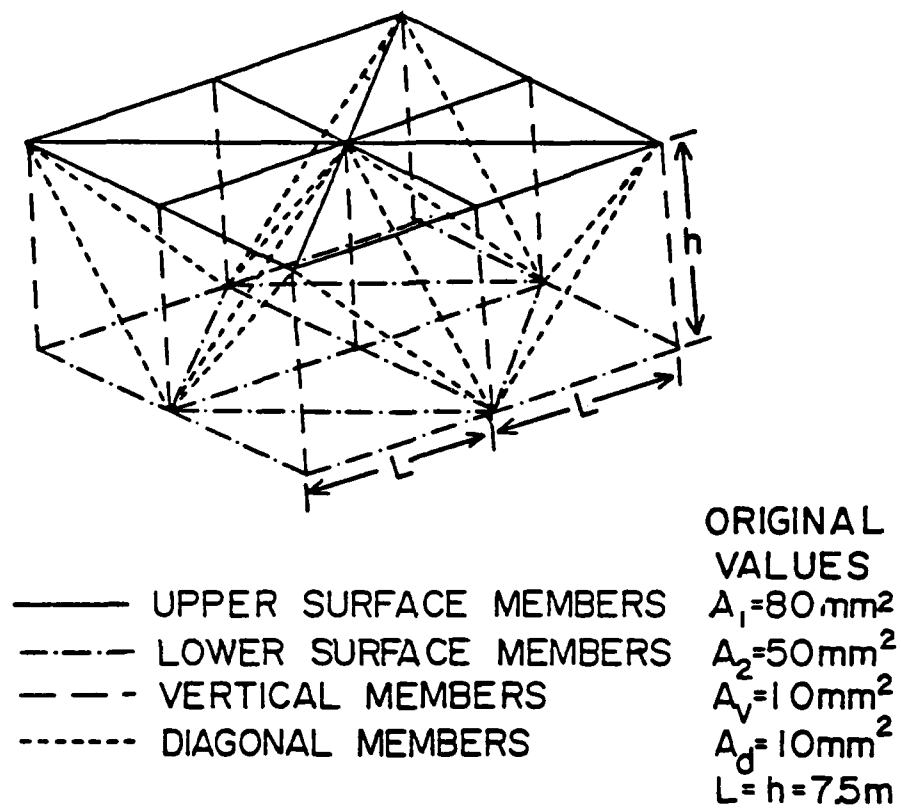
Figure 3. Plate-like Space Lattice Unit Cell

each of two directions (Fig. 4). The resulting structure resembles a plate. The detailed finite element model is made using a pinned truss element for each member. This model is analyzed using NASTRAN. The full model has 1254 d.o.f.'s. The reduced dynamic analysis model has 214 d.o.f.'s as shown in Fig. 5. This structure was chosen to be large enough to allow an equivalent continuum model to be accurate over a significant frequency range, but small enough to be readily analyzed.

### Equivalent Plate Models

The truss properties of the unit cell shown in Fig. 3 are used to generate the strain energy and kinetic energy of the structure in terms of the strain components at an arbitrary point within the cell. The matrices $[W_{eq}]$ and $[M_{eq}]$ in the strain energy expression Eq. (II.21) and kinetic energy expression Eq. (II.24), respectively, are tabulated below and are in agreement with those presented in Ref. 7.

Constitutive Matrix

$$\frac{[W_{eq}]}{10^6 \text{ nt-m}} = \begin{bmatrix} 1.6822 & 0.4394 & 0.0 & 1.4557 & 3.8025 & 0.0 & 0.0 & 0.0 \\ & 1.6822 & 0.0 & 3.8025 & 1.4557 & 0.0 & 0.0 & 0.0 \\ & & 1.7576 & 0.0 & 0.0 & 15.214 & 0.0 & 0.0 \\ & & & 23.6559 & 6.179 & 0.0 & 0.0 & 0.0 \\ & & & & 23.6559 & 0.0 & 0.0 & 0.0 \\ \text{SYMMETRY} & & & & & 24.716 & 0.0 & 0.0 \\ & & & & & & 0.388 & 0.0 \\ & & & & & & & 0.388 \end{bmatrix}$$

(II.39)
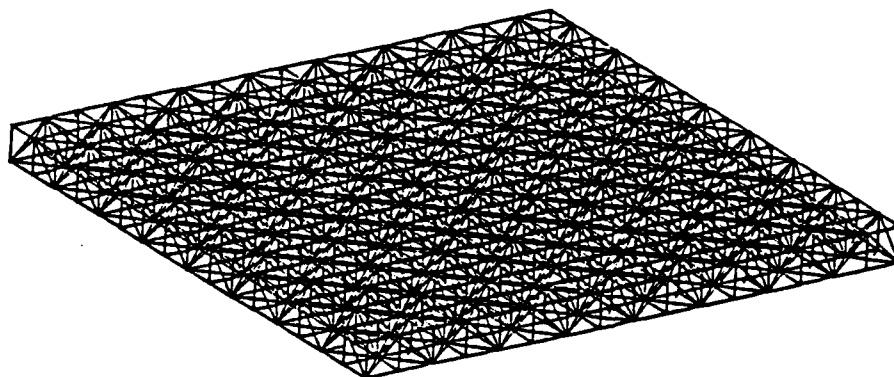
Figure 4. Plate-like Space Lattice
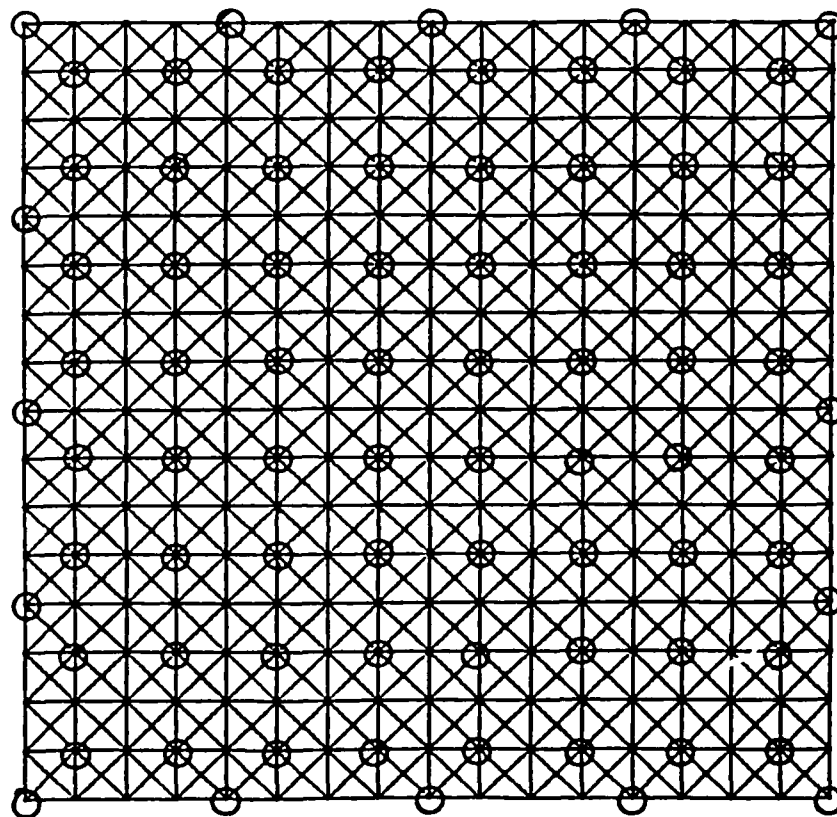
Figure 5. Detailed Finite Element Model
Dynamic Analysis Set.

Mass Density Matrix

$$
\frac{[M_{eq}]}{kg/m^2} =
\begin{bmatrix}
0.17794 & 0.0 & 0.0 & 0.14176m & 0.0 \\
 & 0.17794 & 0.0 & 0.0 & 0.14176m \\
 & & 0.17794 & 0.0 & 0.0 \\
 & & & 2.3698m^2 & 0.0 \\
 & \text{SYMMETRY} & & & 2.3698m^2
\end{bmatrix}
\qquad (II.40)
$$

These expressions are used to derive an equivalent plate finite element. This element is used to form two equivalent plate models, a coarse one (4x4) containing 16 uniform elements, and a more detailed one (8x8) containing 64 uniform elements.

## Free Vibration Analysis

Each of the three finite element models, a complex model (1254 bar elements) and two equivalent plate models (4x4 and 8x8 meshes), was analyzed to determine the natural frequencies and mode shapes of the structure. The lower natural frequencies and the associated mode shapes predicted by the three models are shown in Fig. 6. The mode shapes predicted by all the models are very similar. Contour plots of several of the elastic modes generated for the structure contained in Appendix A. The three sets of frequencies are in good agreement, especially at low frequencies. The relative costs to execute each vibration analysis are given in Table 1. Even with as few as eight cell repetitions in each direction the cost savings using the equivalent plate finite element model are substantial.
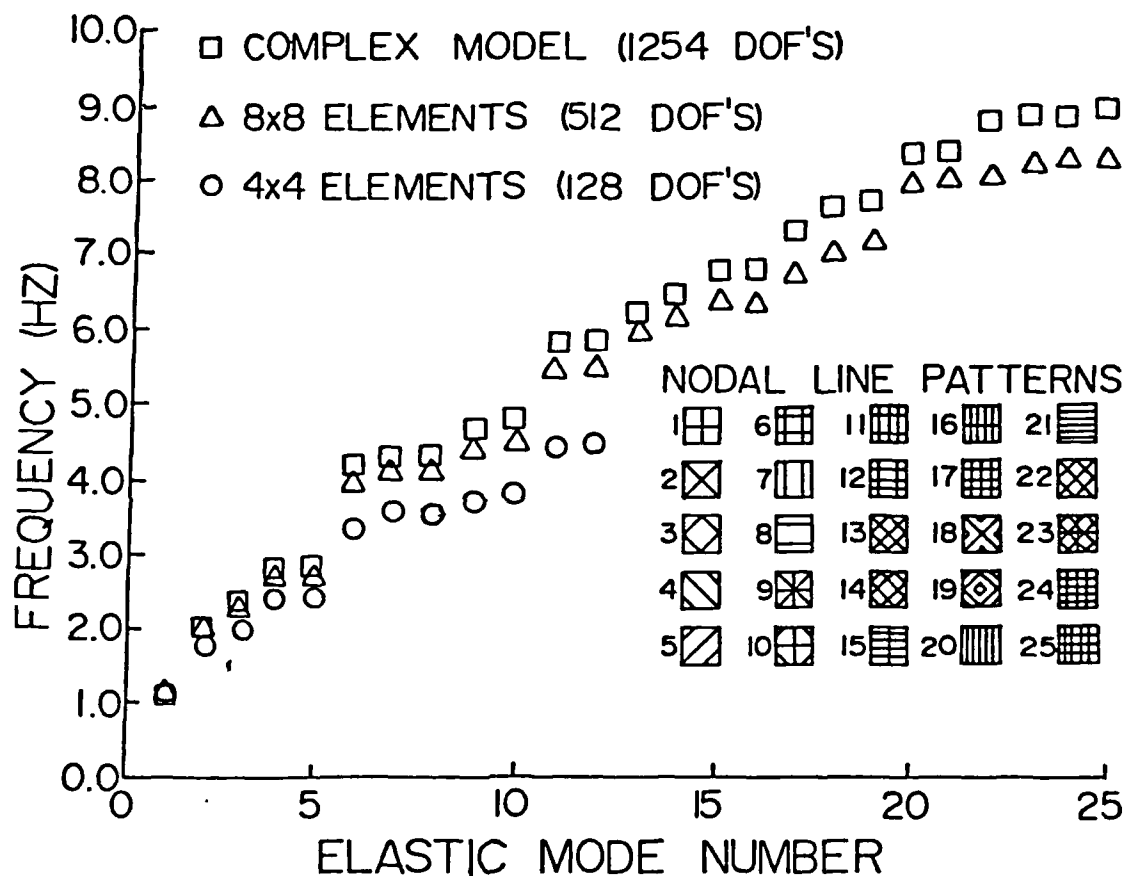
Figure 6. Elastic Modes of the Space
Lattice Structure.

Table 1. Relative Vibration Analysis Costs

| Model | Relative Cost |
|---|---|
| Complex | 1.0000 |
| 4x4 elements | 0.0350 |
| 8x8 elements | 0.1000 |

## Control Problem

The control problem used to evaluate the capability of the equivalent continuum models involves angular sensors and actuators located at the center and the four corners of the structure. This is similar to a case examined for an isotropic plate.[17] It is assumed that the output is measured and the disturbance is acting on these ten rotational d.o.f.'s at the five locations. Therefore, the $[B]$, $[D]$, $[C]^T$, and $[M]^T$ matrices are identical. The output and control weighting matrices are assumed to be identity matrices. The disturbance weighting matrix $[W]$ is assumed to be 0.0001 times the identity matrix. The measurement weight matrix $[V]$ is assumed to be $10^{-12}$ times the identity matrix. The modal damping $\zeta$ is assumed to be 0.005.

## Evaluation Model

A system containing 24 modes was used to design a control system using LQG theory. The evaluation model was chosen to include the two rigid body modes that are both observable and controllable. The frequencies and modal coefficients are given in Table 2.

Table 2. Evaluation Model Rotational Coefficients

| Natural Freq (Hz) | Rotation about the y-axis ($\theta_x$) | | | | | Rotation about the x-axis ($\theta_y$) | | | | |
|---|---|---|---|---|---|---|---|---|---|---|
| | Corner 1 | Corner 2 | Corner 3 | Corner 4 | Center | Corner 1 | Corner 2 | Corner 3 | Corner 4 | Center |
| 0.00 | -3.76 | -3.76 | -3.76 | -3.76 | -3.76 | -3.76 | -3.76 | -3.76 | -3.76 | -3.76 |
| 0.00 | -3.55 | -3.55 | -3.55 | -3.55 | -3.55 | 3.55 | 3.55 | 3.55 | 3.55 | 3.55 |
| 1.16 | 5.88 | 5.88 | -5.88 | -5.88 | 0.00 | 5.88 | -5.88 | -5.88 | 5.88 | 0.00 |
| 1.99 | 6.98 | -6.98 | -7.04 | 6.99 | 0.00 | -6.98 | -6.98 | 7.03 | 6.98 | 0.00 |
| 2.26 | 6.49 | -6.50 | -6.67 | 6.53 | 0.00 | 6.51 | 6.54 | -6.39 | -6.53 | 0.00 |
| 2.76 | -11.72 | 9.35 | -11.97 | 9.29 | 1.45 | -7.57 | 2.75 | -7.21 | 2.75 | 2.95 |
| 2.76 | 2.75 | -7.57 | 2.75 | -7.57 | 2.95 | -9.35 | 11.71 | -9.35 | 11.71 | -1.45 |
| 4.14 | 7.92 | -8.50 | -9.01 | 7.67 | 0.00 | 8.19 | 8.16 | -7.71 | -8.21 | 0.00 |
| 4.23 | 10.75 | 10.17 | 10.79 | 11.08 | -2.87 | .43 | .80 | -.74 | .16 | -.06 |
| 4.23 | .47 | .12 | .47 | .12 | -2.87 | -10.61 | -10.60 | -10.61 | -10.60 | 2.88 |
| 4.67 | -9.54 | -9.63 | 9.81 | 9.49 | 0.00 | 8.82 | -8.68 | -9.40 | 8.68 | 0.00 |
| 4.79 | -10.30 | -10.39 | 10.67 | 10.29 | 0.00 | -10.92 | 11.06 | 10.30 | -11.06 | 0.00 |
| 5.84 | 12.75 | 9.94 | 13.47 | 9.43 | 3.27 | 8.32 | -1.90 | 7.04 | .59 | .94 |
| 5.85 | 2.02 | -8.29 | 2.02 | -8.29 | -.90 | 9.88 | 12.74 | 9.88 | 12.74 | 3.26 |
| 6.30 | -6.47 | 6.03 | 7.00 | -7.02 | 0.00 | 5.81 | 6.19 | -7.25 | -5.92 | 0.00 |
| 6.42 | -5.78 | 5.58 | 6.25 | -6.19 | 0.00 | -6.44 | -6.19 | 5.65 | 6.39 | 0.00 |
| 6.76 | -11.80 | 12.83 | 12.53 | 12.38 | .72 | 2.57 | -4.29 | 4.05 | -4.22 | -2.61 |
| 6.78 | -4.26 | 2.29 | -4.26 | 2.29 | 0.00 | -12.51 | 11.99 | -12.51 | 11.99 | 0.00 |
| 7.31 | -10.13 | -9.36 | 10.04 | 9.75 | 0.00 | -9.76 | 9.56 | 8.97 | -9.72 | 0.00 |
| 7.62 | -12.01 | 12.32 | 12.20 | -11.91 | 0.00 | -10.46 | -10.96 | 9.30 | 10.78 | 0.00 |
| 7.68 | 4.03 | -4.35 | -4.33 | 3.86 | -.05 | -7.23 | -6.68 | 8.65 | 6.90 | .08 |
| 8.38 | 6.67 | 7.37 | 7.21 | 8.43 | 4.20 | -.81 | -4.70 | -3.07 | -4.24 | -1.71 |
| 8.40 | -4.51 | -1.13 | -4.51 | -1.13 | -1.64 | -7.93 | -6.62 | -7.93 | -6.62 | -4.23 |
| 8.81 | 4.81 | 9.41 | -9.20 | -4.69 | .22 | -7.12 | 3.80 | 7.19 | -7.50 | .75 |

## Modal Cost Analysis

The modal costs are calculated for each of the three analysis models and plotted versus frequency in Fig. 7. The 8x8 element model and the complex model have very similar modal cost distributions. Not surprisingly, the 4x4 element does not predict the modal costs as closely. The frequencies and modal coefficients for the two finite element modal models are given in Tables 3 and 4 for the 4x4 and 8x8 meshes, respectively.
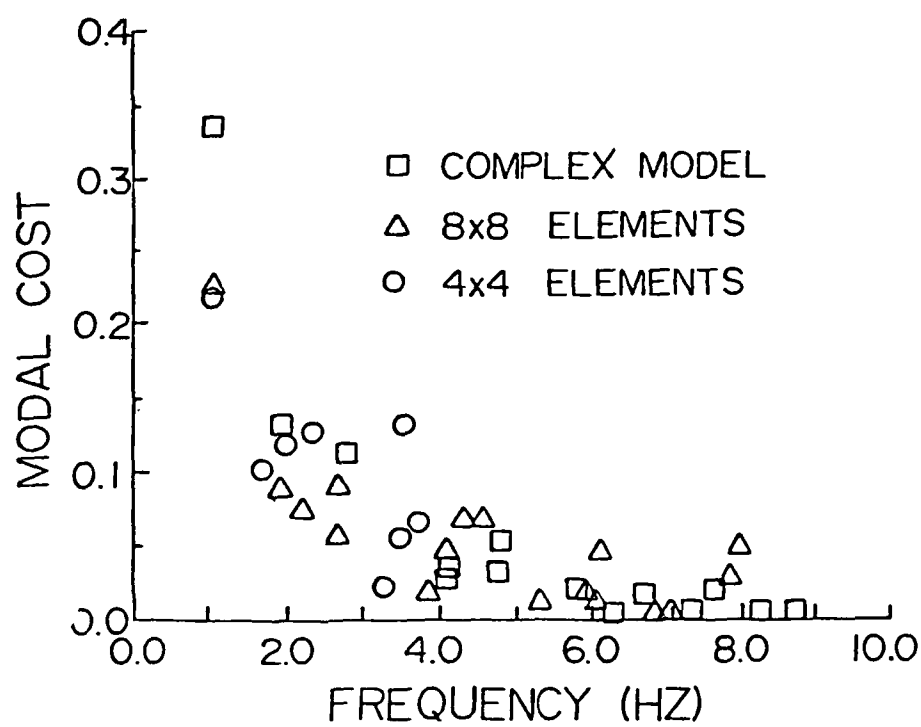
Figure 7. Modal Costs of the Example Lattice Structure

Table 3. 4x4 Equivalent Plate Model
Rotational Coefficients

| Natural Freq. (Hz) | Rotation about the y-axis ($\theta x$) | | | | | Rotation about the x-axis ($\theta y$) | | | | |
|---|---|---|---|---|---|---|---|---|---|---|
| | Corner 1 | Corner 2 | Corner 3 | Corner 4 | Center | Corner 1 | Corner 2 | Corner 3 | Corner 4 | Center |
| 0.00 | -5.35 | -5.35 | -5.35 | -5.35 | -5.35 | -.49 | -.49 | -.49 | -.49 | -.49 |
| 0.00 | .49 | .49 | .49 | .49 | .49 | -5.35 | -5.35 | -5.35 | -5.35 | -5.35 |
| 1.12 | -5.71 | -5.71 | 5.71 | 5.71 | 0.00 | -5.71 | 5.71 | 5.71 | -5.71 | 0.00 |
| 1.80 | 6.66 | -6.66 | -6.66 | 6.66 | 0.00 | -6.66 | -6.66 | 6.66 | 6.66 | 0.00 |
| 2.06 | -7.53 | 7.53 | 7.53 | -7.53 | 0.00 | -7.53 | -7.53 | 7.53 | 7.53 | 0.00 |
| 2.40 | 10.28 | -12.08 | 10.28 | -12.08 | .76 | -1.70 | 6.57 | -1.70 | 6.57 | -2.06 |
| 2.40 | -6.57 | 1.70 | -6.57 | 1.70 | 2.06 | -12.08 | 10.28 | -12.08 | 10.28 | .76 |
| 3.34 | -6.70 | 6.70 | 6.70 | -6.70 | 0.00 | -6.70 | -6.70 | 6.70 | 6.70 | 0.00 |
| 3.56 | 12.02 | 12.50 | 12.02 | 12.51 | -2.14 | -2.92 | -4.53 | -2.92 | -4.53 | .65 |
| 3.56 | 4.53 | 2.92 | 4.53 | 2.92 | -.65 | 12.50 | 12.02 | 12.51 | 12.02 | -2.14 |
| 3.67 | -9.98 | -9.98 | 9.98 | 9.98 | 0.00 | 9.98 | -9.98 | -9.98 | 9.98 | 0.00 |
| 3.80 | -9.87 | -9.87 | 9.87 | 9.87 | 0.00 | -9.87 | 9.87 | 9.87 | -9.87 | 0.00 |

Table 4. 8x8 Equivalent Plate Model
Rotational Coefficients

| Natural Freq. (Hz) | Rotation about the y-axis ($\theta_x$) | | | | | Rotation about the x-axis ($\theta_y$) | | | | |
|---|---|---|---|---|---|---|---|---|---|---|
| | Corner 1 | Corner 2 | Corner 3 | Corner 4 | Center | Corner 1 | Corner 2 | Corner 3 | Corner 4 | Center |
| 0.00 | 5.55 | 5.55 | 5.55 | 5.55 | 5.55 | .26 | .26 | .26 | .26 | .26 |
| 0.00 | .25 | .25 | .25 | .25 | .25 | -5.58 | -5.58 | -5.58 | -5.58 | -5.58 |
| 1.17 | 5.80 | 5.80 | -5.80 | -5.80 | 0.00 | 5.80 | -5.80 | -5.80 | 5.80 | 0.00 |
| 2.00 | -6.88 | 6.88 | 6.88 | -6.88 | 0.00 | 6.88 | 6.88 | -6.88 | -6.88 | 0.00 |
| 2.27 | -7.02 | 7.02 | 7.02 | -7.02 | 0.00 | -7.02 | -7.02 | 7.02 | 7.02 | 0.00 |
| 2.68 | 8.36 | -4.50 | 8.36 | -4.50 | -2.50 | 11.17 | -8.66 | 11.17 | -8.66 | -1.62 |
| 2.68 | 8.66 | -11.17 | 8.66 | -1.62 | 0.00 | -4.50 | 8.36 | -4.50 | 8.36 | -2.50 |
| 3.93 | -7.60 | 7.60 | 7.60 | -7.60 | 0.00 | -7.60 | -7.60 | 7.60 | 7.60 | 0.00 |
| 4.11 | 13.10 | 13.10 | 13.10 | 13.10 | -2.26 | .86 | .77 | .86 | .77 | -.14 |
| 4.11 | -.77 | -.86 | -.77 | -.86 | .14 | 13.10 | 13.10 | -13.10 | 13.10 | -2.26 |
| 4.31 | 11.39 | 11.39 | -11.39 | -11.39 | 0.00 | -11.39 | 11.39 | 11.39 | -11.39 | 0.00 |
| 4.60 | -11.87 | -11.87 | 11.87 | 11.87 | 0.00 | -11.87 | 11.87 | 11.87 | -11.87 | 0.00 |
| 5.41 | -11.73 | -10.26 | -11.73 | -10.26 | -1.03 | -6.21 | -2.48 | -6.21 | -2.48 | -.41 |
| 5.41 | -2.48 | -6.21 | -2.48 | -6.21 | -.41 | 10.26 | 11.73 | 10.26 | 11.73 | 1.03 |
| 5.99 | 11.23 | -11.23 | -11.23 | 11.23 | 0.00 | -11.23 | -11.23 | 11.23 | 11.23 | 0.00 |
| 6.14 | -9.50 | 9.50 | 9.50 | -9.50 | 0.00 | -9.50 | -9.50 | 9.50 | 9.50 | 0.00 |
| 6.29 | 2.79 | -2.06 | 2.79 | -2.07 | -2.24 | -19.02 | 18.93 | -19.02 | 18.93 | .29 |
| 6.29 | 18.93 | -19.02 | 18.93 | -19.02 | .29 | 2.07 | -2.79 | 2.07 | -2.79 | 2.24 |
| 6.68 | 6.65 | 6.65 | -6.65 | -6.65 | 0.00 | 6.65 | -6.65 | -6.65 | 6.65 | 0.00 |
| 6.98 | -9.16 | 9.16 | 9.16 | -9.16 | 0.00 | 9.16 | 9.16 | -9.16 | -9.16 | 0.00 |
| 7.13 | -10.41 | 10.41 | 10.41 | -10.41 | 0.00 | -10.41 | -10.41 | 10.41 | 10.41 | 0.00 |
| 7.92 | 16.27 | 16.37 | 16.27 | 16.37 | 5.32 | -.97 | 19.86 | -.97 | 1.99 | .17 |
| 7.92 | -1.99 | .97 | -1.99 | .97 | -.17 | 16.37 | 16.27 | 16.37 | 16.27 | 5.32 |
| 8.05 | -16.57 | -16.57 | 16.57 | 16.57 | 0.00 | 16.57 | -16.57 | -16.57 | 16.57 | 0.00 |

## Control Design Models

The reduced models chosen contain the two observable and controllable rigid body modes plus up to ten elastic modes. The elastic modes retained are those with the largest modal costs. The performance of several reduced order controllers is shown in Fig. 8.

## Conclusions

A basic procedure to analyze plate-like space lattice structures using finite element models of equivalent continuum formulations of the strain energy and kinetic energy of the structure has been developed and implemeneted. By retaining the transverse shear deformations in the finite element formulation, the equivalent plate finite element models are found to give modal results consistent with those generated from a detailed truss bar element model of the space lattice structure even for small numbers of unit cell repetitions.

The modal models resulting from the finite element model are shown to serve as accurately, yet are more simplified in the control design process compared to the complex truss bar element model for the space-lattice structure. This study has shown that choosing control design models based on modal sequence may involve unnecessary modes. By using Modal Cost Analysis to consider the control problem based on a sequence of lower modes, it is found that several intermediate modes do not contribute much to the control design.
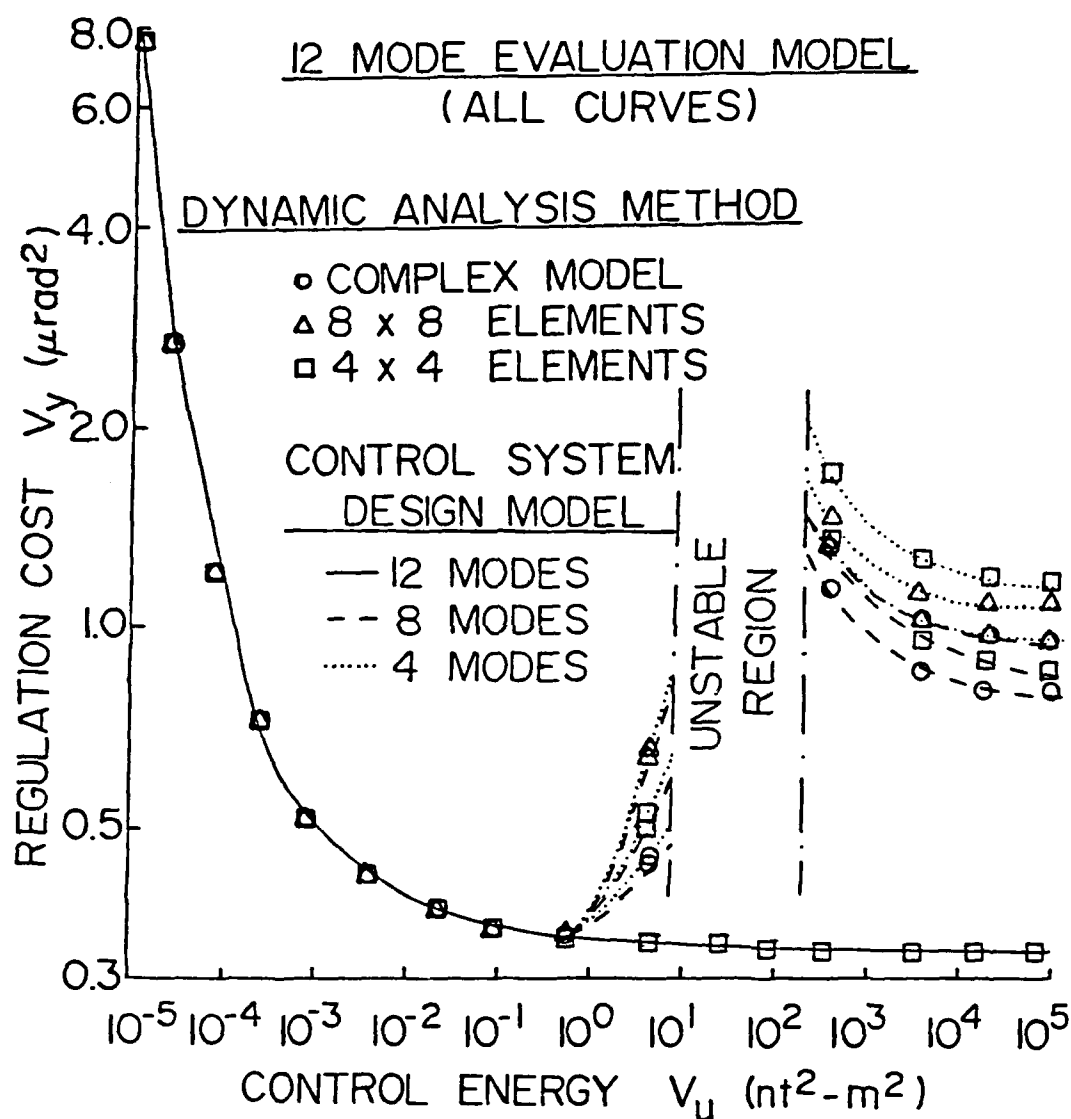
Figure 8. System Performance of the
Example Lattice Structure.

# CHAPTER III - EQUIVALENT MODELLING
## AS A DESIGN TOOL - PARAMETRIC STUDY

Lattice plate finite elements based on a continuum model of a large plate-like lattice space structure are used to examine the effect of variation of several fundamental structural parameters on the natural frequencies and mode shapes of the structure.[18] Reduced order controller design models are developed using modal cost analysis to rank the modes for each set of structural parameter values. The linear quadratic Gaussian (LQG) controller design method is used to develop feedback control systems for each set of structural parameter values. The resulting system performance is then evaluated by examining the steady state regulation cost of the structure as a function of the structural design parameters.

## Problem Statement

The initial space lattice geometry used in this study was used in Chapter II to demonstrate the effectiveness of equivalent finite element models in designing feedback control systems for plate-like lattice space structures. A simple unit cell (Fig. 9) is repeated eight times in two orthogonal directions to generate the lattice space structure. The lattice space structure geometry is defined by six parameters. Four of these are the cross sectional areas of: the upper surface members ($A_1$), the lower surface members ($A_2$), the
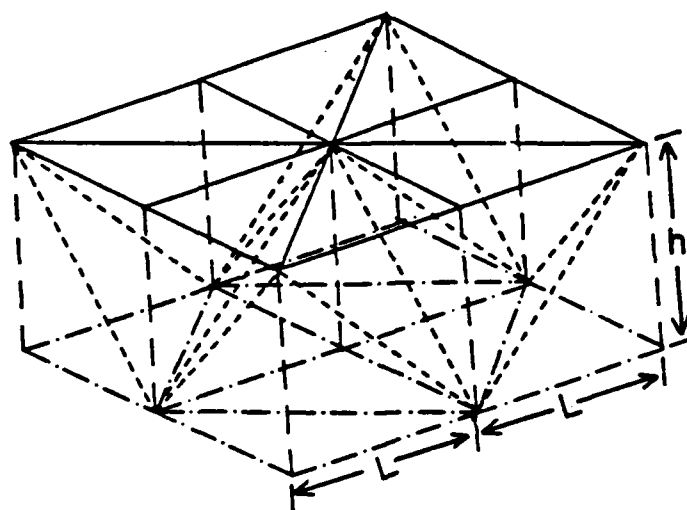
Figure 9. Space Lattice Structure Unit Cell.

vertical members connecting the two surfaces ($A_v$), and the diagonal members connecting the two surfaces ($A_d$). The remaining two parameters are the thickness or height (h) and half-width (L) of the unit cell. For simplicity, it is assumed in this study that all members are of circular hollow cross sections with outer diameter ($d_o$) and inner diameter ($d_i$). The ratio between the two diameters ($d_o/d_i$) is defined as a. The plate-like lattice structure is assumed to be free along all four edges. The control system configuration, shown as a midplane in Fig. 10, consists of a set of four pairs of torque actuators (A) about the x and y axes respectively located along the diagonals of the plate-like structure at a distance of 21.3 meters from each corner. The eight actuators are driven by a feedback control system using eight sensors (M) measuring the angular motion of the structure. These angular sensors are located in pairs at the four corners of the structure. Five pairs of disturbances (D) are used: four pairs are at the same location as the actuators and one pair is at a distance of 21.3 meters from the center of the structure along a diagonal.

## Cross Sectional Area Variation

The first parametric variation performed in this study is optimizing the cross sectional areas ($A_1$, $A_2$, $A_v$ and $A_d$) for fixed lengths (L and h). Examining the strain energy terms calculated for the equivalent continuum formulation (see Table 2 of Ref. 7), it is apparent that the bending stiffnesses depend on the sum of $A_1$ and $A_2$ and the transverse shear stiffness depends on $A_d$. The natural frequencies and mode shapes for small amplitude transverse vibration of the lattice are virtually independent of the in-plane stiffness
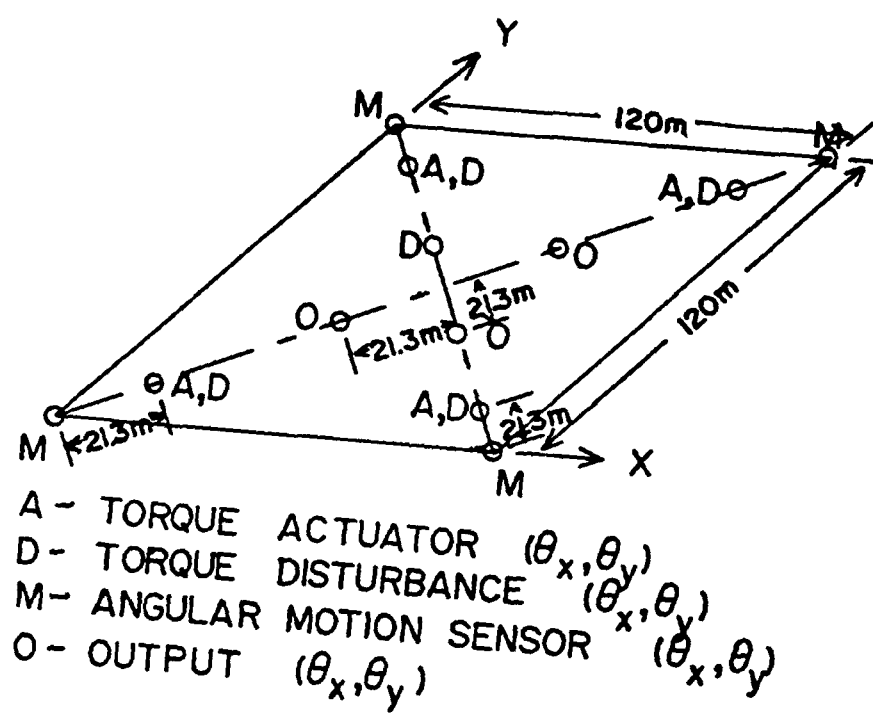
A - TORQUE ACTUATOR $(\theta_x, \theta_y)$
D - TORQUE DISTURBANCE $(\theta_x, \theta_y)$
M - ANGULAR MOTION SENSOR $(\theta_x, \theta_y)$
O - OUTPUT $(\theta_x, \theta_y)$

Figure 10. Control System Configuration.

which depends on the difference between $A_1$ and $A_2$ (see Table 2 of Ref. 7). Therefore, the natural frequencies and mode shapes for transverse vibration of the lattice are independent of the relative magnitude of $A_1$ and $A_2$. For simplicity of this study, the cross sectional areas $(A_s)$ of all the members in the upper and lower surfaces is assumed to be the same.

$$A_s = A_1 = A_2 \tag{III.1}$$

The cross sectional area $A_v$ is held constant at its original value. The total mass of the structure, which is held constant, is given by:

$$M = \frac{2\rho\, AREA}{L} \left[ \left(1 + \frac{1}{\sqrt{2}}\right)(A_1 + A_2) + \frac{1}{2}\frac{h}{L}A_v + \frac{d}{L}A_d \right] \tag{III.2}$$

where $\rho$ is the mass density of the structural members and $d = \sqrt{h^2 + L^2}$. Substituting the assumed parameter values into Eq. (III.2) yields the following relation between $A_s$ and $A_d$.

$$A_s = (69.167 - 4.167 \times 10^5 A_d) \times 10^{-6} m^2 \tag{III.3}$$

The members of the lattice structure are extremely slender. Before examining the effect of varying $A_s$ and $A_d$ on the natural frequencies, mode shapes, and performance, their effect on the Euler buckling load capacity of each member of the lattice is examined and shown in Fig. 11. Since $A_2$ is related to $A_d$ by Eq. (III.3), only $A_d$ is used in presenting results. The buckling load of each tubular member is nondimensionalized by dividing its value by the buckling load of the initial lower surface members
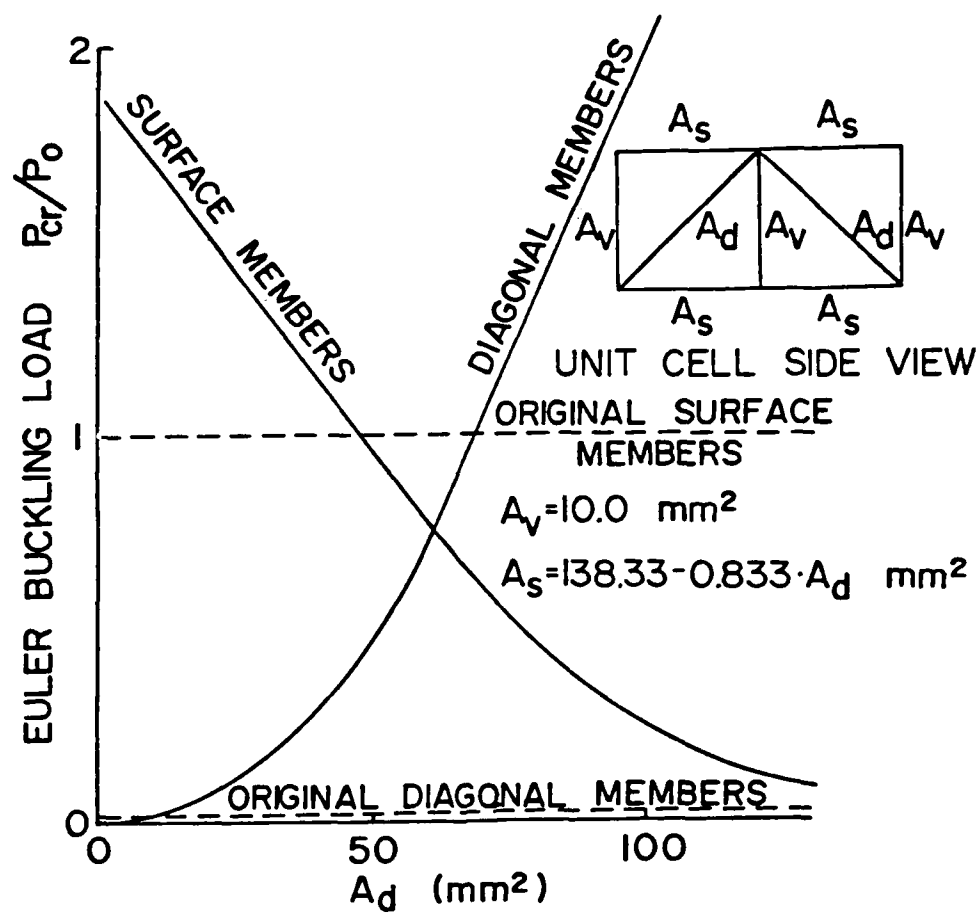
Figure 11. Allowable Buckling Load vs. Diagonal
Member Area.

$$P_0 = \frac{\pi E I_0}{L} \tag{III.4}$$

where

$$E = 71.7 \times 10;$$

$$I_0 = \frac{\pi(a^4-1)d_1^4}{b4} ; \quad \text{and}$$

$$d_0 = a d_i \quad .$$

Figure 12 shows that as $A_d$ is varied to either extreme, $A_d$ or the inversely related $A_s$ will become very small causing the members to have unacceptably low values of the Euler buckling load. For reference, the Euler buckling loads of the surface and diagonal members in the initial configuration are shown in Fig. 11 as dashed lines. Figure 12 shows the effect of the cross section area $A_d$ (and the inversely related $A_s$) on the natural frequencies of various modes. It is noted that modes 4,5 and modes 7,8 are double modes. It is interesting to note that all of the present natural frequencies for the ten lowest modes approach maxima when $A_d$ is between 30 and 50 $mm^2$. Apparently, the trends of these curves result from the compensating effects of three factors: the bending stiffness, the transverse shear stiffness, and the rotatory inertia. When $A_d$ decreases (or $A_s$ increases) both the bending stiffness and the rotatory inertia increase, whereas the transverse shear stiffness decreases. Figure 13 shows the effect of $A_d$ on the modal cost for each mode. As the $A_d$ value decreases, the modal cost of the first mode becomes increasingly dominant, whereas the modal cost curves for
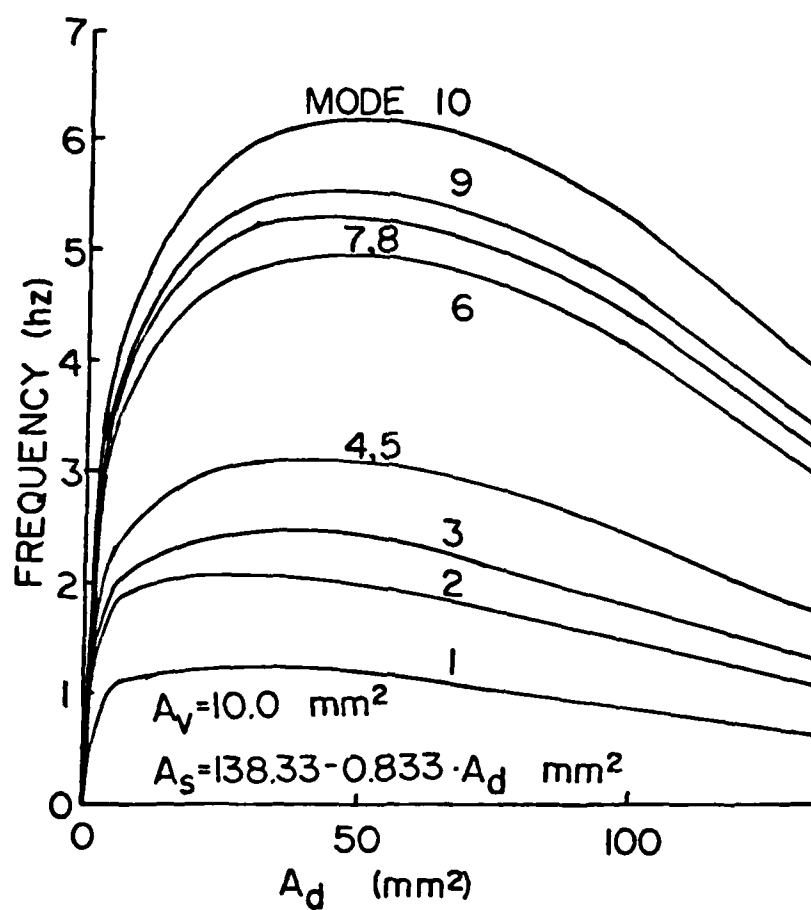
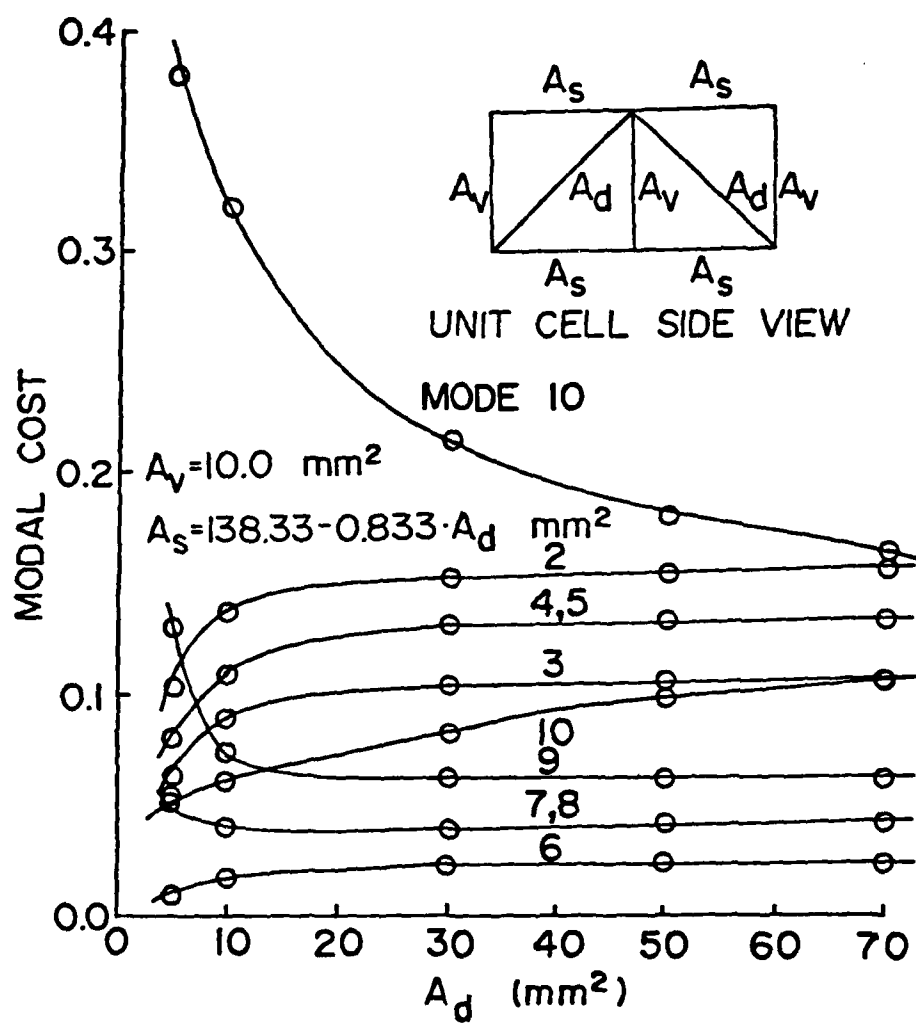Figure 12. Natural Frequency vs. Diagonal
Member Area.

Figure 13. Modal Cost vs. Diagonal Member Area.

several other modes cross each other. Such crossings indicate that different modes are retained at different $A_d$ values in the reduced order feedback control system design models.

For each set of parameter values, a series of reduced order controllers are designed using the LQG method. The system performance is evaluated using the full evalation model driven by the reduced order controller. A typical performance curve (Fig. 14) relating regulation cost ($V_y$) to control energy ($V_u$) is generated by varying $\rho$ in Eq. (II.27). The performance curves for all of the cases studied are very similar and are contained in Appendix B. Figure 15 shows the regulation cost ($V_y$) versus $A_d$ for various constant values of (solid curves) and for the minimum $V_y$ (circled points). These results are for a controller designed retaining two rigid body modes and three elastic modes in the reduced order controller design model. The results for other reduced order controllers were similar and are also in Appendix B. The minimum regulation cost is obtained for $A_d$ values between 10 and 30 mm$^2$. It is interesting to see that designs near the $A_d$ value of the original configuration perform better than designs near the peak frequency.

## Thickness or Height Variation

As a second parametric study, the effect of varying the depth of the structure (h) is examined. The variation is performed such that the buckling load in the slender truss members connecting the surfaces and the total mass of the structure is held constant. For tubular members with a constant ratio of outer and inner diameters, the moment of inertia (I) is proportional to the cross
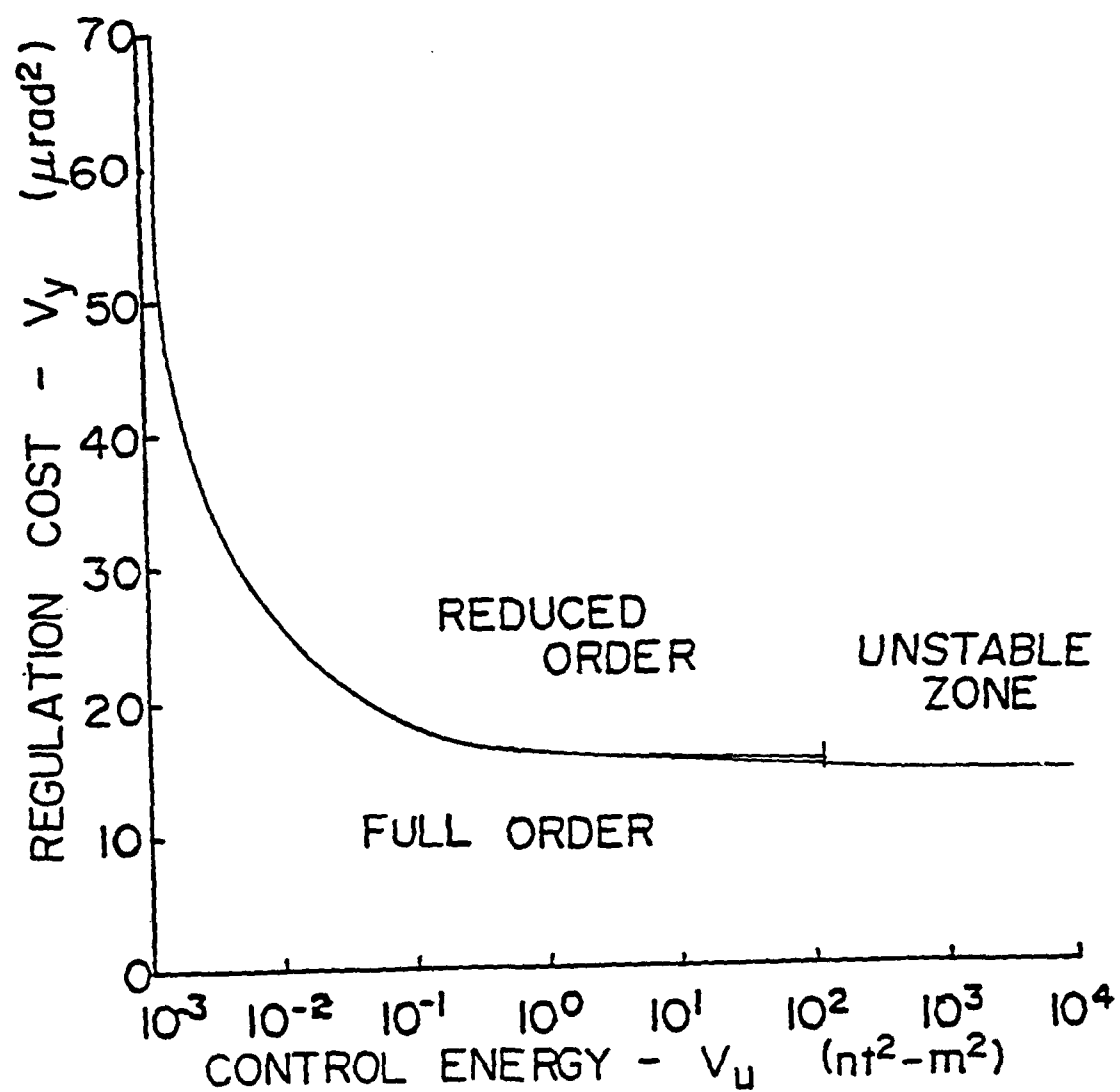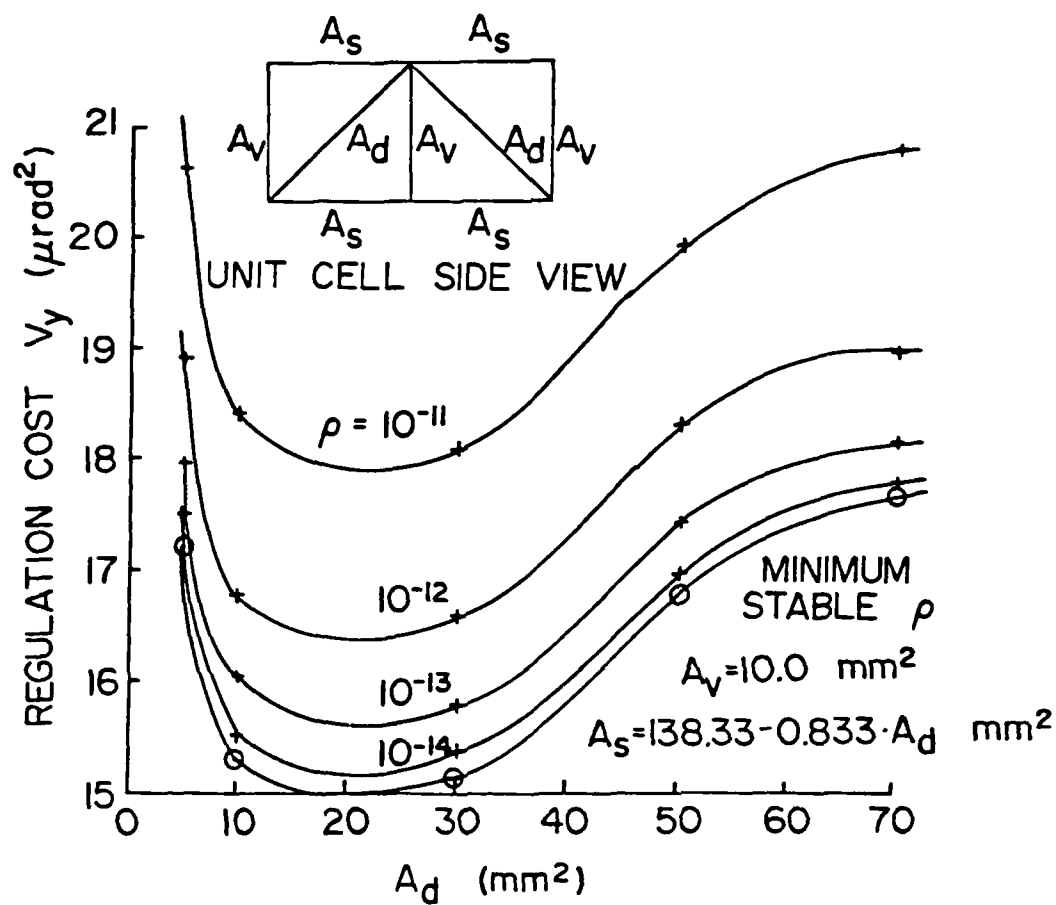
Figure 14. Typical Performance Plot

Figure 15. System Performance vs. Diagonal
Member Area.

sectional area ($A_v$). Thus the Euler buckling load in the vertical members is held constant by maintaining a constant ratio between the cross sectional area ($A_v$) and the height (h). For simplicity, the cross sectional area $A_d$ is assumed equal to $A_v$.

$$A_v = A_d = (\frac{1.33 \times 10^{-6} m}{7.5}) \; h \qquad (III.5)$$

Substituting the assumed parameter values into the mass Eq. (III.2) yields the relation between $A_s$ and h.

$$A_s = 141.2 \times 10^{-6} - \frac{h'}{2} + \frac{\sqrt{1+(h')^2}}{1 + \frac{1}{\sqrt{2}}} \qquad (III.6)$$

where

$$h' = h/7.5m.$$

As h increases, the nondimensionalized Euler buckling load in the surface members (Fig. 16) decreases, eventually indicating that these members are too slender. The natural frequencies of the first ten elastic modes of the structure are shown in Fig. 17. Note that the maximum frequency of the present ten modes occurs at thicknesses near 22.5 meters. The trend in these curves is caused by the compensating effects of $A_s$ and h on the bending stiffness, transverse shear stiffness, and rotatory inertia. As h increases, $A_s$ increases Eq. (III.6). Therefore, the increase in stiffness due to increasing h is offset by the reduction in stiffness due to decreasing $A_s$.
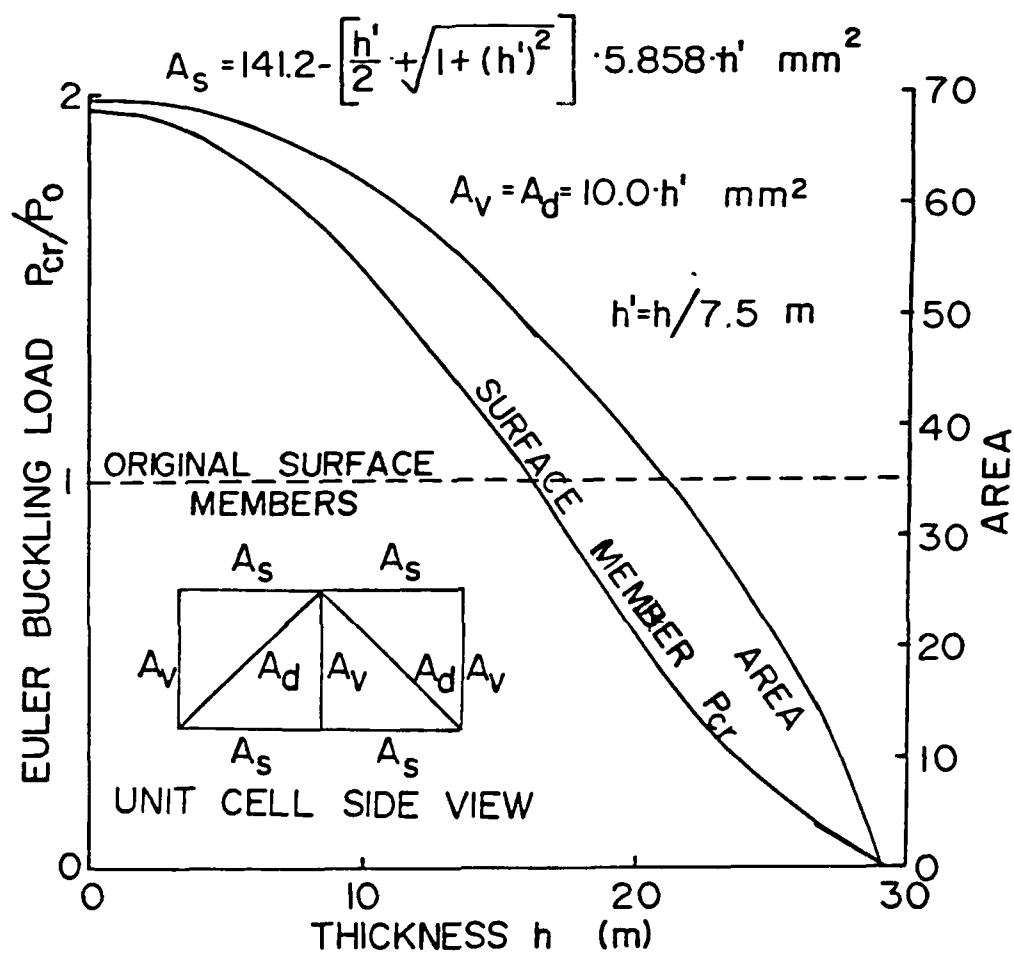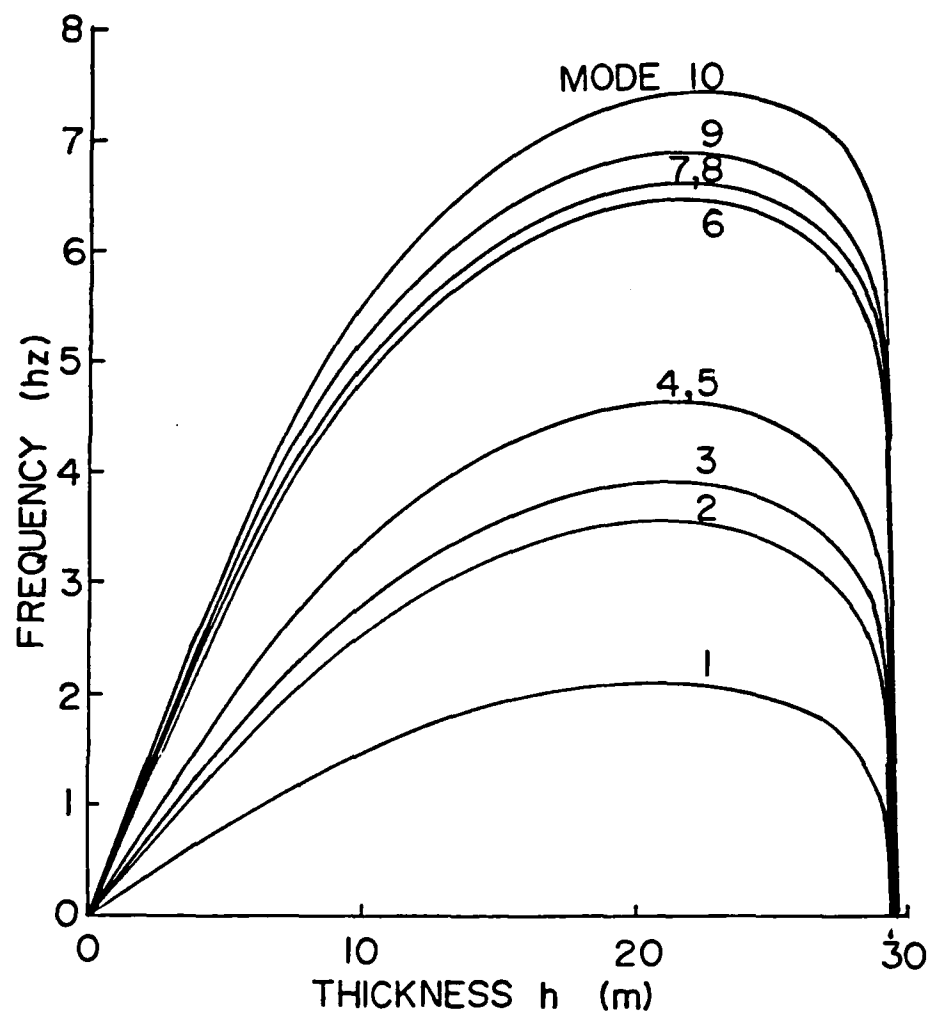
Figure 16. Allowable Buckling Load vs. Thickness.

Figure 17. Natural Frequency vs. Thickness.

The modal cost as a function of thickness (h) for the various modes is shown in Fig. 18. Since the modal cost curves show some crossings, different elastic modes will be retained in the reduced order models for different ranges of thickness (h). Figure 19 shows the regulation cost $(V_y)$ versus thickness for various constant values of $\rho$ (solid curves) and for the minimum $V_y$ value obtainable (circled points). The reduced order controllers for thicknesses less than 15.0 meters at $\rho = 1.0 \times 10^{-15}$ were unstable. The performance results are for LQG controllers based on two rigid body modes and three elastic modes. Similar results were obtained for reduced order controllers of other orders (see Appendix B). It is interesting to point out that for this example the optimal performance always occurs when the thickness (h) is near 7.5 meters, whereas a local maxima occurs when h is near 15 meters.

A procedure has been demonstrated to utilize equivalent continuum finite element modelling methods to efficiently examine the effects of parametric variation of the cross sections of plate-like space lattice structures. Using a specific space lattice structural configuration, two sets of parameter variations were performed. In the first case, the length of all the members as well as the mass of the structure were held constant. This caused the area of the surface members to be a function of the area of the internal diagonal members. The second case involved the variation in the thickness of the space lattice structure. Again, the length and total mass of the structure were held constant. The allowable buckling load of the slender internal members was also held constant. Thus the
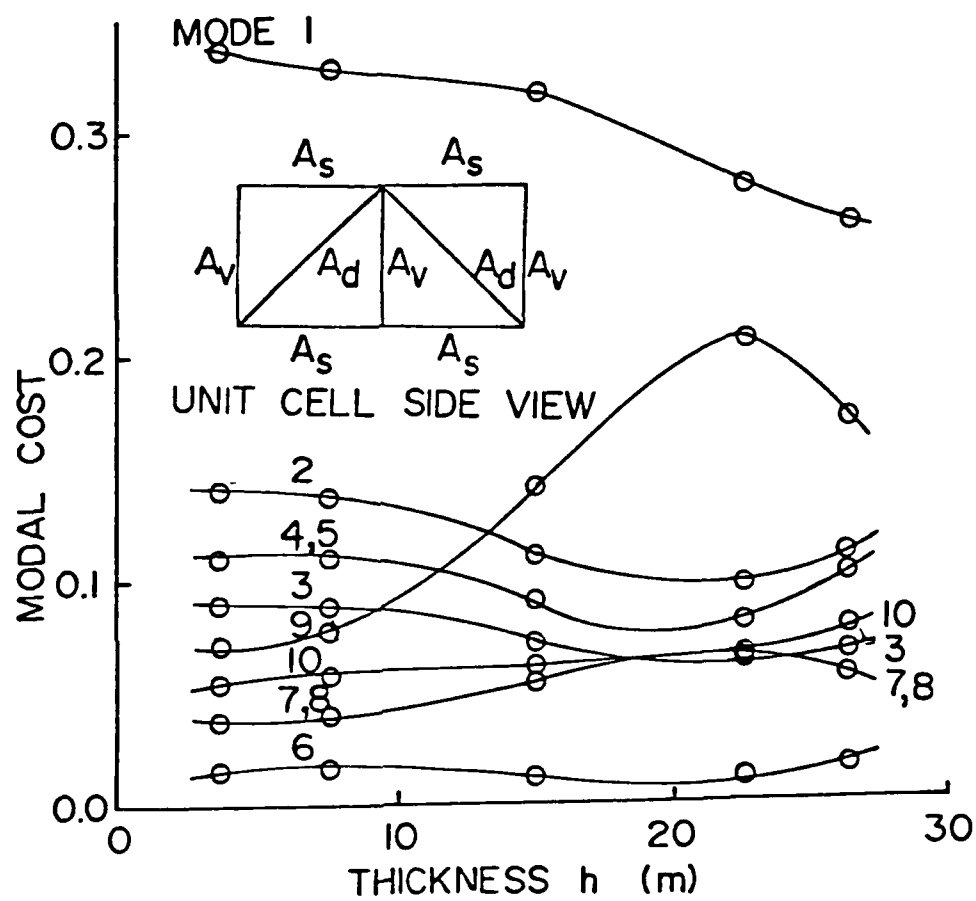
Figure 18. Modal Cost vs. Thickness.

$$\dot{A}_s = 141.2 - \left[\frac{h'}{2} + \sqrt{1 + (h')^2}\right] \cdot 5.858 \cdot h' \ \ mm^2$$

$$A_v = A_d = 10.0 \cdot h' \ \ mm^2 \qquad h' = h/7.5 \ m$$
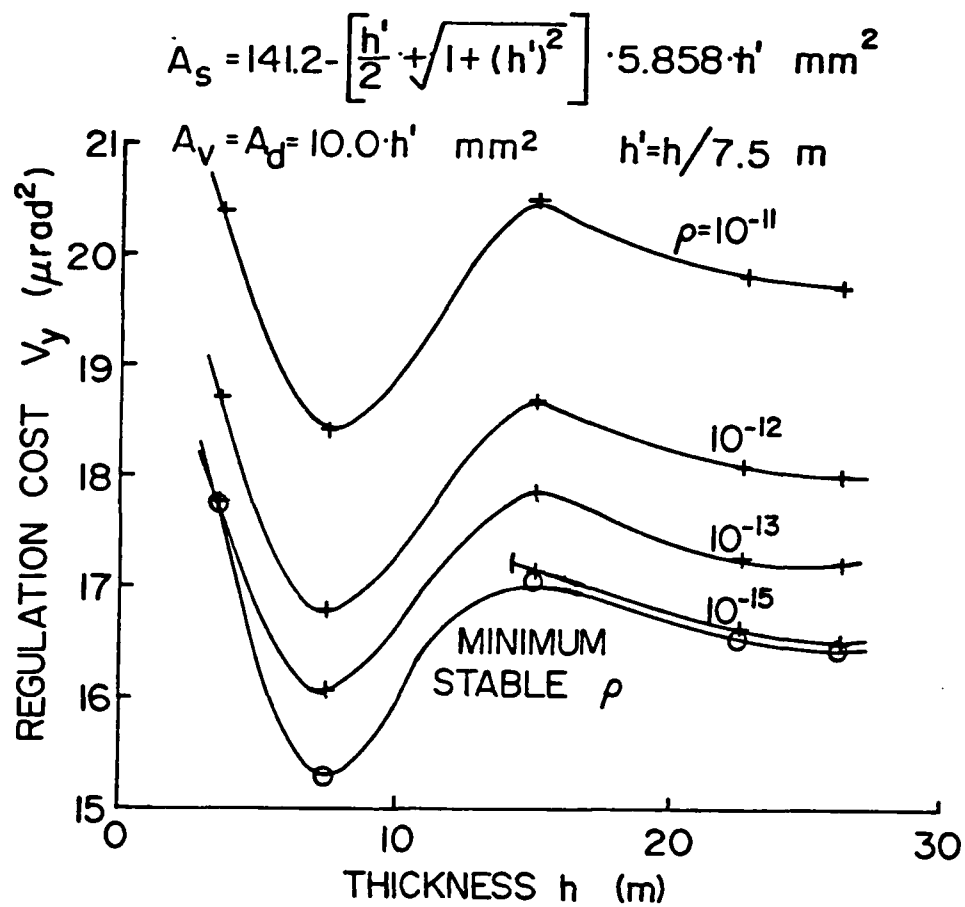
Figure 19. System Performance vs. Thickness.

cross sectional area of the surface and internal members was determined to be a function of the thickness. For both cases, maxima were obtained in the natural frequencies and optimal performance values of the design parameter were calculated. Modelling the structure using the finite element continuum model is seen to allow more flexibility in treating geometry, boundary conditions, attachments, and other structural complexities.

## CHAPTER IV - EQUIVALENT MODELLING OF
## FRAME STUCTURES WITH RIGID JOINTS

In this chapter a micropolar plate continuum model of plate-like space lattices whose frame members are connected with rigid joints is derived. The resulting continuum model is used to derive an equivalent plate finite element including micropolar rotations and transverse shear deformations as nodal d.o.f.'s in addition to displacements and displacement derivatives.[19]

A hexahedral space lattice structure with rigidly connected frame members is used as a demonstration problem. Several sets of frame member cross sectional properties are used. The exemplary plate-like space lattice structure is assumed as rectangular in shape with rigid joints and with four repeating cells along each edge. The natural frequencies and mode shapes of this structure with all edges free are calculated with and without the micropolar strains and rotations using the micropolar plate finite element. The natural frequencies and mode shapes are also calculated using a detailed finite element model (with every structural member modelled by a beam-column element) of the plate-like space lattice structure. The natural frequencies and mode shapes obtained using the micropolar theory are shown to be in good agreement with those obtained using the detailed finite element modelling, for the present example. The

natural frequencies and mode shapes calculated neglecting the micro-
polar terms are found to differ substantially from those obtained
by the detailed finite element model. A static analysis is also
performed for a rectangular plate-like space lattice structure with
rigid joints and with eight repeating cells along each edge. The
plate structure is simply supported at four corners and loaded at
the center by a transverse concentrated load. The static deflections
of the structure are calculated using the same three types of
modellings. Again, the static deflections obtained using the micro-
polar plate finite element model are in good agreement with those
from the detailed finite element model, while neglecting the micropolar
terms causes substantial discrepancies.

## Equivalent Continuum Representation

The repetitive nature of many large space lattice structures
allows them to be modelled as an equivalent continuum. The smallest
fundamental building block of such a structure is called a unit cell.
The strain energy expression of the unit cell is obtained using a
finite element model with each frame member modelled with a one
dimensional beam-column element containing both axial and flexural
rigidity.

$$U_{cell} = \frac{1}{2} \{q\}^T [K_{cell}]\{q\} \tag{IV.1}$$

where

$U_{cell}$ is the strain energy of the unit cell;

$$\{q\}^T = (\{q_1\}^T, \{q_2\}^T, \ldots \{q_n\}^T);$$

$$\{q_i\}^T = (u_i, v_i, w_i, \beta_{x_i}, \beta_{y_i}, \beta_{z_i});$$

$(u_i, v_i, w_i)$ are the translations in the $(x,y,z)$ directions at node i;

$(\beta_{x_i}, \beta_{y_i}, \beta_{z_i})$ are the rotations about the $(x,y,z)$ axes at node i;

$[K_{cell}]$ is the stiffness matrix of the unit cell; and

n is the number of joints in the unit cell.

In this study, the stiffness matrix was computed using the NASA Structural Analysis (NASTRAN) code, with each frame member modelled as a CBAR type element.[14]

The derivation which follows is equally valid for unit cells containing other structural elements such as plates and membranes. The translation and micro-rotations in the unit cell are assumed to vary linearly through the thickness (h) of the plate-like structure. The orientations of the various translations and rotations are expanded as a first order Taylor's series in the z direction yielding ten displacement components at the midplane (see Fig. 20).

$$u_i = u(x_i, y_i) + z_i \phi_x(x_i, y_i)$$

$$v_i = v(x_i, y_i) + z_i \phi_y(x_i, y_i)$$
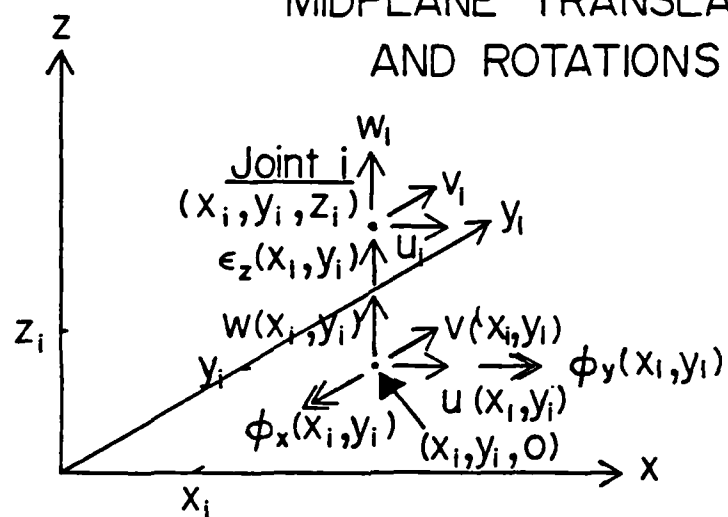
Figure 20. Orientations of Translation, Rotation, and Microrotation.

$$w_i = w(x_i, y_i) + z_i \, \epsilon_z(x_i, y_i)$$

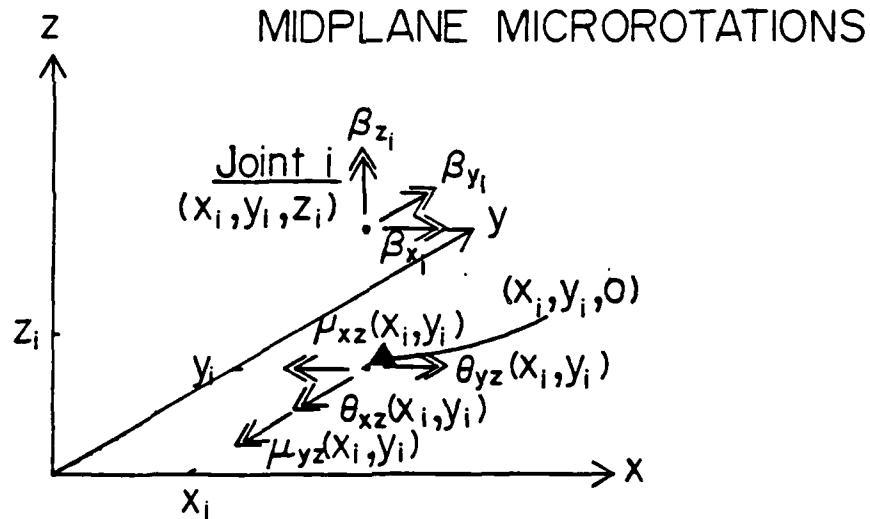$$\beta_{yi} = \theta_x(x_i, y_i) + z_i \, \mu_{xz}(x_i, y_i) \qquad \text{(IV.2)}$$

$$\beta_{xi} = \theta_y(x_i, y_i) + z_i \, \mu_{yz}(x_i, y_i)$$

where $(u, v, w)$ are the translations in the $(x, y, z)$ directions; $(\phi_x, \phi_y)$ are the rotations about the $(-y, x)$ axes; $(\theta_x, \theta_y)$ are the microrotations about the $(-y, x)$ axes; $\epsilon_z = \frac{dw}{dz}$ ; $\mu_{xz} = d\theta_x/dz$; and $\mu_{yz} = d\theta_y/dz$ all at the midplane of the plate continuum. The rotation $(\beta_{z_i})$ about the axis normal to the plate is ignored. It is noted that the positive sign convention of each rotation is based on the right hand rule. Each of these ten displacement components at the plate midplane is expanded as a second order Taylor's series in $x$ and $y$ about the center of the unit cell. For example, three are shown below.

$$u(x,y) = a_1 + x a_2 + y a_3 + \frac{x^2}{2} a_4 + \frac{xy}{2} a_5 + \frac{y^2}{2} a_6$$

$$v(x,y) = a_7 + x a_8 + y a_9 + \frac{x^2}{2} a_{10} + \frac{xy}{2} a_{11} + \frac{y^2}{2} a_{12} \qquad \text{(IV.3)}$$

$$\mu_{yz}(x,y) - a_{55} + x a_{56} + y a_{57} + \frac{x^2}{2} a_{58} + \frac{xy}{2} a_{59} + \frac{y^2}{2} a_{60}$$

Using Eq. (IV.2) and Eq. (IV.3) the nodal displacement vector $\{q\}$ can be expressed in terms of the displacement Taylor's series coefficient vector $\{a\}$.

$$\{q\}_{6n \times 1} = [T] \{a\}_{60 \times 1} \qquad \text{(IV.4)}$$

where

$$[T] = \begin{bmatrix} T_1 \\ T_2 \\ \vdots \\ T_n \end{bmatrix} \quad ; \quad [T_i] = [[S] \quad z_i[S]]$$

$$[S] = \begin{bmatrix} s_i & 0 & 0 & 0 & 0 \\ 0 & s_i & 0 & 0 & 0 \\ 0 & 0 & s_i & 0 & 0 \\ 0 & 0 & 0 & 0 & s_i \\ 0 & 0 & 0 & -s_i & 0 \\ 0 & 0 & 0 & 0 & 0 \end{bmatrix} \tag{IV.5a}$$

where

$$[s_i] = [1 \quad x_i \quad y_i \quad \frac{x_i^2}{2} \quad \frac{x_i y_i}{2} \quad \frac{y_i^2}{2}]$$

Substituting Eq. (IV.4) into Eq. (IV.1) yields the strain energy expression of the unit cell in terms of the displacement Taylor's series coefficient vector.

$$U_{cell} = \frac{1}{2} \{a\}^T [T]^T [K_{cell}][T]\{a\} \tag{IV.5b}$$

The fundamental assumption of micropolar continuum theory is that the local rotation at a point (microrotation) is independent of the translations.[20] The strain components of the micropolar continuum are defined in terms of the ten midplane displacement components.

classical plate strains:

$$\epsilon_{xx} = \frac{du}{dx} \;;\quad \epsilon_{yy} = \frac{dv}{dy} \;;\quad 2\epsilon_{xy} = \frac{du}{dy} + \frac{dv}{dx} \;;$$

$$\kappa_{xx} = \frac{d\phi_x}{dx} \;;\quad \kappa_{yy} = \frac{d\phi_y}{dy} \;;\quad 2\kappa_{xy} = \frac{d\phi_x}{dy} + \frac{d\phi_y}{dx} \;;$$

transverse shear strains:

$$2\epsilon_{xz} = \frac{dw}{dx} + \phi_x \;;\quad 2\epsilon_{yz} = \frac{dw}{dy} + \phi_y : \tag{IV.6}$$

micropolar strains:

$$r_x = \frac{1}{2}\left(\frac{dw}{dx} - \phi_x\right) - \theta_x; \quad r_y = \frac{1}{2}\left(\frac{dw}{dy} - \phi_y\right) - \theta_y;$$

$$\mu_{xx} = \frac{d\theta_x}{dx} \;;\quad \mu_{yy} = \frac{d\theta_y}{dy} \;;\quad \mu_{xy} = \frac{1}{2}\left(\frac{d\theta_x}{dy} + \frac{d\theta_y}{dx}\right)$$

These strains are expanded in a strain Taylor's series in x and y about the center of the unit cell.

$$\epsilon_{xx} = \epsilon_x^0 + \epsilon_{x,x}^0 \; x + \epsilon_{x,y}^0 \; y$$

$$\epsilon_{yy} = \epsilon_y^0 + \epsilon_{y,y}^0 \; y + \epsilon_{y,y}^0 \; y$$

$$\epsilon_{xy} = \epsilon_{xy}^0 + \epsilon_{xy,x}^0 \; x + \epsilon_{xy,y}^0 \; y$$

$$\kappa_{xx} = \kappa_{xy}^0 + \kappa_{xy,x}^0 \; x + \kappa_{xy,y}^0 \; y$$

$$\kappa_{yy} = \kappa_{yy}^0 + \kappa_{yy,x}^0 \; x + \kappa_{yy,y}^0 \; y$$

$$\kappa_{xy} = \kappa_{xy}^{0} + \kappa_{xy,x}^{0} \, x + \kappa_{xy,y}^{0} \, y$$

$$\varepsilon_{xz} = \varepsilon_{xz}^{0} + \varepsilon_{xz,x}^{0} \, x + \varepsilon_{xz,y}^{0} \, y + \varepsilon_{xz,x2}^{0} \, \frac{x^2}{2} + \varepsilon_{xz,xy}^{0} \, xy + \varepsilon_{xz,y2}^{0} \, \frac{y^2}{2}$$

$$\varepsilon_{yz} = \varepsilon_{yz}^{0} + \varepsilon_{yz,x}^{0} \, x + \varepsilon_{yz,y}^{0} \, y + \varepsilon_{yz,x2}^{0} \, \frac{x^2}{2} + \varepsilon_{yz,xy}^{0} \, \frac{xy}{2} + \varepsilon_{yz,y2}^{0} \, \frac{y^2}{2}$$

$$r_x = r_x^{0}$$

$$r_y = r_y^{0} \qquad\qquad (IV.7)$$

$$\mu_{xx} = \mu_{xx}^{0} + \mu_{xx,x}^{0} \, x + \mu_{xx,y}^{0} \, y$$

$$\mu_{yy} = \mu_{yy}^{0} + \mu_{yy,x}^{0} \, x + \mu_{yy,y}^{0} \, y$$

$$\mu_{xy} = \mu_{xy}^{0} + \mu_{xy,x}^{0} \, x + \mu_{xy,y}^{0} \, y$$

$$\varepsilon_{z} = \varepsilon_{z}^{0} + \varepsilon_{z,x}^{0} \, x + \varepsilon_{z,y}^{0} \, y + \varepsilon_{z,x2}^{0} \, \frac{x^2}{2} + \varepsilon_{z,xy}^{0} \, \frac{xy}{2} + \varepsilon_{z,y2}^{0} \, \frac{y^2}{2}$$

$$\mu_{xz} = \mu_{xz}^{0} + \mu_{xz,x}^{0} \, x + \mu_{xz,y}^{0} \, y + \mu_{xz,x2}^{0} \, \frac{x^2}{2} + \mu_{xz,xy}^{0} \, \frac{xy}{2} + \mu_{xz,y2}^{0} \, \frac{y^2}{2}$$

From Eq. (IV.3), EQ. (IV.6), and Eq. (IV.7) we can generate a relationship between the strain Taylor's series vector $\{\varepsilon\}$ and the displacement Taylor's series vector $\{a\}$.

$$\{\varepsilon\}_{53\times1} = [A] \, \{a\}_{60\times1} \qquad\qquad (IV.8)$$

where

$$\varepsilon_1 \equiv \varepsilon_{xx}^{0} = u_{,x}^{0} \equiv a_2; \quad \varepsilon_2 \equiv \varepsilon_{yy}^{0} = v_{,y}^{0} \equiv a_9;$$

$$\varepsilon_3 \equiv \varepsilon_{xy} = \frac{1}{2}(u^0_{,y} + v^0_{,x}) \equiv \frac{a_3 + a_8}{2} \; ; \quad \varepsilon_4 \equiv \kappa^0_{xx} = \phi^0_{x,x} \equiv a_{32};$$

$$\varepsilon_5 \equiv \kappa^0_{yy} = \phi^0_{y,y} \equiv a_{39}; \; \varepsilon_6 \equiv \kappa^0_{xy} = \frac{1}{2}(\phi^0_{x,y} + \phi^0_{y,x}) = \frac{a_{33} + a_{38}}{2}$$

$$\varepsilon_7 \equiv \varepsilon^0_{xx,x} = u^0_{,x2} \equiv a_4; \quad \varepsilon_8 \equiv \varepsilon^0_{xx,y} = u^0_{,xy} \equiv a_5; \; \varepsilon_9 \equiv \varepsilon^0_{yy,x}$$

$$= v^0_{,xy} \equiv a_9;$$

$$\varepsilon_{10} \equiv \varepsilon^0_{yy,y} = v^0_{,y2} \equiv a_{12}; \; \varepsilon_{11} \equiv \varepsilon^0_{xy,x} = \frac{1}{2}(u^0_{,xy}) + v^0_{,x2}) \equiv a_5 + a_{10};$$

$$\varepsilon_{12} \equiv \varepsilon^0_{xy,y} = \frac{1}{2}(u^0_{,y2} + v^0_{,xy}) \equiv a_6 + a_{11}; \; \varepsilon_{13} \equiv \kappa^0_{xx,x} = \phi^0_{x,x2} \equiv a_{34};$$

$$\varepsilon_{14} \equiv \kappa^0_{xx,y} = \phi^0_{x,xy} \equiv a_{35}; \; \varepsilon_{15} \equiv \kappa^0_{yy,x} = \phi^0_{y,xy} \equiv a_{41};$$

$$\varepsilon_{16} \equiv \kappa^0_{yy,y} = \phi^0_{y,y2} \equiv a_{42}; \; \varepsilon_{17} \equiv \kappa^0_{xy,x} = \frac{1}{2}(\phi^0_{x,xy} + \phi^0_{y,x2})$$

$$= \frac{a_{35} + a_{40}}{2};$$

$$\varepsilon_{18} \equiv \kappa^0_{xy,y} = \frac{1}{2}(\phi^0_{x,y2} + \phi^0_{y,xy}) \equiv \frac{a_{36} + a_{41}}{2};$$

$$\varepsilon_{19} \equiv \varepsilon^0_z = \varepsilon^0_z \equiv a_{43}; \; \varepsilon_{20} \equiv 2\varepsilon^0_{xz} = w^0_{,x} + \phi^0_x \equiv a_{14} + a_{31};$$

$$\varepsilon_{21} \equiv 2\varepsilon^0_{yz} = w^0_{,y} + \phi^0_y \equiv a_{15} + a_{37}; \; \varepsilon_{22} \equiv 2\varepsilon_{xz,x} = w^0_{,x2} + \phi^0_{x,x}$$

$$= a_{16} + a_{32};$$

$$\varepsilon_{23} \equiv 2\varepsilon_{xz,y} = w^o_{,xy} + \phi^o_{x,y} \equiv a_{17} + a_{33}; \quad \varepsilon_{24} \equiv 2\varepsilon_{yz,x} = w^o_{,xy}$$

$$+ \phi^o_{y,x} \equiv a_{17} + a_{38};$$

$$\varepsilon_{25} \equiv 2\varepsilon_{yz,y} = w^o_{,y2} + \phi^o_{y,y} \equiv a_{18} + a_{39}; \quad \varepsilon_{26} \equiv \varepsilon^o_{z,x} \equiv a_{44};$$

$$\varepsilon_{27} \equiv \varepsilon^o_{z,y} \equiv a_{45}$$

$$\varepsilon_{28} \equiv \varepsilon^o_{z,x2} \equiv a_{46}; \quad \varepsilon_{29} \equiv \varepsilon^o_{z,xy} \equiv a_{47}; \quad \varepsilon_{30} \equiv \varepsilon^o_{z,y2} \equiv a_{48}$$

$$\varepsilon_{31} \equiv r^o_x = \frac{1}{2}(w^o_{,x} - \phi^o_x) - \theta^o_x \equiv \frac{a_{14}}{2} - \frac{a_{31}}{2} - a_{19};$$

$$\varepsilon_{32} \equiv r^o_y = \frac{1}{2}(w^o_{,y} - \phi^o_y) - \theta^o_y \equiv \frac{a_{15}}{2} - \frac{a_{37}}{2} - a_9$$

$$\varepsilon_{33} \equiv \mu^o_{xz} \equiv a_{49}; \quad \varepsilon_{34} \equiv \mu^o_{xz,x} \equiv a_{50}; \quad \varepsilon_{35} \equiv \mu_{xz,y} \equiv a_{51};$$

$$\varepsilon_{36} \equiv \mu^o_{xz,x2} \equiv a_{52}; \quad \varepsilon_{37} \equiv \mu^o_{xz,xy} \equiv a_{53}; \quad \varepsilon_{38} \equiv \mu^o_{xz,y2} \equiv a_{54};$$

$$\varepsilon_{39} \equiv \mu^o_{yz} \equiv a_{55}; \quad \varepsilon_{40} \equiv \mu^o_{yz,x} \equiv a_{56}; \quad \varepsilon_{41} \equiv \mu^o_{yz,y} \equiv a_{57};$$

$$\varepsilon_{42} \equiv \mu^o_{yz,x2} \equiv a_{58}; \quad \varepsilon_{43} \equiv \mu^o_{yz,xy} \equiv a_{59}; \quad \varepsilon_{44} \equiv \mu^o_{yz,y2} \equiv a_{60};$$

$$\varepsilon_{45} \equiv \mu^o_{yy} = \theta^o_{x,x} \equiv a_{20}; \quad \varepsilon_{46} \equiv \mu^o_{xx,x} = \theta^o_{x,x2} = a_{22}; \quad \varepsilon_{47} \equiv \mu^o_{xx,y}$$

$$= \theta^o_{x,xy} \equiv a_{23};$$

$$\epsilon_{48} \equiv \mu^0_{yy} = \theta^0_{y,y} = a_{27}; \quad \epsilon_{49} \equiv \mu^0_{yy,x} = \theta^0_{y,xy} \equiv a_{29}; \quad \epsilon_{50} \equiv \mu^0_{yy,y}$$

$$= \theta^0_{y,y2} \equiv a_{30}; \quad \epsilon_{51} \equiv \mu^0_{xy} = \frac{1}{2}(\theta^0_{x,y} + \theta^0_{y,x}) \equiv \frac{a_{21}+a_{51}}{2} ,$$

$$\epsilon_{52} \equiv \mu^0_{xy,x} = \frac{1}{2}(\theta^0_{x,xy} + \theta^0_{y,x2}) \equiv \frac{a_{23}+a_{28}}{2} ; \quad \text{and}$$

$$\epsilon_{53} \equiv \mu_{xy,y}0 = \theta^0_{x,y2} + \theta^0_{y,yxy}) = \frac{a_{24}+a_{29}}{2}$$

The rigid body motions of the structure {b} can also be expressed in terms of the displacement Taylor's series vector {a}.

$$\{b\} = [A_b]\{a\} \tag{IV.9}$$

where

$$\{b\}^T = (u^0, v^0, w^0, \phi^0_x, \phi^0_y, \theta, \Omega) ;$$

$$\theta = \frac{1}{2}(u^0_{,y} - v^0_{,x}); \quad \text{and} \quad \Omega = \frac{1}{2}(\theta_{x,y} - \theta_{y,x}) .$$

Equation (IV.8) is merged with (IV.9)

$$\left\{ \begin{array}{c} \epsilon \\ b \end{array} \right\} = \left[ \begin{array}{c} A_\epsilon \\ A_b \end{array} \right] \{a\} \tag{IV.10}$$

This equation is inverted.

$$\{a\} = [B_\epsilon \quad B_b] \left\{ \begin{array}{c} \epsilon \\ b \end{array} \right\} \tag{IV.11}$$

where

$$B_{b1,1} = 1.0; \quad B_{b3,6} = 1.0; \quad B_{b7,2} = 1.0; \quad B_{b8,6} = -1.0; \quad B_{b13,3} = 1.0;$$

$$B_{b14,4} = -1.0; \quad B_{b15,5} = -1.0; \quad B_{b21,7} = 0.0; \quad B_{b25,5} = -1.0;$$

$$B_{b26,7} = -1.0; \quad B_{b31,4} = B_{b31,4} = 1.0; \quad B_{b37,4} = 1.0; \quad B_{\varepsilon2,1} = 1.0;$$

$$B_{\varepsilon3,3} = 1.0; \quad B_{\varepsilon4,7} = 1.0; \quad B_{\varepsilon5,8} = 1.0; \quad B_{\varepsilon6,9} = -1.0; \quad B_{\varepsilon6,12} = 2.0;$$

$$B_{\varepsilon8,3} = 1.0; \quad B_{\varepsilon9,2} = 2.0; \quad B_{\varepsilon10,8} = -1.0; \quad B_{\varepsilon10,11} = 2.0;$$

$$B_{\varepsilon11,9} = 1.0; \quad B_{\varepsilon12,10} = 1.0; \quad B_{\varepsilon14,20} = 1.0; \quad B_{\varepsilon15,21} = 1.0;$$

$$B_{\varepsilon16,22} = 1.0; \quad B_{\varepsilon17,6} = 1.0; \quad B_{\varepsilon17,24} = 0.5; \quad B_{\varepsilon17,23} = 0.5;$$

$$B_{\varepsilon18,25} = -1.0; \quad B_{\varepsilon19,20} = 0.5; \quad B_{\varepsilon19,31} = -1.0; \quad B_{\varepsilon20,45} = 1.0;$$

$$B_{\varepsilon21,51} = 1.0; \quad B_{\varepsilon22,46} = 1.0; \quad B_{\varepsilon23,47} = 1.0; \quad B_{\varepsilon24,49} = 1.0;$$

$$B_{\varepsilon24,53} = 1.0; \quad B_{\varepsilon25,21} = 0.5; \quad B_{\varepsilon25,32} = -1.0; \quad B_{\varepsilon26,51} = 1.0;$$

$$B_{\varepsilon27,48} = 1.0; \quad B_{\varepsilon27,47} = -1.0; \quad B_{\varepsilon27,52} = 2.0; \quad B_{\varepsilon29,49} = 1.0;$$

$$B_{\varepsilon30,50} = 1.0; \quad B_{\varepsilon32,4} = 1.0; \quad B_{\varepsilon36,6} = 1.0; \quad B_{\varepsilon36,23} = 0.5;$$

$$B_{\varepsilon36,24} = -0.5; \quad B_{\varepsilon34,13} = 1.0; \quad B_{\varepsilon35,14} = 1.0; \quad B_{\varepsilon36,15} = -1.0;$$

$$B_{\varepsilon36,18} = 2.0; \quad B_{\varepsilon38,6} = 1.0; \quad B_{\varepsilon39,5} = 1.0; \quad B_{\varepsilon40,14} = -1.0;$$

$$B_{\varepsilon 40,17} = 2.0; \quad B_{\varepsilon 41,15} = 1.0; \quad B_{\varepsilon 42,16} = 1.0; \quad B_{\varepsilon 47,29} = 1.0;$$

$$B_{\varepsilon 48,30} = 1.0; \quad B_{\varepsilon 49,33} = 1.0; \quad B_{\varepsilon 50,34} = 1.0; \quad B_{\varepsilon 51,35} = 1.0;$$

$$B_{\varepsilon 52,36} = 1.0; \quad B_{\varepsilon 53,37} = 1.0; \quad B_{\varepsilon 54,38} = 1.0; \quad B_{\varepsilon 55,39} = 1.0;$$

$$B_{\varepsilon 56,40} = 1.0; \quad B_{\varepsilon 57,41} = 1.0; \quad B_{\varepsilon 58,42} = 1.0; \quad B_{\varepsilon 59,43} = 1.0;$$

$$B_{\varepsilon 60,44} = 1.0; \quad \text{and all other terms of } B \text{ and } B_b \text{ are equal}$$

to zero.

Substituting Eq. (IV.11) into Eq. (IV.5) and taking advantage of the
fact that the strain energy is independent of rigid body motion of
the structures gives the expression for the strain energy of a unit
cell in terms of the strain Taylor's series coefficient vector $\{\varepsilon\}$.

$$U_{cell} = \frac{1}{2} \{\varepsilon\}^T [K] \{\varepsilon\} \tag{IV.12}$$

where

$$[K_\varepsilon] = [B_\varepsilon]^T [T]^T [K_{cell}] [T] [B_\varepsilon] \ .$$

Strain components in the plane connecting two unit cells must have
identical values to maintain compatability. This is satisfied by
taking the origin of the Taylor's series expansions at the center of
the unit cell and requiring that the expansions for these strain
components be even, insuring that these strains are identical on
opposite sides of the cell. Therefore, the odd derivatives of

these strain components are set to zero by removing the appropriate rows and columns from $[K_\epsilon]$.

$$\epsilon^0_{xzy,} = \epsilon^0_{yz,x} = \epsilon^0_{z,x} = \epsilon^0_{z,y} = \mu^0_{xx,y} = u^0_{yy,x} = 0 \qquad (IV.13)$$

The strain gradients are retained in the Taylor's series expansions to allow internal motion within the cell. There is no loading associated with these strain gradients and the partial derivative of the strain energy with respect to these terms should be zero.

$$\frac{\partial U_{cell}}{\partial \epsilon^0_{xx,x}} = \frac{\partial U_{cell}}{\partial \epsilon^0_{xx,y}} = \frac{\partial U_{cell}}{\partial \epsilon^0_{yy,x}} = \frac{\partial U_{cell}}{\partial \epsilon^0_{yy,y}} = \frac{\partial U_{cell}}{\partial \epsilon^0_{xy,x}} = \frac{\partial U_{cell}}{\partial \epsilon^0_{xy,y}} = 0$$

$$\frac{\partial U_{cell}}{\partial \kappa^0_{xx,x}} = \frac{\partial U_{cell}}{\partial \kappa^0_{xx,y}} = \frac{\partial U_{cell}}{\partial \kappa^0_{yy,x}} = \frac{\partial U_{cell}}{\partial \kappa^0_{yy,y}} = \frac{\partial U_{cell}}{\partial \kappa^0_{xy,x}} = \frac{\partial U_{cell}}{\partial \kappa^0_{xy,y}} = 0$$

$$\frac{\partial U_{cell}}{\partial \epsilon^0_{z}} = \frac{\partial U_{cell}}{\partial \epsilon^0_{xz,x}} = \frac{\partial U_{cell}}{\partial \epsilon^0_{yz,y}} = \frac{\partial U_{cell}}{\partial \epsilon^0_{z,x^2}} = \frac{\partial U_{cell}}{\partial \epsilon^0_{z,xy}} = \frac{\partial U_{cell}}{\partial \epsilon^0_{z,y^2}} = 0$$

$$\qquad\qquad (IV.14)$$

$$\frac{\partial U_{cell}}{\partial \mu^0_{xz}} = \frac{\partial U_{cell}}{\partial \mu^0_{xz,x}} = \frac{\partial U_{cell}}{\partial \mu^0_{xz,y}} = \frac{\partial U_{cell}}{\partial \mu^0_{xz,x^2}} = \frac{\partial U_{cell}}{\partial \mu^0_{xz,xy}} = \frac{\partial U_{cell}}{\partial \mu^0_{xz,y^2}} = 0$$

$$\frac{\partial U_{cell}}{\partial \mu_{yz}} = \frac{\partial U_{cell}}{\partial \mu_{yz,x}} = \frac{\partial U_{cell}}{\partial \mu_{yz,y}} = \frac{\partial U_{cell}}{\partial \mu_{yz,x^2}} = \frac{\partial U_{cell}}{\partial \mu_{yz,xy}} = \frac{\partial U_{cell}}{\partial \mu_{yz,y^2}} = 0$$

$$\frac{\partial U_{cell}}{\partial \mu^0_{xx,x}} = \frac{\partial U_{cell}}{\partial \mu^0_{yy,y}} = \frac{\partial U_{cell}}{\partial \mu^0_{xy,x}} = \frac{\partial U_{cell}}{\partial \mu^0_{xy,y}} = 0$$

Using Castigliano's Theorem, this is the same as requiring that the row of $[K_\epsilon]$ corresponding to the strain gradient times $\{\epsilon\}$ be equal

to zero. $[K_\epsilon]$ is partitioned so that all of the constrained terms in Eq. (IV.1) fall at the end of the vector $\{\epsilon\}$.

$$U_{cell} = \frac{1}{2} \begin{Bmatrix} \epsilon_r \\ \epsilon_0 \end{Bmatrix}^T \begin{bmatrix} K_{\epsilon_{rr}} & K_{\epsilon_r} \\ K_{\epsilon_{ro}} & K_{\epsilon_{0\theta}} \end{bmatrix} \begin{Bmatrix} \epsilon_r \\ \epsilon_0 \end{Bmatrix} \qquad (IV.15)$$

where $\{\epsilon_r\}^T = (\epsilon_{xx}^0, \ \epsilon_{yy}^0, \ \epsilon_{xy}^0, \ \kappa_{xx}^0, \ \kappa_{yy}^0, \ \kappa_{xy}^0, \ 2\epsilon_{xz}^0, \ 2\epsilon_{yz}^0, \ r_x^0, \ r_y^0, \ \mu_{xx}^0, \ \mu_{yy}^0$ $\mu_{xy}^0)$ are the strain terms which are constrained; and $\{\epsilon_0\}^T = (\epsilon_{xx,x}^0,$ $\epsilon_{xx,y}^0, \ \ldots, \ \mu_{xy,y}^0)$ are the strain terms constrained in Eq. (IV.14). The constraints, Eq. (IV.14) are then rewritten.

$$\{0\} = \begin{bmatrix} K_{\epsilon_{ro}}^T & K_{\epsilon_{00}} \end{bmatrix} \begin{Bmatrix} \epsilon_r \\ \epsilon_0 \end{Bmatrix} \qquad (IV.16)$$

This equation is rewritten as an expression for $\{\epsilon_0\}$ the constrained strain vector.

$$\{\epsilon_0\} = -[K_{\epsilon_{00}}]^{-1} \ [K_{\epsilon_{ro}}] \ \{\epsilon_r\} \qquad (IV.17)$$

Substituting Eq. (IV.17) into Eq. (IV.15) yields the strain energy expression in terms of the retained terms.

$$U_{cell} = \frac{1}{2} \{\epsilon_r\}^T [K_{eq}] \{\epsilon_r\} \qquad (IV.18)$$

where

$$[K_{eq}] = [K_{\epsilon_{rr}}] - [K_{\epsilon_{ro}}][K_{\epsilon_{00}}]^{-1}[K_{\epsilon_{ro}}]^T$$
$$13\times13$$

It is assumed that $[K_{eq}]$ divided by the area of the unit cell $(A_{cell})$ forms the constitutive matrix of the continuum at all points

$$U_{structure} = \frac{1}{2} \int_{\substack{Area\ of \\ the\ structure}} \{\epsilon_r\}^T \frac{[K_{eq}]}{A_{cell}} \{\epsilon_r\}\ dA \qquad (IV.19)$$

### Equivalent Finite Element Model

The 16 d.o.f. rectangular plate element[15] is modified to include in-plane, transverse shear, and micropolar rotational terms yielding a 40 d.o.f. element. The interpolation functions are assumed as linear except for the out-of-plane displacement which is assumed as a bicubic Hermite polynomial.

$$u^0 = c_1 + c_2 x + c_3 y + c_4 xy$$

$$v^0 = c_5 + c_6 x + c_7 y + c_8 xy$$

$$w^0 = c_9 + c_{10}x + c_{11}y + c_{12}x^2 + c_{13}xy + c_{14}y^2 + c_{15}x^3$$
$$+ c_{16}x^2 y + c_{17}xy^2 + c_{18}y^3 + c_{19}x^3 y + c_{20}x^2 y^2 + c_{21}xy^3$$
$$+ c_{22}x^3 y^2 + c_{23}x^2 y^3 + c_{24}x^3 y^3 \qquad (IV.20)$$

$$2\epsilon_{xz}^0 = c_{25} + c_{26}x + c_{27}y + c_{28}xy$$

$$2\epsilon_{yz}^0 = c_{29} + c_{30}x + c_{31}y + c_{32}xy$$

$$\theta_x^0 = c_{33} + c_{34}x + c_{35}y + c_{36}xy$$

$$\theta_y^0 = c_{37} + c_{38}x + c_{39}y + c_{40}xy$$

Using the strain definition, Eqs. (IV.6) and the interpolation functions (IV.20), the strain vector $\{\epsilon_r\}$ is related to the interpolation coefficient vector $\{c\}$.

$$\{\epsilon_r\} = [C]\{c\} \qquad\qquad (IV.21)$$

where

$$[C] = \begin{bmatrix} C_1 & 0 & 0 \\ 0 & C_2 & 0 \\ 0 & C_{23} & C_3 \end{bmatrix} \quad ;$$

$$[C_1] = \begin{bmatrix} 0 & 1 & 0 & y & 0 & 0 & 0 & 0 \\ 0 & 0 & 0 & 0 & 0 & 0 & 1 & x \\ 0 & 0 & 0.5 & 0.5x & 0 & 0.5 & 0 & 0.5x \end{bmatrix} \quad ;$$

$$[C_{2a}] = \begin{bmatrix} 0 & 0 & 0 & -2 & 0 & 0 & -6x & -2y & 0 & 0 & -6xy \\ 0 & 0 & 0 & 0 & 0 & -2 & 0 & 0 & -2x & -6y & 0 \\ 0 & 0 & 0 & 0 & -1 & 0 & 0 & -2x & -2y & 0 & -3x^2 \\ 0 & 0 & 0 & 0 & 0 & 0 & 0 & 0 & 0 & 0 & 0 \\ 0 & 0 & 0 & 0 & 0 & 0 & 0 & 0 & 0 & 0 & 0 \end{bmatrix} \quad ;$$

$$[C_{2b}] = \begin{bmatrix} -2y^2 & 0 & -6xy^2 & -2y^3 & -6xy^3 \\ -2x^2 & -6xy & -2x^3 & -6x^2y & -6x^3y \\ -4x & -3y^2 & -6x^2y & -6xy^2 & -9x^2y^2 \\ 0 & 0 & 0 & 0 & 0 \\ 0 & 0 & 0 & 0 & 0 \end{bmatrix} \quad ;$$

$$[C_{2c}] = \begin{bmatrix} 0 & 1 & 0 & y & 0 & 0 & 0 & 0 \\ 0 & 0 & 0 & 0 & 0 & 0 & 1 & x \\ 0 & 0 & 0.5 & 0.5x & 0 & 0.5 & 0 & 0.5y \\ 1 & x & y & xy & 0 & 0 & 0 & 0 \\ 0 & 0 & 0 & 0 & 1 & x & y & xy \end{bmatrix} \quad ;$$

$$[C_{23}] = \begin{bmatrix} C_{23a} & C_{23b} & C_{23c} \\ 0 & 0 & 0 \end{bmatrix} \quad ;$$

$$[C_{23a}] = \begin{bmatrix} 0 & 1 & 0 & 2x & y & 0 & 3x^2 & 2xy & y^2 & 0 & 3x^2y \\ 0 & 0 & 1 & 0 & x & 2y & 0 & x^2 & 2xy & 3y^2 & x^3 \end{bmatrix} \quad ;$$

$$[C_{23b}] = \begin{bmatrix} 2xy^2 & y^3 & 3x^2y^2 & 2xy^3 & 3x^2y^3 \\ 2x^2y & 3xy^3 & 2x^3y & 3x^2y^2 & 3x^3y^3 \end{bmatrix} \quad ;$$

$$[C_{23c}] = \begin{bmatrix} 0.5 & 0.5x & 0.5y & 0 & 0 & 0 & 0 \\ 0 & 0 & 0 & 0.5 & 0.5x & 0.5y & 0.5xy \end{bmatrix} \quad ;$$

$$[C_3] = \begin{bmatrix} -1 & -x & -y & -xy & 0 & 0 & 0 & 0 \\ 0 & 0 & 0 & 0 & -1 & -x & -y & -xy \\ 0 & 1 & 0 & y & 0 & 0 & 0 & 0 \\ 0 & 0 & 0 & 0 & 0 & 0 & 1 & x \\ 0 & 0 & 0.5 & 0.5x & 0 & 0.5 & 0 & -0.5y \end{bmatrix}$$

The strain energy expression, Eq. (IV.19) for the structure is used to derive a finite element representing a portion of the structure. Substituting Eq. (18) into Eq. (16) and limiting the integration to a specific element gives the strain energy expression of the element.

$$U_{el} = \frac{1}{2a_{cell}} \{c\}^T \int_{\substack{\text{Area of} \\ \text{the element}}} [C]^T [K_{eq}][C] dA \{c\} \qquad (IV.22)$$

The 40 d.o.f. of the element can be expressed in terms of the interpolation function coefficients $\{c\}$ by using Eq. (17) and the x,y location of each node point of the element.

$$g_{el} = [R]\{c\}$$

where

$$\{g_{el}\}^T = [g_1{}^T \quad g_2{}^T \quad g_3{}^T \quad g_4{}^T] ; \qquad (IV.23)$$

$$\{g_i\}^T = [u_i \quad v_i \quad \frac{dw_i}{dx} \quad \frac{dw_i}{dy} \quad \frac{d^2w_i}{dxdy} \quad 2\kappa^o_{xz_i} \quad 2\kappa^o_{yz_i} \quad \theta^o_{x_i} \quad \theta^o_{y_i}] ;$$

and i refers to node c of the element.

The strain energy expression of the element is then expressed in terms

of the nodal d.o.f.'s.

$$U_{el} = \frac{1}{2} \{g_{el}\}^T [K_{el}]\{g_{el}\} \tag{IV.24}$$

where

$$[K_{el}] = \frac{1}{A_{cell}} [R]^{-T} \int\limits_{\substack{\text{Area of} \\ \text{the element}}} [C]^T[K_{eq}][C]dA[R] \ .$$

The same lumped mass matrix used for the repetitive space lattice with pinned joints Eq. (II.25) is used in this chapter.

## Results

### Space Lattice Structure Configuration

The hexahedral space lattice geometry (Fig. 21) is used as a demonstration problem. The space lattice is generated by repeating a unit cell (Fig. 22) several times in two orthogonal directions. The initial properties of the structure were chosen to be similar to several box truss geometries which have been developed.[21,22] The length of each main structural member, which is equal to the thickness of the space lattice structure, is 4 meters. The main structural members are 6.1 mm thick Graphite Epoxy Tubes, 11.7 cm in diameter. The diagonal braces are aluminum tubes, 5.657 meters long with a thickness of 0.5 mm and a diameter of 1.58 cm. The natural frequencies and mode shapes are calculated for a repetitive plate-like space lattice structure with four cells in each direction. The static displacements are calculated for a centrally loaded plate-like space lattice structure with eight cells in each direction.
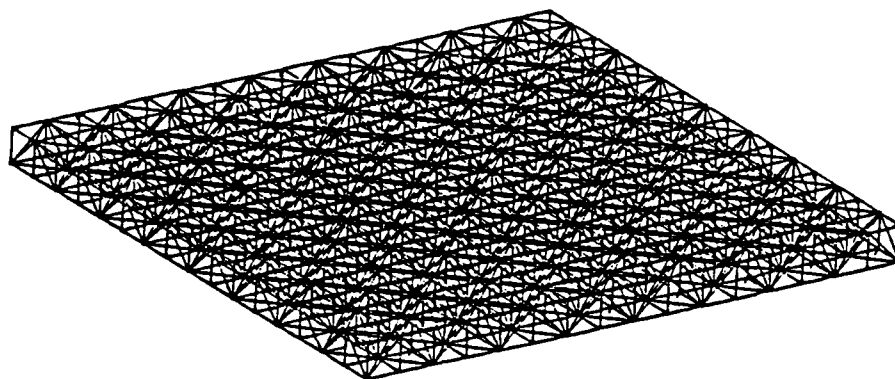
Figure 21. Hexahedral Space Lattice.

L = h = 4.0 m

MEMBER CROSS
SECTION

—————— MAIN STRUCTURAL MEMBERS
(GRAPHITE EPOXY)

$t_0 = 6.1$ mm $d_0 = 11.7$ cm $A_0 = 22.35$ cm$^2$
$I_0 = 380.25$ cm$^4$ E $= 20.0 \times 10^{10}$ N/m$^2$
$\rho = 1550$ kg/m3

— — — DIAGONAL BRACES
(ALUMINUM)

$t_0 = 0.5$ mm $d_0 = 1.58$ cm $A_0 = 25.0$ mm$^2$
$I_0 = 781.25$ mm$^4$ E $= 7.17 \times 10^{10}$ N/m$^2$
$\rho = 2768$ kg/m3
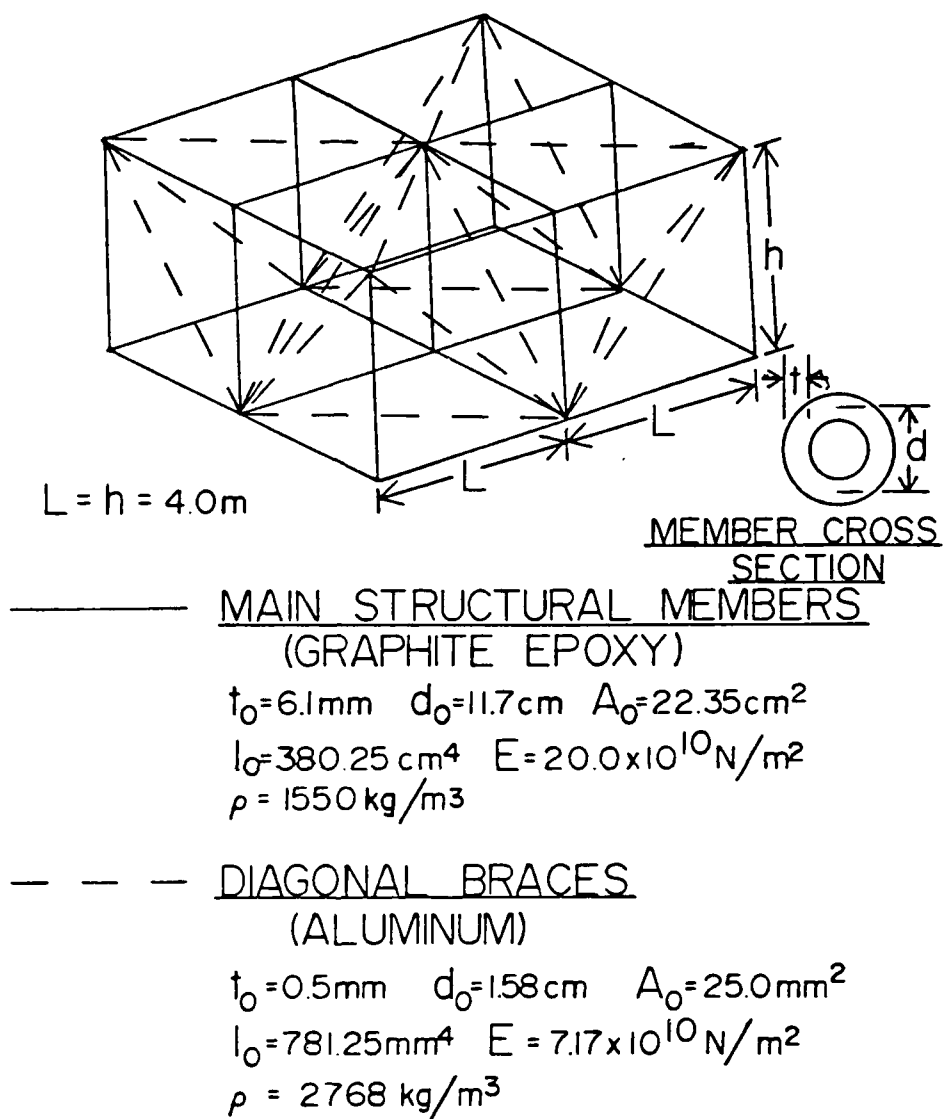
Figure 22. Hexahedral Space Lattice Unit Cell.

## Natural Frequencies and Mode Shapes

The natural frequencies and mode shapes of this space lattice, with free edge conditions, are calculated using three different finite element models. The most accurate solution among the three is the "detailed" finite element mode, which is obtained using NASTRAN, with each frame member of the structure modelled as a single CBAR type finite element. Guyan reduction is used and the six rigid body modes, are calculated using the NASTRAN free body support option, Eqs. (II.7) to (II.16). The flexible natural frequencies and mode shapes are shown in Fig. 23 as the solid curves. Four sets of frequencies are obtained by assuming four values of $A/A_o$, where the value of cross sectional area $A_o = 2.235 \times 10^{-3} m^2$ for the main structural members is used as a basis for nondimensionalization. It is assumed that the ratios of cross sectional areas and moments of inertia between the main structural members and the diagonal braces are as follows:

$$\frac{A_o}{\bar{A}_o} = 89.4 \; ; \quad \text{and} \quad \frac{I_o}{\bar{I}_o} = \frac{t_o}{\bar{t}_o} \frac{d_o}{\bar{d}_o} (\frac{A_o}{\bar{A}_o})^2 \; .$$

Therefore the main structural member properties scale as follows:

$$t = (\frac{A}{A_o})^{1/2} t_o; \quad d = \frac{A}{A_o}^{1/2} d_o; \quad I = (\frac{A}{A_o})^2 \tag{IV.25}$$

the diagonal brace properties also scale using Eq. (IV.25). The equivalent micropolar plate finite element developed above is then used to calculate the natural frequencies and mode shapes which appear
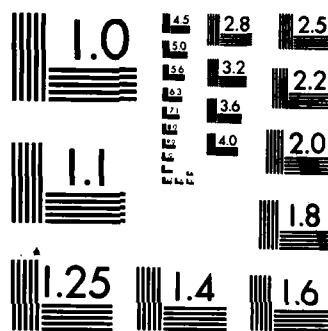
END

FILMED

DTIC
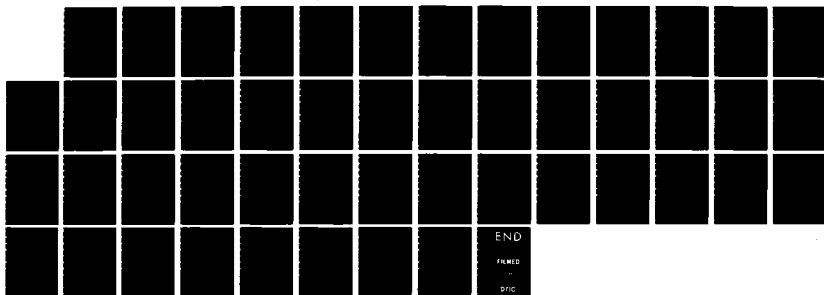
MICROCOPY RESOLUTION TEST CHART

NATIONAL BUREAU OF STANDARDS-1963-A

as the dashed curves in Fig. 23. The agreement between the results

obtained by the micropolar and the detailed finite element models

is good, especially for the relative small number (four) of cells

assumed. The equivalent micropolar plate finite element can be

reduced to a transverse shear type plate finite element by removing

the terms of $[K_{eq}]$ associated with the micropolar strains and con-

straining $\theta_x$ and $\theta_y$ to zero. The natural frequencies and mode shapes

calculated using this equivalent plate model are shown as the dashed

dotted curve in Fig. 23. It should be noted that except for the

first flexible mode the transverse shear continuum plate model

frequencies deviate significantly from those results obtained by

the micropolar plate finite element model and the detailed finite

element model. These discrepancies are small for very flexible

tube members (as $A/A_0$ is small) and they increase as the tube

members become stiffer (as $A/A_0$ increases).

## Static Analysis

The static deflection is also calculated using these three

different finite element models. The detailed model described above

is used to model a quadrant of a statically loaded plate-like space

lattice structure with a central concentrated load normal to the

plane of the structure. The structure is constrained against

translation normal to its plane at each corner. As in the calculation

of the natural frequencies, four values of cross section areas

$(A/A_0)$ are used. The resulting nondimensional central deflection

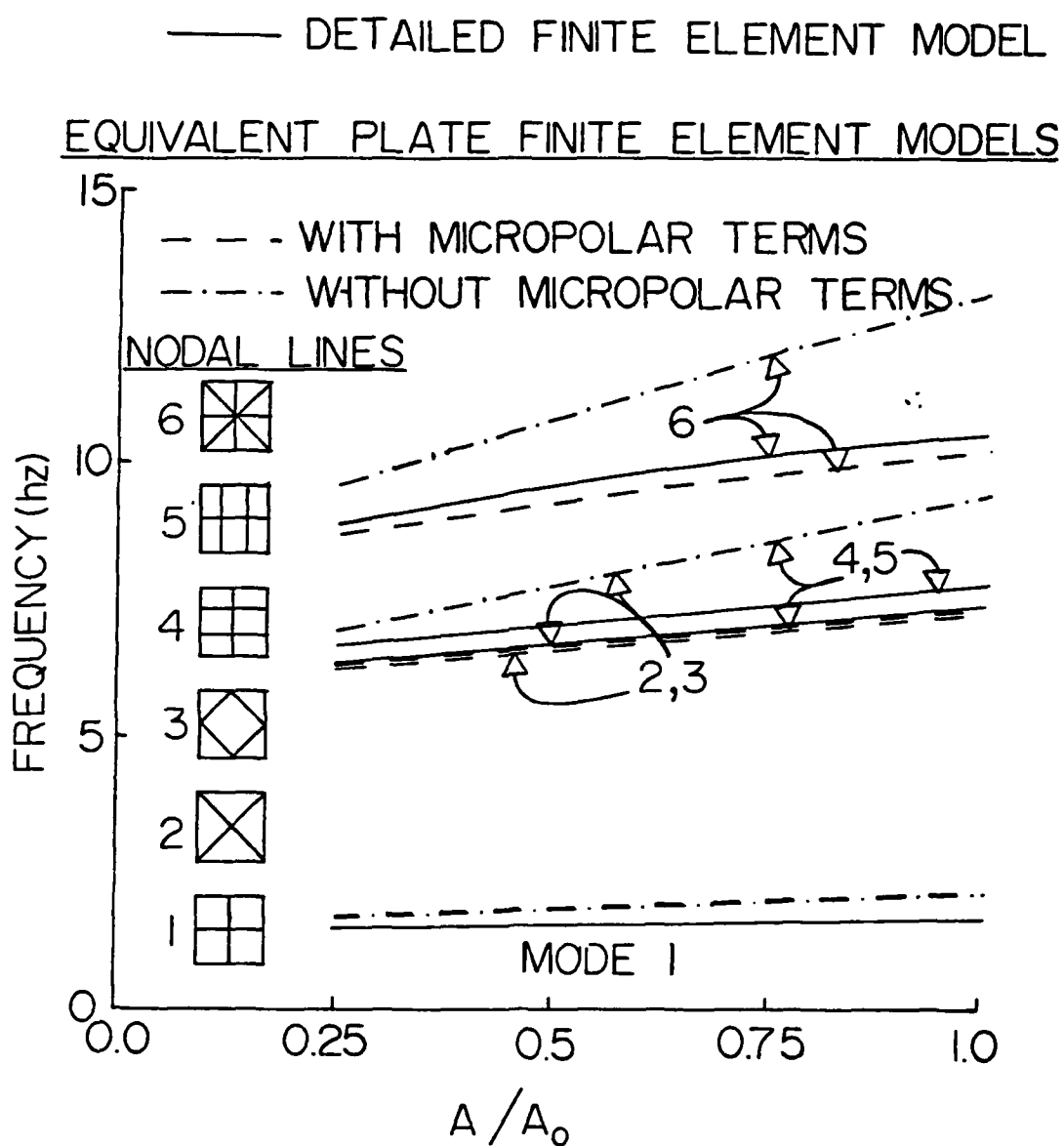$(w/h)$ is shown as the solid curve in Fig. 24, where h is the thickness

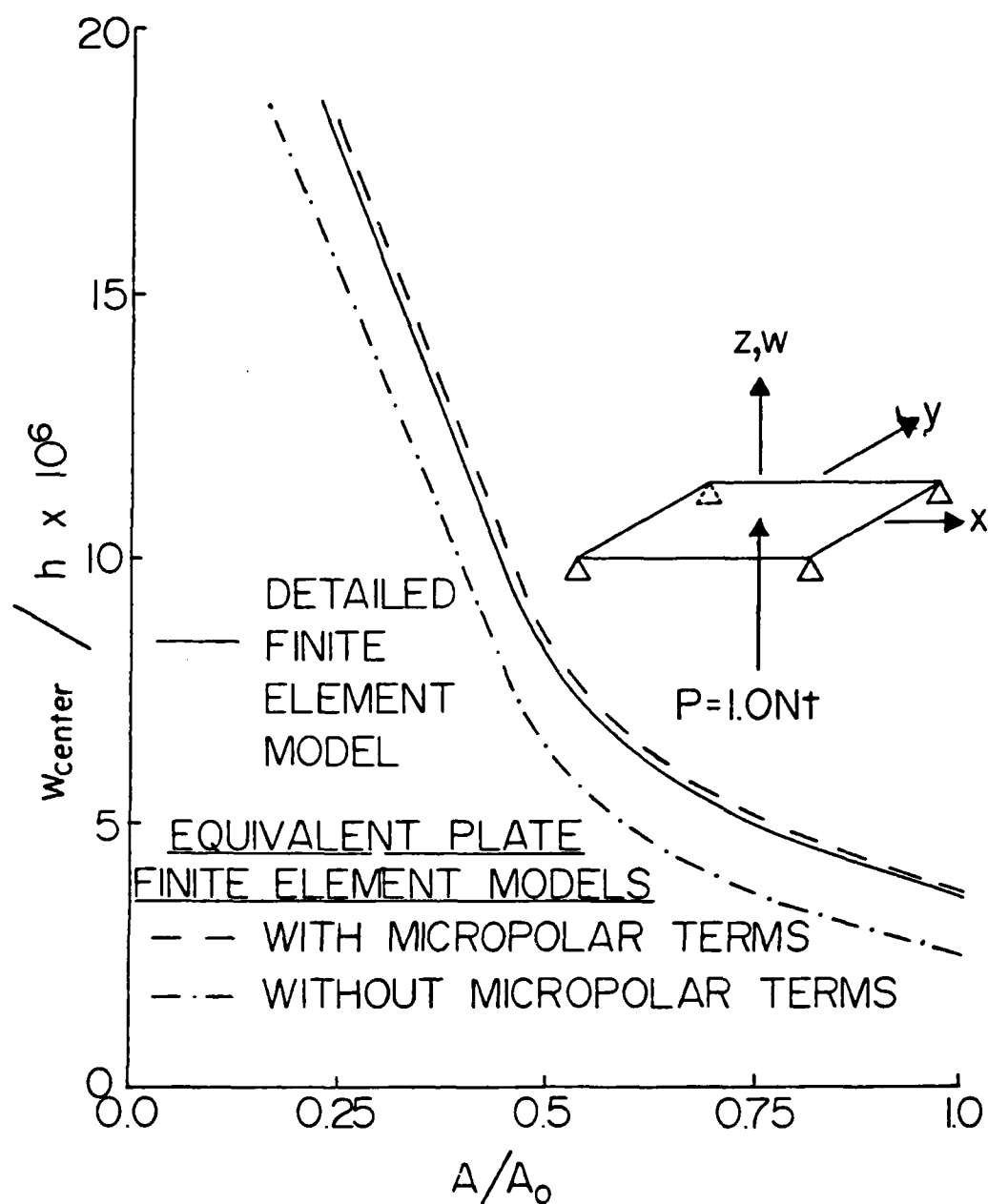Figure 23. Flexible Natural Frequencies
and Mode Shapes.

Figure 24. Nondimensionalized Central Deflections of
a Corner Supported, Centrally Loaded
Space Lattice.

of the plate-like lattice structure as shown in Fig. 22. The micropolar finite element models, with and without the micropolar rotational terms, are also used to calculate the static deflections which are shown in Fig. 24 for the four cross sectional areas as the dashed and dashed-dotted curves, respectively. As in the case of the natural frequencies the results obtained using the micropolar finite element model agree well with those obtained using the detailed finite element model. Both sets of results deviate significantly from those obtained by the finite element model that omits the micropolar rotational degrees of freedom as the structural members become stiffer (as $A/A_0$ increases).

## Conclusion

A method has been developed to allow repetitive plate-like space lattice structures with rigid joints to be modelled effectively as an equivalent micropolar plate continuum. A micropolar plate finite element has been developed using the strain energy expression of this continuum model. This allows considerable simplicity and flexibility in tresting geometry, boundary conditions, attachments, and other structural complexities.

It is found that the present micropolar plate finite elements can accurately predict the static deflection and natural frequencies of the plate-like lattice structures. This is done by comparing the results with those obtained using a detailed finite element model where each structural member is modelled using one CBAR (6 d.o.f.'s per node beam-column) element in NASTRAN. The present example study

shows that the micropolar plate finite element is considerably more accurate than the one without micropolar rotation but with transverse shear d.o.f.'s.

While numerical results have only been generated for structures built with frame members connected by rigid joints, the method would certainly apply to a general class of repetitive plate-like structures with either rigid or pinned joints. The present unit cell modelling method as described in Eq. (1) could certainly be generalized to include plate, membrane, or other types of finite elements, without changing any subsequent portion of the method. Logical next steps would include incorporating semirigid joints into the continuum model, extension of the method to model member and joint damping as continuum properties for forced response analysis, including geometric nonlinearities, and applying this finite element model for feedback control system design.

## CHAPTER V - CONCLUSIONS

### Further Developments

In this section several potential extensions of this work will be discussed. In general, the theoretical basis of the idea is presented without supporting numerical examples.

### Semirigid Joints

The first extension considered is the application of the micropolar plate finite elements developed in Chapter IV to model large repetitive plate-like space lattices with semirigid joints. In order to use this element for these type structures, the detailed finite element model of the unit cell would be developed with each frame member modelled as a single beam-column type element as before. However, there would be a separate nodal point at each joint connected to each element. The value of the translational displacements for each of these nodes would be equated.

$$u_i = u_{i_1} = u_{i_2} = u_i m_i$$

$$v_i = v_{i_1} = v_{i_2} = v_i m_i \qquad (V.1)$$

$$w_i = w_{i_1} = w_{i_2} = \ldots = w_i m_i$$

where

$(u_{ij}, v_{ij}, w_{ij})$ are the translations along $(x,y,z)$ of

the jth frame member; and

$m_i$ is the number of frame members of the unit cell which

intersect at joint i.

Each rotational d.o.f. would be connected with rotational spring
elements of zero length (Fig. 25). The stiffness matrix of such a
spring element in terms of the torsional stiffness (J) of the spring
is given by:[12]

$$[K_{rot.spr}] = \begin{bmatrix} J & -J \\ -J & J \end{bmatrix} \tag{V.2}$$

with this stiffness matrix connecting the rotational d.o.f. pairs
$(\beta_{x_{i_j}}, \beta_{x_{i_j}})$, $(\beta_{y_i}, \beta_{y_{i_j}})$, and $(\beta_{z_i}, \beta_{z_{i_j}})$, where $(\beta_{x_{i_j}}, \beta_{y_{i_j}}, \beta_{z_{i_j}})$
are the rotational d.o.f. about the $(x,y,z)$ axes at joint i for the
jth frame and j varies from 1 to the number of frame members of the
unit cell intersecting at joint i ($m_i$).

The equations of constraint Eq. (V.1) would be used to
substantially reduce the order of the stiffness matrix $[K_{cell}]$ of
the unit cell. First the d.o.f.'s {q} are reorganized into three
vectors $\{q_r\}$ containing one set of translation and rotation d.o.f.'s
at each joint, $\{q_o\}$ containing the remaining rotational d.o.f.'s
at each joint, and $\{q_c\}$ conaining the remaining translational
d.o.f.'s at each joint. The matrix $[K_{cell}]$ is similarly reorganized
and partitioned.
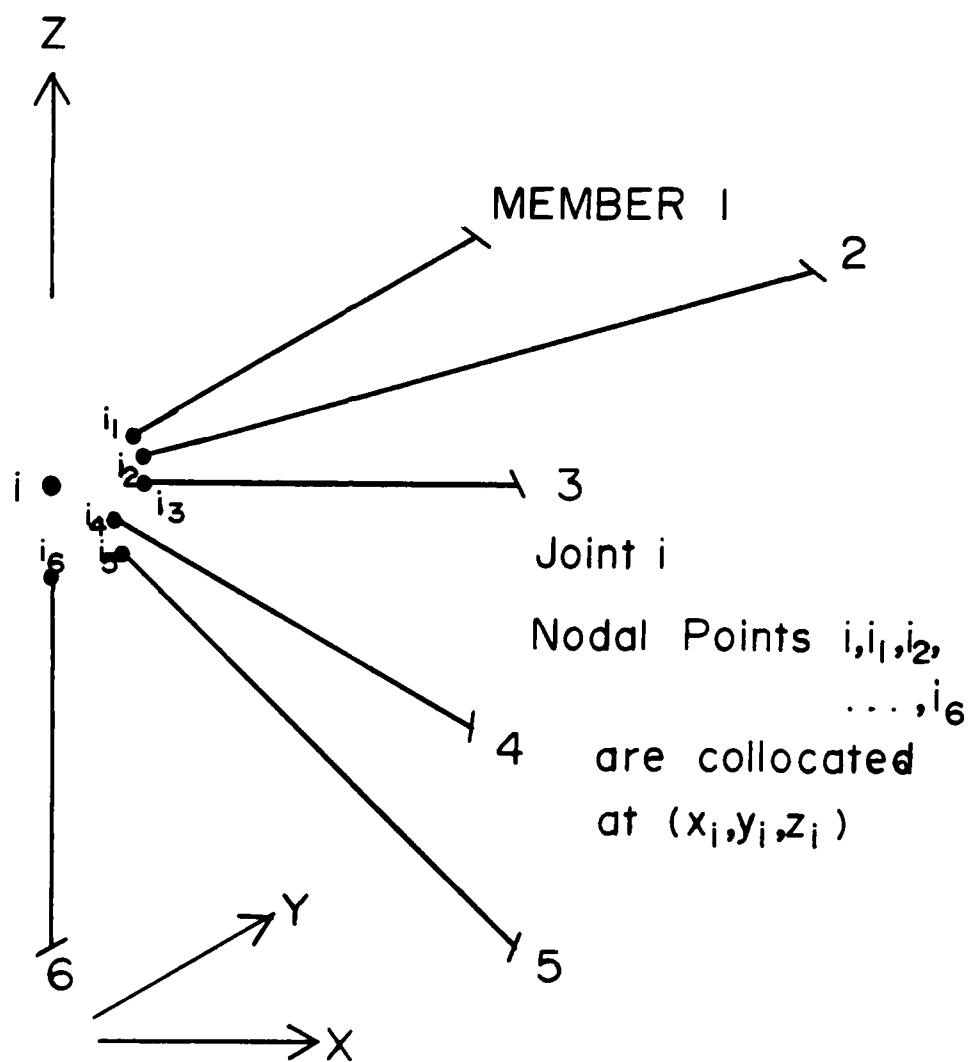
Figure 25. Semirigid Joint Model.

$$[K_{cell}] = \begin{bmatrix} K_{rr} & K_{ro} & K_{rc} \\ K_{ro}^T & K_{oo} & K_{oc} \\ K_{rc}^T & K_{oc}^T & K_{cc} \end{bmatrix} \qquad (V.3)$$

The equality constraints Eq. (V.1) can be rewritten

$$\{q_c\} = [G]\{q_r\} \qquad (V.4)$$

The strain energy expression is given as:

$$U_{cell} = \frac{1}{2} \begin{Bmatrix} q_r \\ q_o \\ q_c \end{Bmatrix}^T \begin{bmatrix} K_{rr} & K_{ro} & K_{rc} \\ K_{ro}^T & K_{oo} & K_{oc} \\ K_{rc}^T & K_{oc}^T & K_{cc} \end{bmatrix} \begin{Bmatrix} q_r \\ q_o \\ q_c \end{Bmatrix} \qquad (V.5)$$

Substituting constraint Eq. (V.4) into the strain energy expression Eq. (V.5) yields an equivalent strain energy expression.[13]

$$U_{cell} = \frac{1}{2} \begin{Bmatrix} q_r \\ q_o \end{Bmatrix}^T \begin{bmatrix} \bar{K}_{rr} & \bar{K}_{ro} \\ \bar{K}_{ro}^T & \bar{K}_{oo} \end{bmatrix} \begin{Bmatrix} q_r \\ q_o \end{Bmatrix} \qquad (V.6)$$

where

$$[\bar{K}_{rr}] = [K_{rr}] + [K_{rr}] + [K_{rc}][G] + [G]^T[K_{rc}]^T + [G]^T[K_{cc}][G];$$

$$[\bar{K}_{ro}] = [K_{ro}] + [G]^T[K_{oc}]^T; \quad \text{and} \quad [\bar{K}_{oo}] = [K_{oo}] .$$

For the micropolar plate finite element which is developed in Chapter IV the mass associated with the rotational d.o.f. at the joints of

the unit cell is ignored since the "lumped mass" description of each individual frame member is used. This element is shown to yield good natural frequencies and mode shapes using a specific space lattice geometry. It is consistent with this assumption to utilize static condensation Eq. (II.4) to reduce the strain energy expression to contain only terms associated with $\{q_r\}$.

$$U_{cell} = \frac{1}{2} \{q_r\}^T [\bar{K}_{cell}]\{q_r\} \qquad\qquad (V.7)$$

where

$$[\bar{K}_{cell}] = [\bar{K}_{rr}] - [\bar{K}_{ro}][\bar{K}_{oo}]^{-1}[\bar{K}_{ro}]^T .$$

It can be seen from Eq. (II.5) that the Guyan reduction is exact if there are no mass terms associated with the omitted d.o.f.'s ($[M_{ro}] = 0$ and $[M_{oo}] = 0$). Therefore, the reduction in Eq. (V.7) causes no additional error beyond that generated when lumped mass matrices are used for the beam-column elements. It should be noted that the strain energy expression Eq. (V.7) is equivalent in both order and form to Eq. (IV.1) and could be used to derive a micropolar plate finite element for repetitive plate-like space lattices with semirigid joints. These results would be compared with those obtained with a detailed finite element model developed for the entire structure in the manner described above for the unit cell. Numerical results were not generated using this method since the resulting detailed finite element model is larger than can be effectively analyzed using NASTRAN as installed at Purdue University.

## Consistent Mass Matrices

The results obtained in this study were obtained using lumped mass matrices for the individual frame members. Such matrices contain half the mass of the member at the diagonal location associated with each of the translation d.o.f. of the element. This ignores any rotatory inertia effects within the individual frame members. The results of the numerical examples in Chapter IV show that the lumped mass assumption for the individual members is reasonable. One obvious extension of this work is to develop the mass matrix in terms of consistent mass matrices for each frame member. One way to implement this would be to assume that the spatial derivatives of the velocity components at the plate midplane are zero, implying that the velocity components are only functions of time for each unit cell. Using this assumption the kinetic energy expression of the unit cell in terms of the joint velocities and angular velocities can be transformed to a kinetic energy expression in terms of the midplane velocity components. This has been done for the beam-like micropolar continuum representation.[8] This kinetic energy expression could be integrated over each element to yield the mass matrix of each element.

An alternative method would be to apply the consistent mass matrix method (where the kinetic energy expression is used to generate the mass matrix of the element in the same manner that the strain energy expression is used to generate the stiffness matrix of the element) to the equivalent model.[3] The kinetic energy expression of the unit cell calculated using a detailed finite element model

of the unit cell is used as the initial kinetic energy expression for the unit cell.

$$K.E._{cell} = \frac{1}{2} \{\dot{q}\}^T [M_{cell}]\{\dot{q}\} \qquad (V.8)$$

where $\{q\}$ is the vector of nodal velocities of the unit cell and $[M_{cell}]$ is the mass matrix of the unit cell from the detailed finite element model of the unit cell. If identical transformations, reductions, and integrations were applied to this expression that were used in Chapter IV with the strain-energy expression Eq. (IV.1), the result would give the consistent mass matrix of each micropolar plate finite element $[M_{el}]$ defined as an analog to $[K_{el}]$ of Eq. (IV.24).

## Joint and Member Damping

There is considerable ongoing research to develop space lattice frame members and joints with significantly larger damping than that of traditional metal components.[23] In this study all of the control system results have been generated using an assumed value of modal damping ($\zeta = 0.005$). For structures with larger damping associated with specific motions of the structure, it might be desirable to include damping effects in the continuum model. One method of doing this would be to build a detailed model similar to that derived in the paragraph above dealing with rigid joints except that the element damping matrices would be assembled and condensed to yield a system damping matrix for the unit cell. This unit cell damping matrix could be substituted for the unit cell stiffness matrix in Eq. (IV.1). As for the consistent mass matrix in the preceeding paragraph, the same procedure used to transform, reduce

and integrate from the unit cell stiffness matrix to the micropolar plate finite element stiffness matrix, could be used to calculate the damping matrix of each micropolar plate finite element. Once assembled this would yield the equation of motion of the structure as;

$$[K]\{q\} + [B]\{\dot{q}\} + [M]\{\ddot{q}\} = \{P\} \qquad (V.9)$$

where

> [K] is the stiffness matrix of the micropolar plate finite element model;

> [B] is the damping matrix of the micropolar plate finite element model;

> [M] is the mass matrix of the micropolar plate finite element; and

> {q} is the vector of nodal displacement d.o.f.'s associated with the micropolar plate finite element model of the space lattice structure.

This equation could be solved to yield complex eigenvalues and eigenvectors, which could be used in a similar manner to that described in Chapter II for feedback control system design and system performance. Alternatively, structural dynamic response could be generated using direct integration analysis methods.

### Application to Non-Lattice Type Structures

While the equivalent continuum models in this study were specifically developed for large repetitive space lattice structures, their usefulness should extended to many other types of structures. As an example, one such application will be discussed. Large mirrors are often designed as a surface plate which can be coated, supported by a backup structure which is often made up of web type structure (for example, see Fig. 26). Detailed finite element models of this type of structure can be too large and cumbersome to use effectively. As an alternative, the micropolar plate finite element developed in Chapter IV could be calculated from the stiffness matrix of the unit cell based on a detailed model of the unit cell (such as in Fig. 27) and used to solve for the structural response of the large mirror.

### Summary

A basic procedure to analyze large repetitive plate-like space lattice structures with pinned joints using finite element models of equivalent continuum representations of the strain energy and kinetic energy of the structure has been developed and implemented. By retaining the transverse shear deformations in the finite element formulation, the equivalent plate finite element models are found to give modal results consistent with those generated from a detailed truss bar element model of the space lattice structure even for small numbers of unit cell repetitions.

The modal models resulting from the finite element model are shown to serve as accurately, yet are more simplified in the control

PORTION OF A
LARGE WEB STIFFENED MIRROR
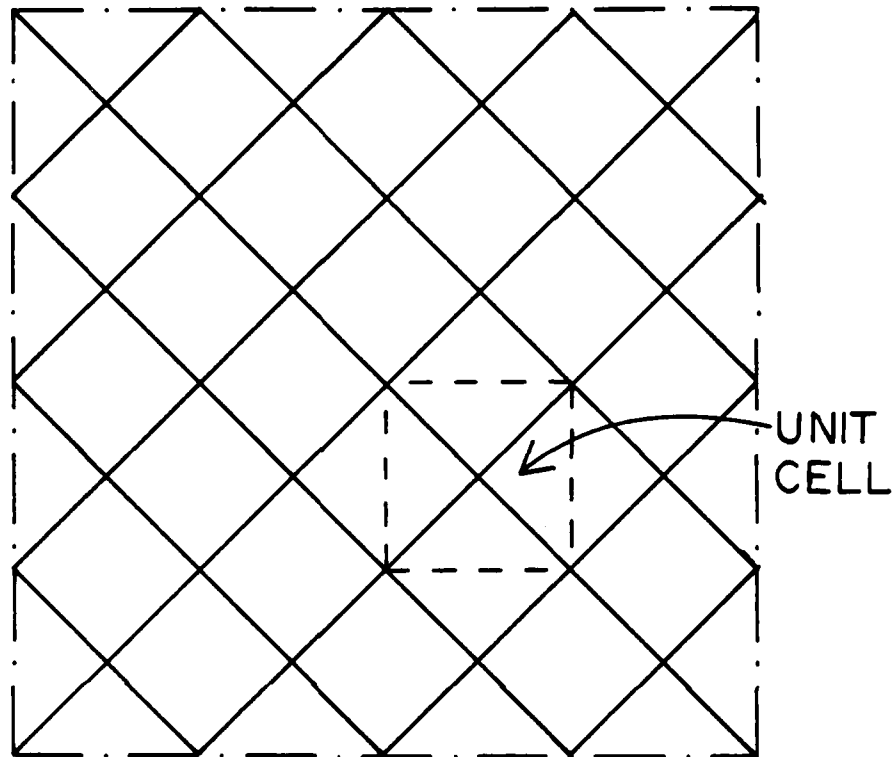


UNIT
CELL

BOTTOM VIEW

SURFACE PLATE
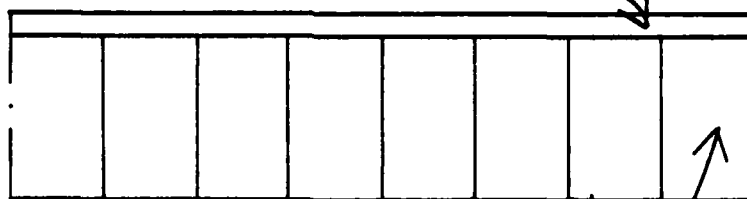
END VIEW

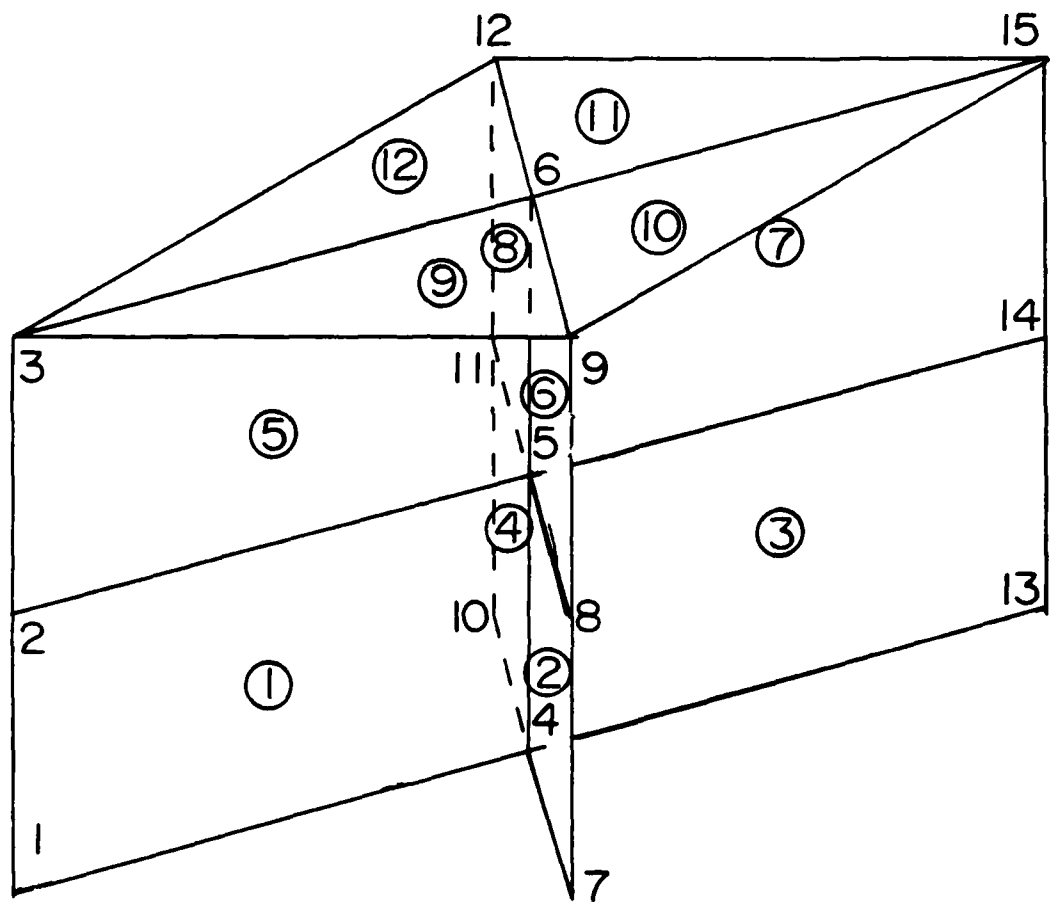SUPPORTING WEB

Figure 26. Large Mirror Example Problem.

Figure 27. Detailed Plate Unit Cell
Finite Element Model.

design process compared to the complex truss bar element model for a specific large plate-like repetitive space lattice structure. This study has shown that choosing control design models based on a modal sequence may involve unnecessary modes. By using Modal Cost Analysis to consider the control problem based on a sequence of lower modes, it is found that several intermediate modes do not contribute much to the control design.

A procedure has been demonstrated to utilize equivalent continuum finite element modelling methods to efficiently examine the effects of parametric variation of the cross sections of large repetitive plate-like space lattice structures. Using a specific space lattice structural configuration, two sets of parameter variations were performed. In the first case, the length of all the members as well as the mass of the structure were held constant. This caused the area of the surface members to be a function of the area of the internal diagonal members. The second case involved the variation in the thickness of the space lattice structure. Again, the length and total mass of the structure were held constant. The allowable buckling load of the slender internal members was held constant. Thus the cross sectional area of the surface and internal members was determined to be a function of the thickness. For both cases, maxima were obtained in the natural frequencies and optimal performance values of the design parameter were calculated. Modelling the structure using the finite element continuum model is seen to allow more flexibility in treating geometry, boundary conditions, attachments, and other structural complexities.

A method was developed to allow repetitive plate-like space lattice structures with rigid joints to be modelled effectively as an equivalent micropolar plate continuum. A micropolar plate finite element has been developed using the strain energy expression of this continuum model. This allows considerable simplicity and flexibility in treating geometry, boundary conditions, attachments, and other structural complexities.

It was found that the present micropolar plate finite elements can accurately predict the static deflection and natural frequencies of the plate-like lattice structures. This was done by comparing the results with those obtained using a detailed finite element model where each structural member was modelled using one CBAR (6 d.o.f.'s per node beam-column) element in NASTRAN. The present example study shows that the micropolar plate finite element is considerably more accurate than the one without micropolar rotation but with transverse shear d.o.f.'s.

Several extensions to equivalent plate modelling methods have been examined. These include techniques to allow the existing equivalent micropolar plate finite element modelling method to solve structural dynamics problems of large plate-like repetitive space lattices with semi rigid joints, consistent mass matrices for the individual frame members, and element damping for the frame members and joints; as well as non-lattice repetitive plate-like structures (such as mirrors). The equivalent plate modelling methods could also be extended to include geometrically nonlinear terms allowing buckling of the structure to be examined.

## Conclusion

As the size and complexity of large repetitive space lattice structure increases the need for accurate, efficient, analysis methods to allow the structural response (both static and dynamic) of these structures to be predicted efficiently also increases. Developing detailed finite element models of large, complex structures is extremely time consuming and cumbersome. Analyzing structural response for such complex structures is also extremely costly and for sufficiently large and complicated structures may be impractical, particularly in the design phase where many analyses are required. Numerous methods have been developed to simplify and automate the analysis of large, complicated structures. While these advances are crucial, particularly for large repetitive structures, even with extremely refined software to manage the generation, assembly, and transfer of large data files from different portions of the structure to some system model, most of these methods achieve the model reduction by removing internal d.o.f.'s from portions of the structure (substructures) and representing these portions of the structure in terms of the deformation at the boundary points with adjacent substructures (retaining sufficient internal d.o.f. to represent the loading and internal dynamics of the substructure). In these methods, the resulting model of the system is tied to the internal geometry of the fundamental structure. In general, the locations where node points of the system model can be loaded are limited.

As an alternative to potentially cumbersome detailed modelling, numerous studies have been performed where a standard continuum finite element (such as a plate element) is used to model a discrete structure by using an equivalent set of fundamental properties (such as E, $\nu$, $\rho$, t, ...). Several studies have been conducted to develop systematic methods for determining these properties. Recently, methods have been developed to systematically generate constitutive matrices of equivalent continuum representations, where higher order strain terms have been retained consistent with the motion the unit cell of the repetitive structure is capable of. In a few cases, these have been used with existing finite elements to analyze specific space lattice geometries. However, in general the equations of motion have been solved in closed form or numerically, usually for simply supported structures. To the authors knowledge, no systematic effort has been made to develop higher order plate finite elements with displacement functions specifically chosen to be consistent with the higher order strain terms in these equivalent continuum representations.

This research effort has extended the existing equivalent continuum representations where necessary (no such representation existed for large repetitive space lattices with rigid joints). Rectangular plate type finite elements have been developed whose displacement functions are consistent with the equivalent continuum representation containing transverse shear deformations, with and without micropolar strain terms. While these elements are intended to model structures with many repeating unit cells per plate-type

finite element, it is gratifying to see that the elements accurately predict the response of the current examples even for very small numbers of unit cells per element.

The equivalent plate finite elements representing large repetitive space lattice structures have many advantages compared to more conventional methods. One significant advantage of this method over detailed modelling using a substructuring method is that the number of and location of nodal points required to model very large, complex, repetitive plate-like space lattices is determined by the number and accuracy of the modes required, not by the internal geometry of the space lattice. Specifically, there is no requirement that (or advantage to) having internal node points of the structure located at unit cell boundaries or joint locations in the lattice. Large repetitive plate-like space lattice structures of the type considered in this study will be used as space platforms to which will be attached various other structural members. While solving the equations of motion of the equivalent continuum representation of a free floating space platform with attachments can certainly be done numerically, it is simpler and more convenient to model the space platform as an equivalent higher order plate-type element which can be coupled with other structural components and analyzed in the free floating configuration using existing finite element solution techniques. Some space lattices will be generated with different lattice configurations in different regions of the structure. The equivalent plate finite element formulation applies directly to this type

of structure by simply using different higher order constitutive matrices in different regions of the structure. While the elements developed in this study were rectangular in shape, for simplicity, elements of other shape could be developed using similar methods. Thus, plate-like space lattices of arbitrary geometry can be readily analyzed using this method.

This research represents a new philosophy to the structural analysis of discrete structures. That is, an equivalent continuum representation of suitable order to account for the possible motion within a unit cell is used as a bridge connecting a repetitive discrete structure with a consistent order discrete finite element model of the structure. This method gives accurate results while greatly simplifying the modelling process over more direct methods of going from the discrete structure to a reduced finite element model of the structure for large, complex, repetitive structures.

LIST OF REFERENCES

# LIST OF REFERENCES

[1]Guyan, R.J., "Reduction of stiffness and mass matrices," AIAA Journal, Vol. 3, 1965, p. 380.

[2]Jerrard, A.J., ed., MSC Application Manual, MacNeal-Schwendler corp., April 1981, Sec. 2.4.

[3]MacNeal, R.H., "Vibration of Composite Systems," Air Research and Development Command, TR-55-120, 1955.

[4]Arnold, R.H., Citerley, N.L., Chardin, M., and Galani, S., "Application of Ritz Vectors for Dynamic Analysis of Large Structures," Computers and Structures, (to appear).

[5]Sun, C.T., and Yang, T.Y., "A continuum approach towards dynamics of Gridworks," Journal of Applied Mechanics, ASME, Vol. 40, 1973, pp. 186-192.

[6]Aswani, M., Au, M.N., and Lin, S.N., "Development of an analytical model for large space structures," AIAA Journal, Vol, 1981, pp. 41-48.

[7]Noor, A.K., Anderson, M.S., and Greene, W.H., "Continuum models for beam- and plate-like lattice structures," AIAA Journal, Vol. 16, 1978, pp. 1219-1228.

[8]Noor, A.K., and Nemeth, M.P., "Micropolar beam models for lattice grids with rigid joints," Computer Methods in Applied Mechanics and Engineering, Vol. 21, 1980, pp. 249-263.

[9]Johnson, C.D., Gibson, W., Kienholz, D., and Paxson, E., Angular Vibration of Aircraft, Air Force Flight Dynamics Laboratory, TR-79-30-5, April 1979.

[10]Kwakernaak, H., and Sivan, R., Linear Optimal Control Systems, Wiley and Sons, New York, 1982.

[11]Skelton, R.E., and Yousuff, A., "Component cost analysis of large scale systems," International Journal of Control, Vol. 37, 1983, pp. 285-304.

[12]Lamberson, S.E., and Yang, T.Y., "Continuum plate finite elements for vibration analysis and feedback control of large space structures," Computers and Structures, to appear.

[13]Martin, H.C., Introduction to Matrix Methods of Structural Analysis, McGraw-Hill, 1966.

[14]MacNeal, R.H., NASTRAN Theoretical Manual, NASA, SP-221, April 1972.

[15]Bogner, F.K., Fox, R.L., and Schmit, L.A., "Generation of interelement-compatible stiffness and mass matrices by the use of interpolation formulas," Proceedings of the First Conference on Matrix Methods in Structural Mechanics, Air Force Flight Dynamics Laboratory, TR-66-80, 1966, pp. 397-443.

[16]Skelton, R.E., Yousuff, A., and Dornseif, M., "Case Studies of Model Reduction of Flexible Structures by Modal Cost Analysis," Report to Control Dynamics Co., Huntsville, Alabama, February 1983.

[17]Skelton, R.E., Hughes, P.C., and Hablani, H.B., "Order reduction for models of space structures using modal cost analysis," Journal of Guidance, Control, and Dynamics, Vol. 5, 1982, pp. 351-357.

[18]Lamberson, S.E., and Yang, T.Y., "Optimization using lattice plate finite elements for feedback control of space structures," Proceedings of the 26th Structures, Structural Dynamics and Materials Conference, AIAA/ASME/ASCE/AHS, 1985.

[19]Lamberson, S.E. and Yang, T.Y., "Micropolar finite element modelling of plate-like structures," AIAA Journal, (submitted for publication).

[20]Eringen, A.C., "Linear theory of micropolar elasticity," Journal of Mathematics and Mechanics, Vol. 15, 1966, pp. 909-923.

[21]Mikulas, M.M., and Bush, H.G., "Advances in structural concepts," Proceedings of the Large Space Antenna Systems Technology Conference, NASA, cp 2269, Part 1, 1982, pp. 257-258.

[22]Coyner, J.V., "Box truss development and applications," Proceedings of the Large Space Antenna Systems Technology Conference, NASA, cp 2269, Part 1, 1982, pp. 527-543.

[23]Pinson, L.D., and Amos, A.K., "NASA/USAF research in structural dynamics," Proceedings of the Large Space Antenna Systems Technology Conference, NASA, cp 2269, Part 1, 1982, pp. 301-344.

APPENDICES

APPENDIX A

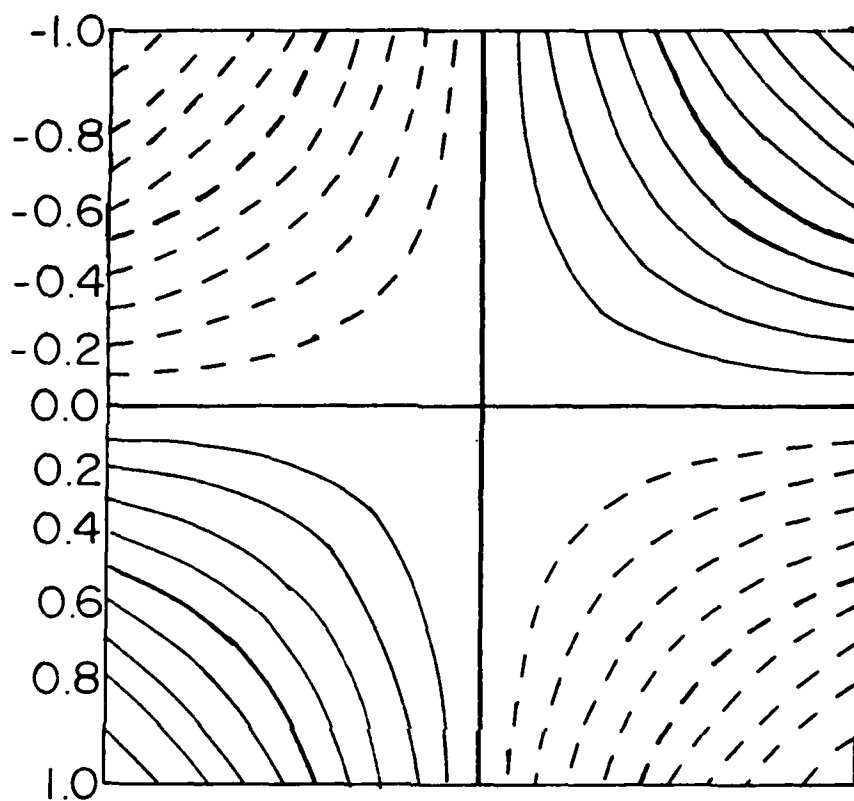Pin Jointed Truss Mode Shapes

# APPENDIX A
## Pin Jointed Truss Mode Shapes



Figure A.1. Flexible Mode 1 - Contour Plots.
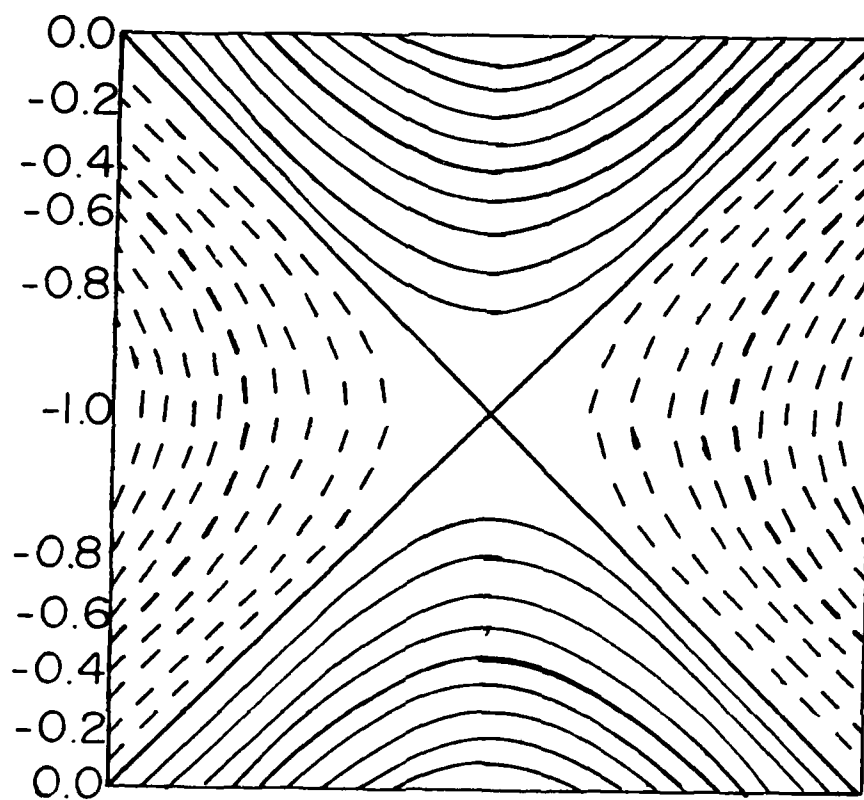
Figure A.2. Flexible Mode 2 - Contour Plots
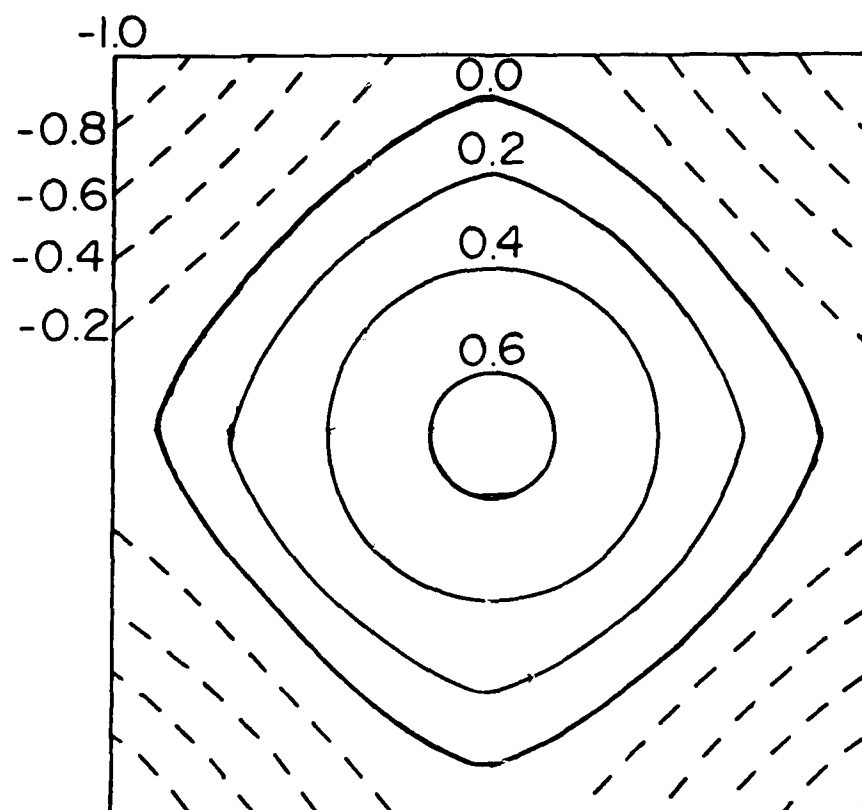
Figure A.3. Flexible Mode 3 - Contour Plots.
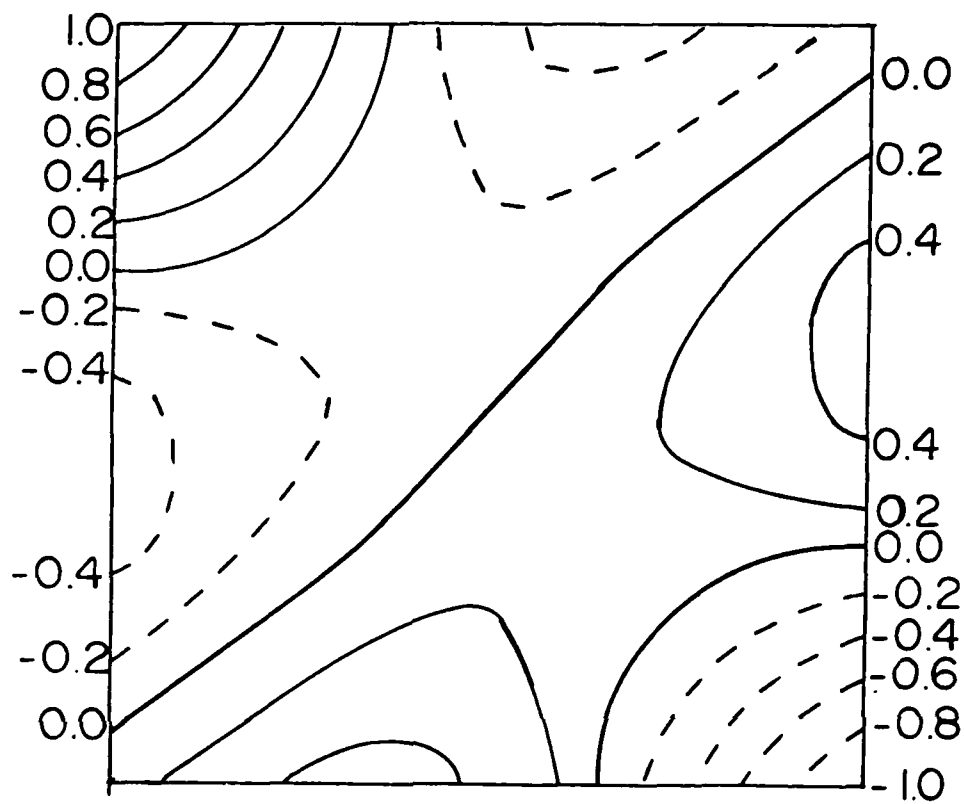
Figure A.4. Flexible Mode 4 - Contour Plots.

APPENDIX B

Parametric Study Performance Plots

# APPENDIX B

## Parametric Study Performance Plots
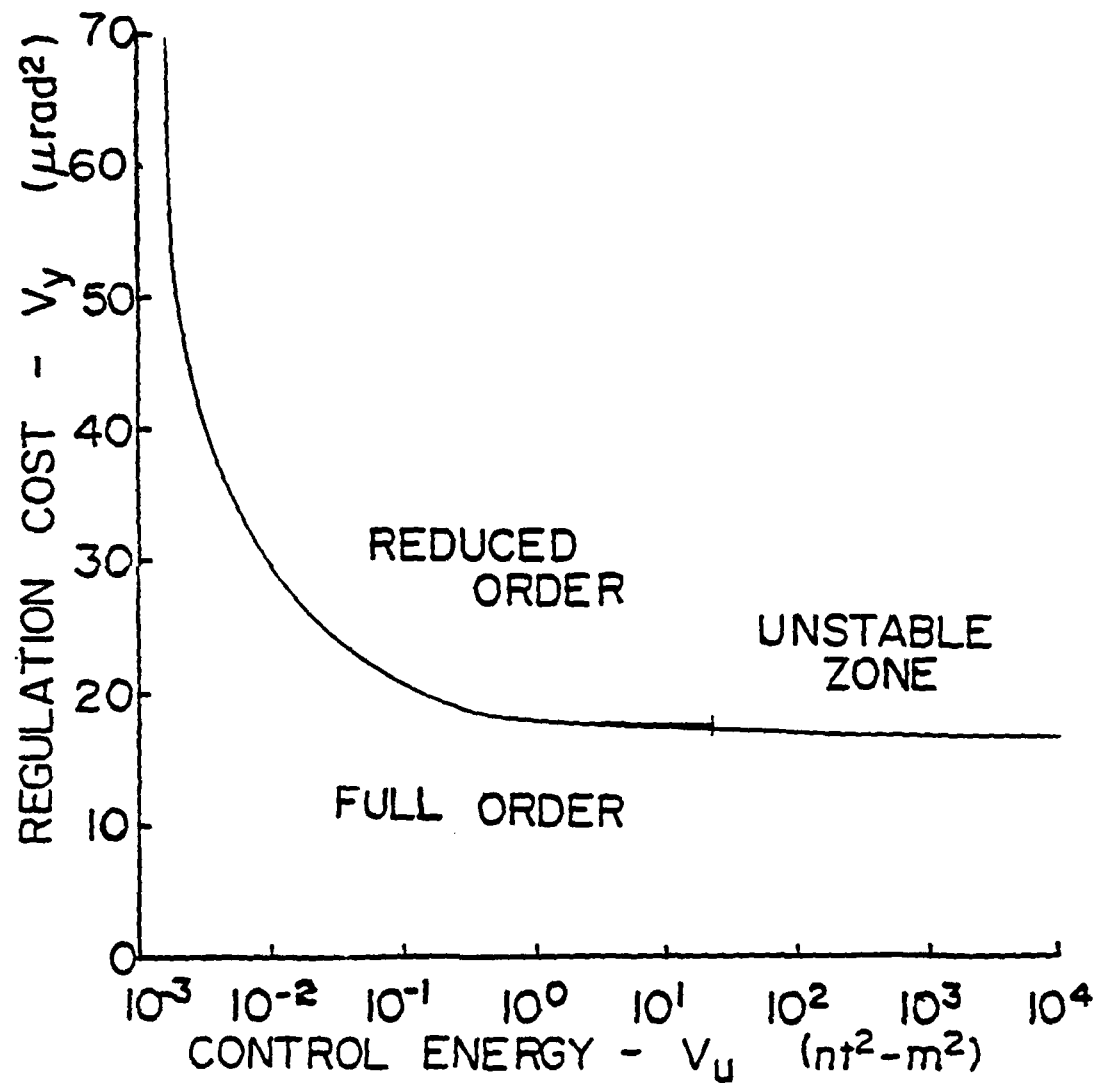


Figure B.1. System Performance Plot ($A_d = 5$ mm$^2$).
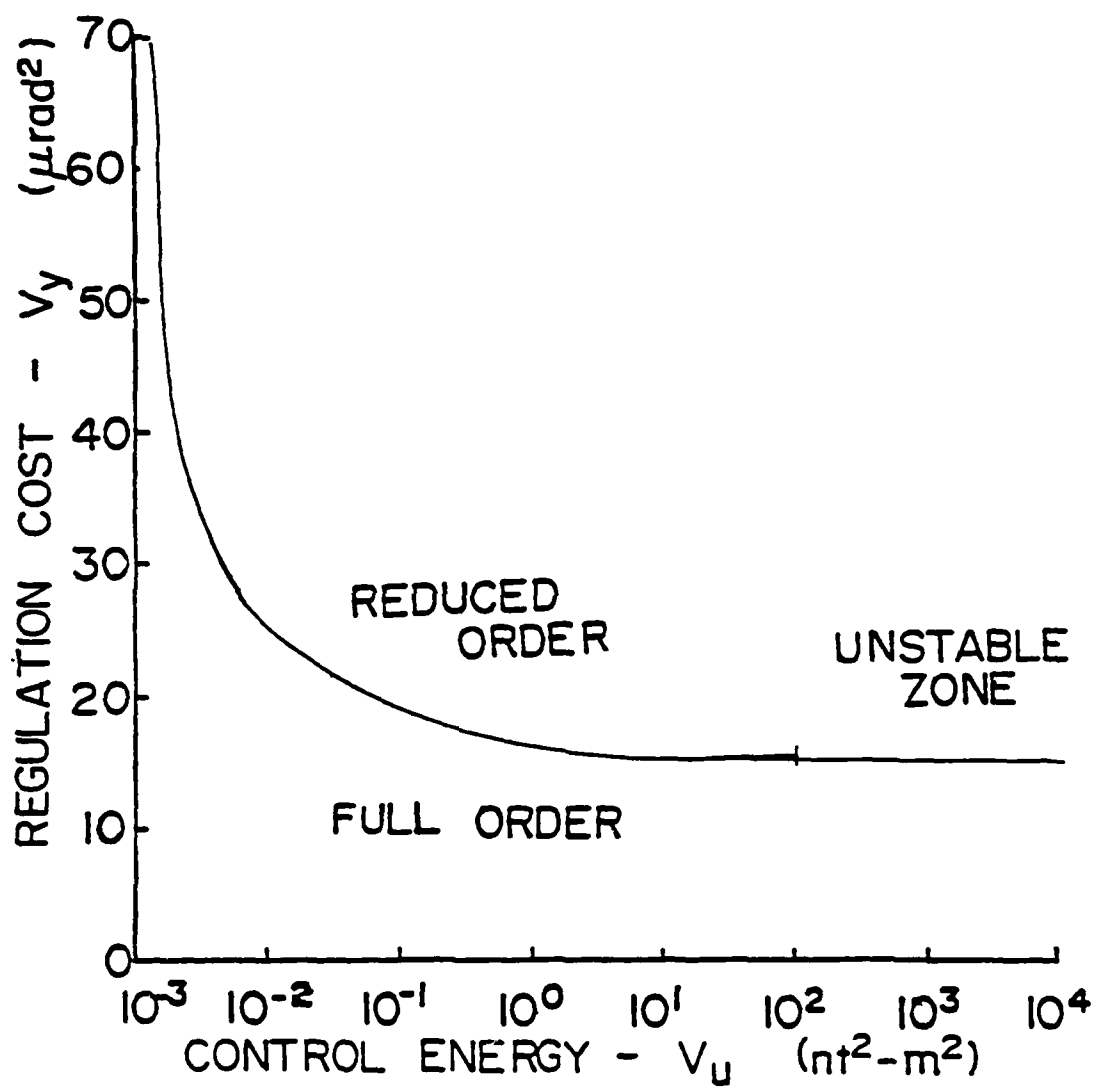
Figure B.2. System Performance Plot ($A_d$ = 10 mm$^2$).
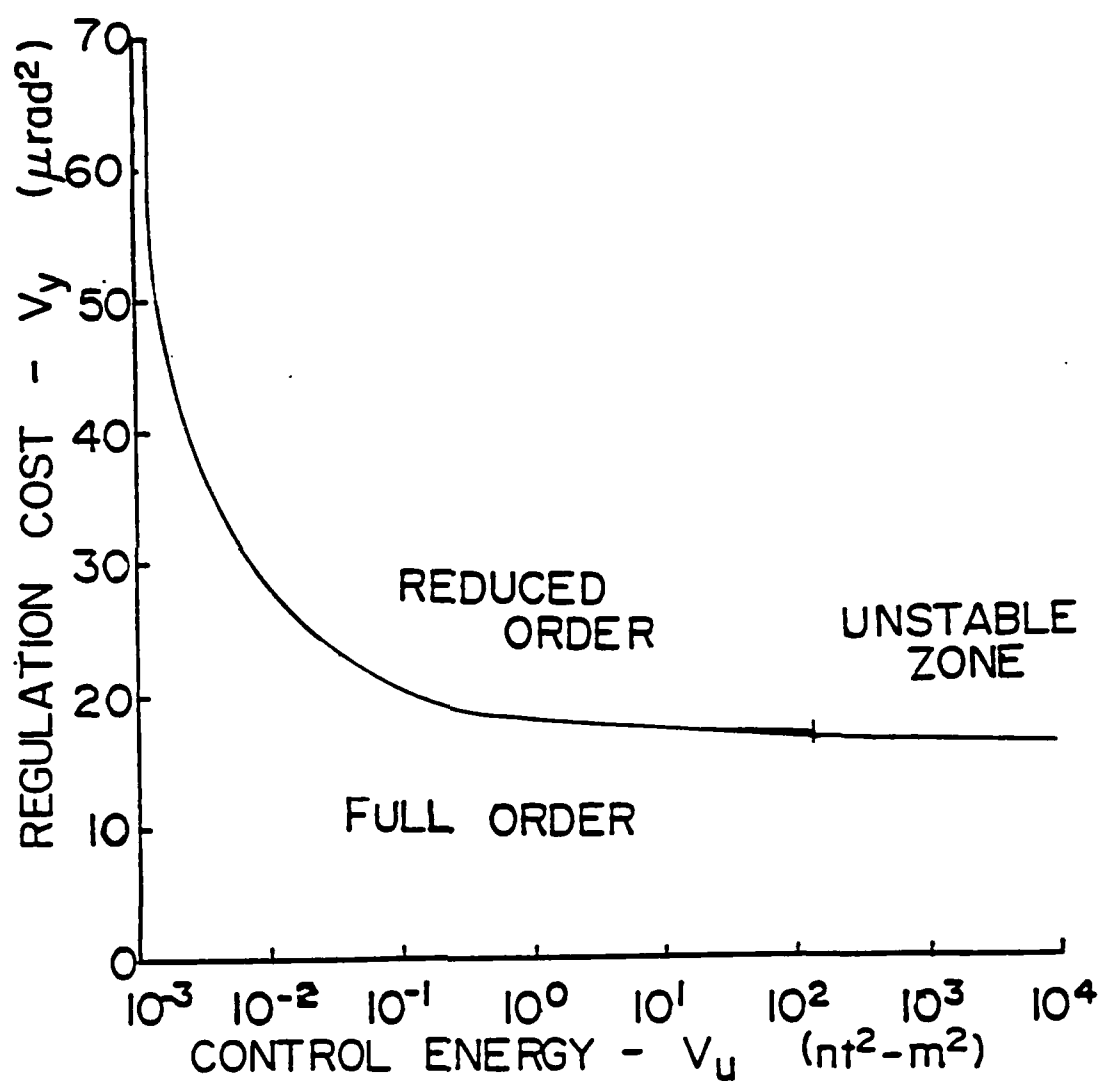
Figure B.3. System Performance Plot ($A_d$ = 30 mm$^2$).
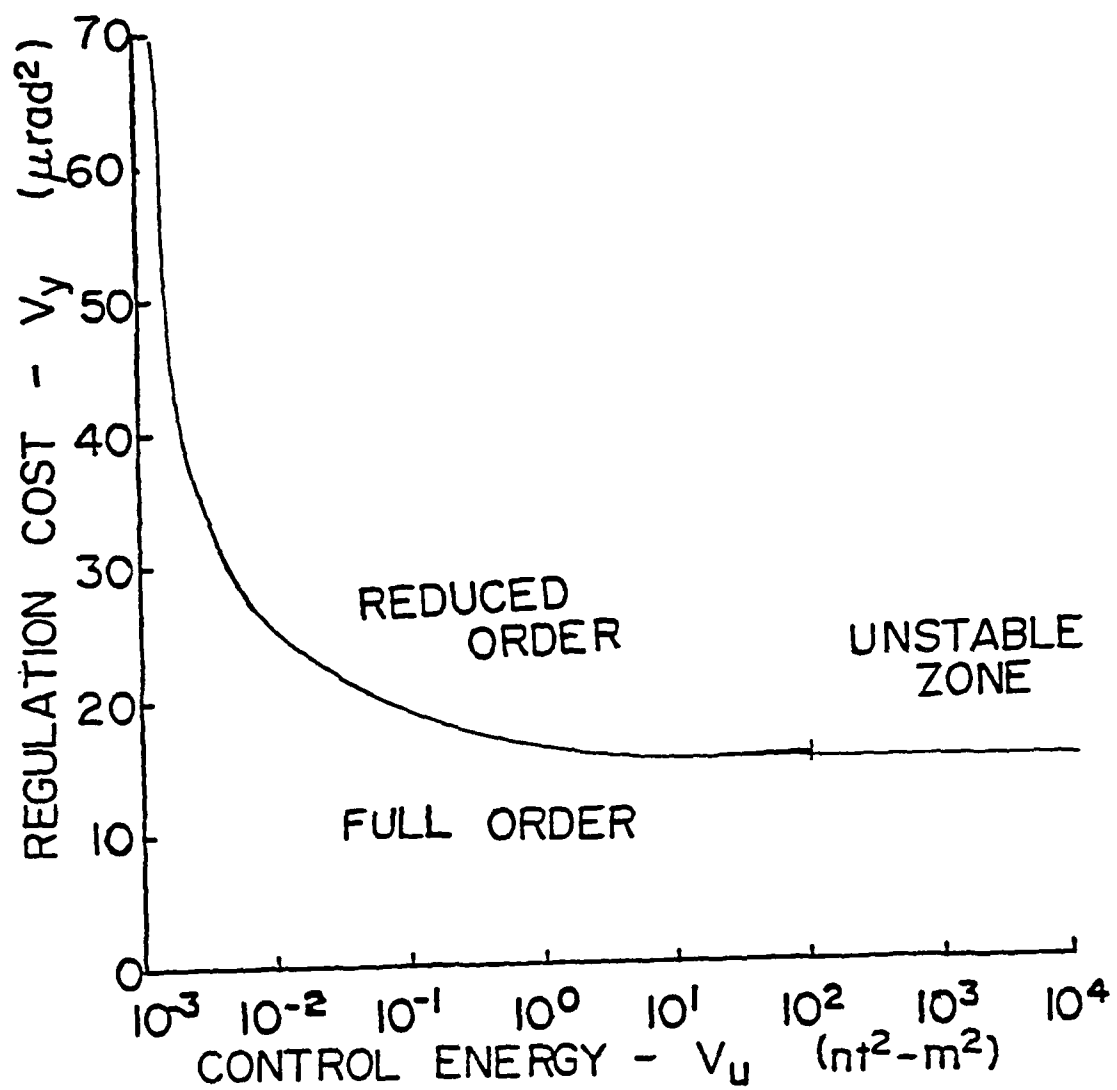
Figure B.4. System Performance Plot ($A_d$ = 50 mm$^2$).
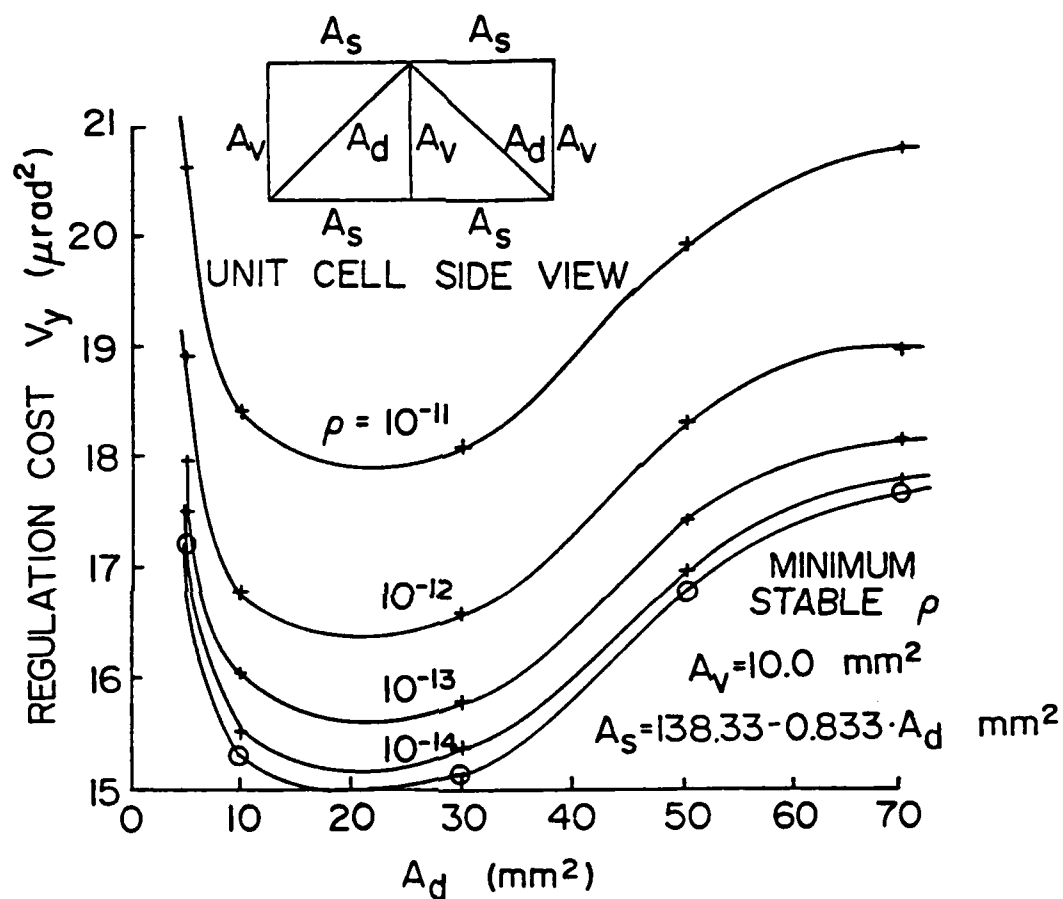
Figure B.5. System Performance vs. Diagonal
Member Area (Controller Order = 8).
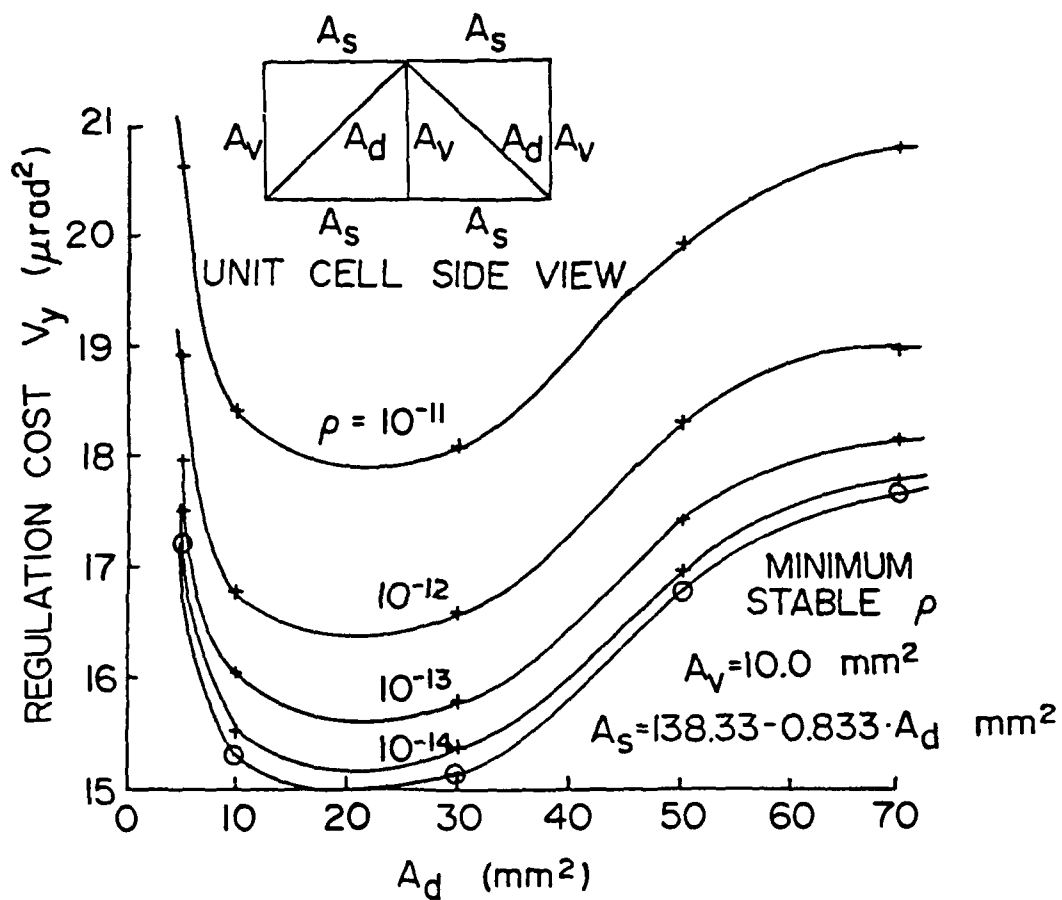
Figure B.6. System Performance vs. Diagonal
Member Area (Controller Area = 12).
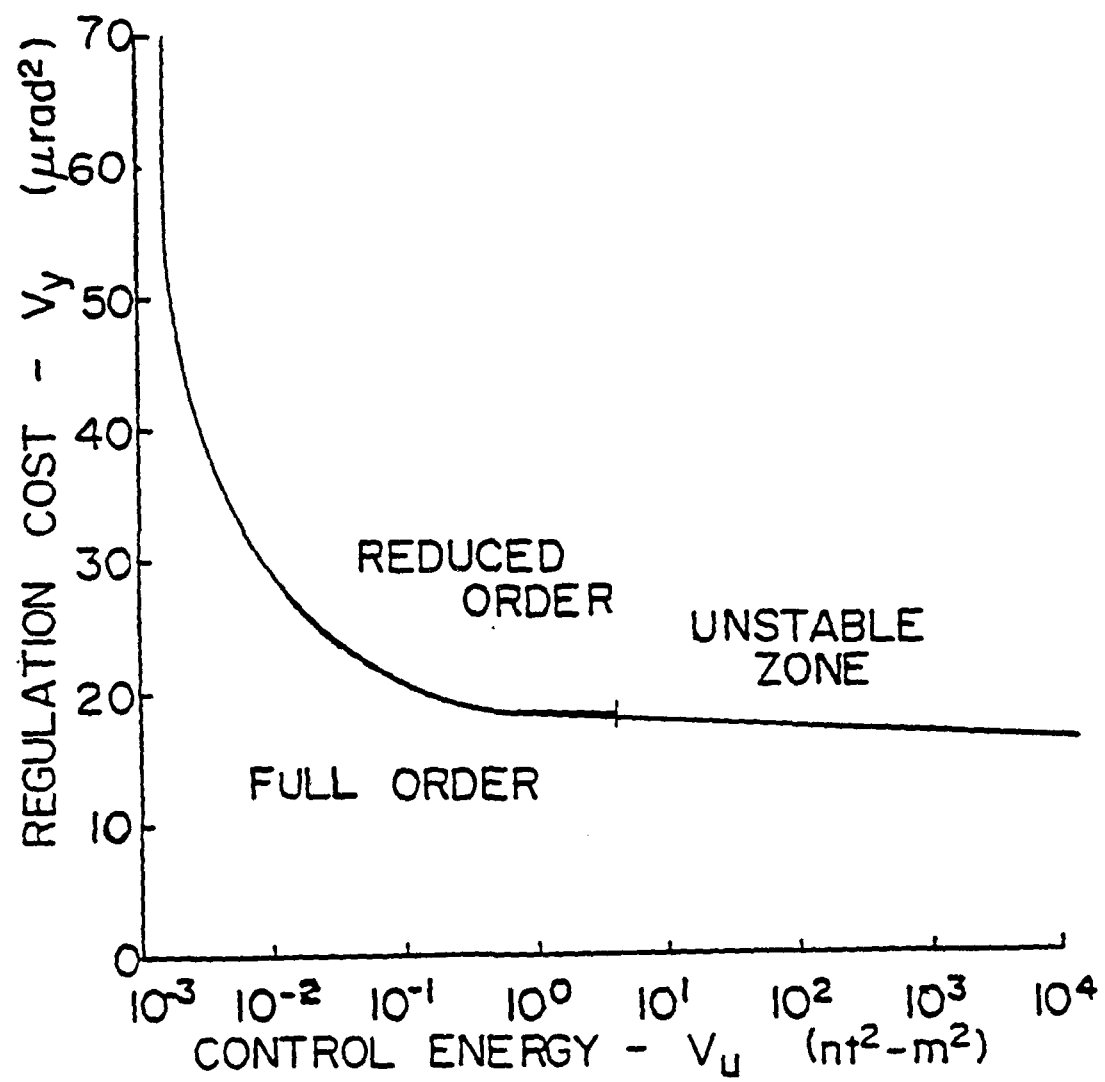
Figure B.7. System Performance Plot (h = 3.75m).
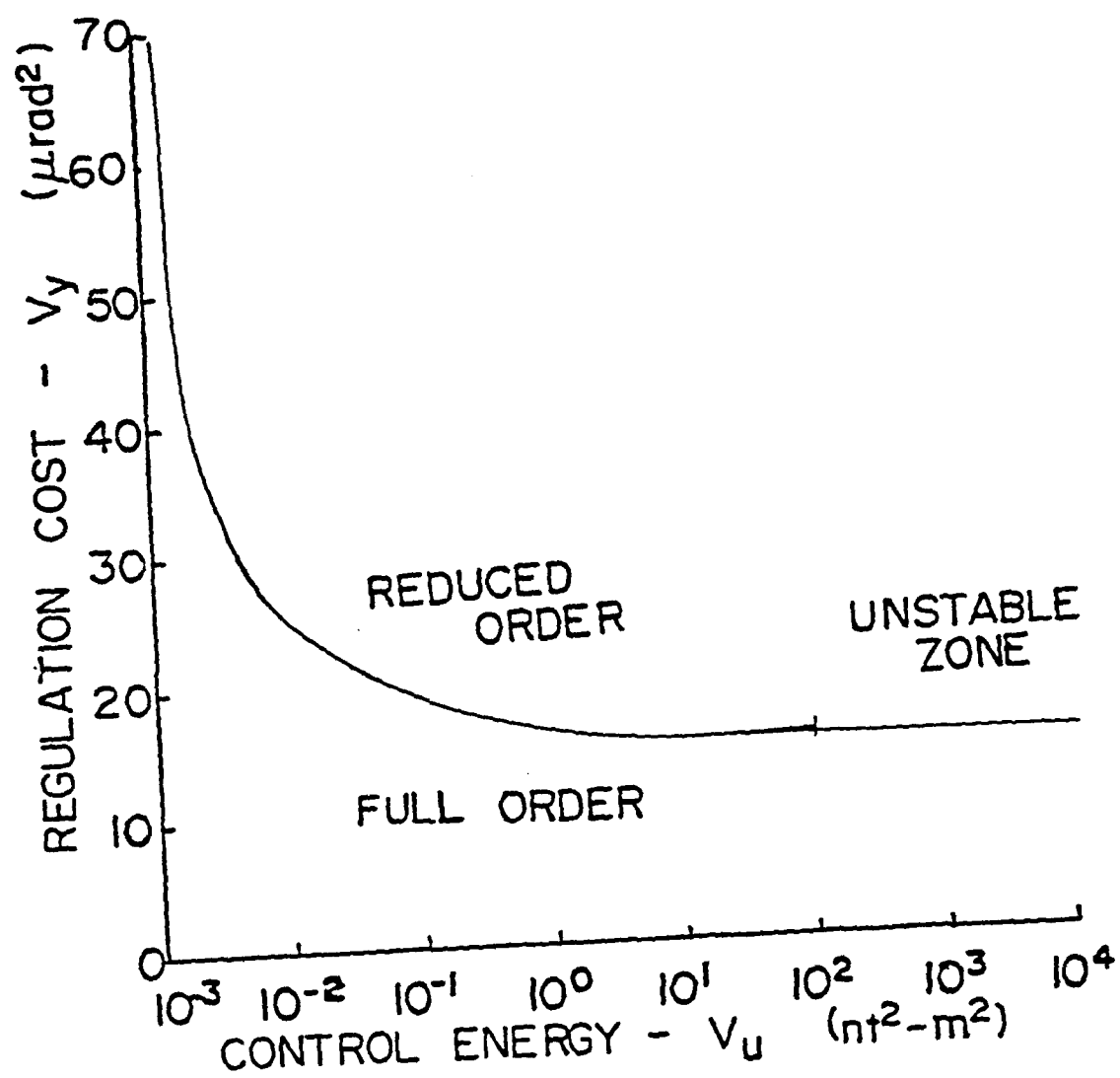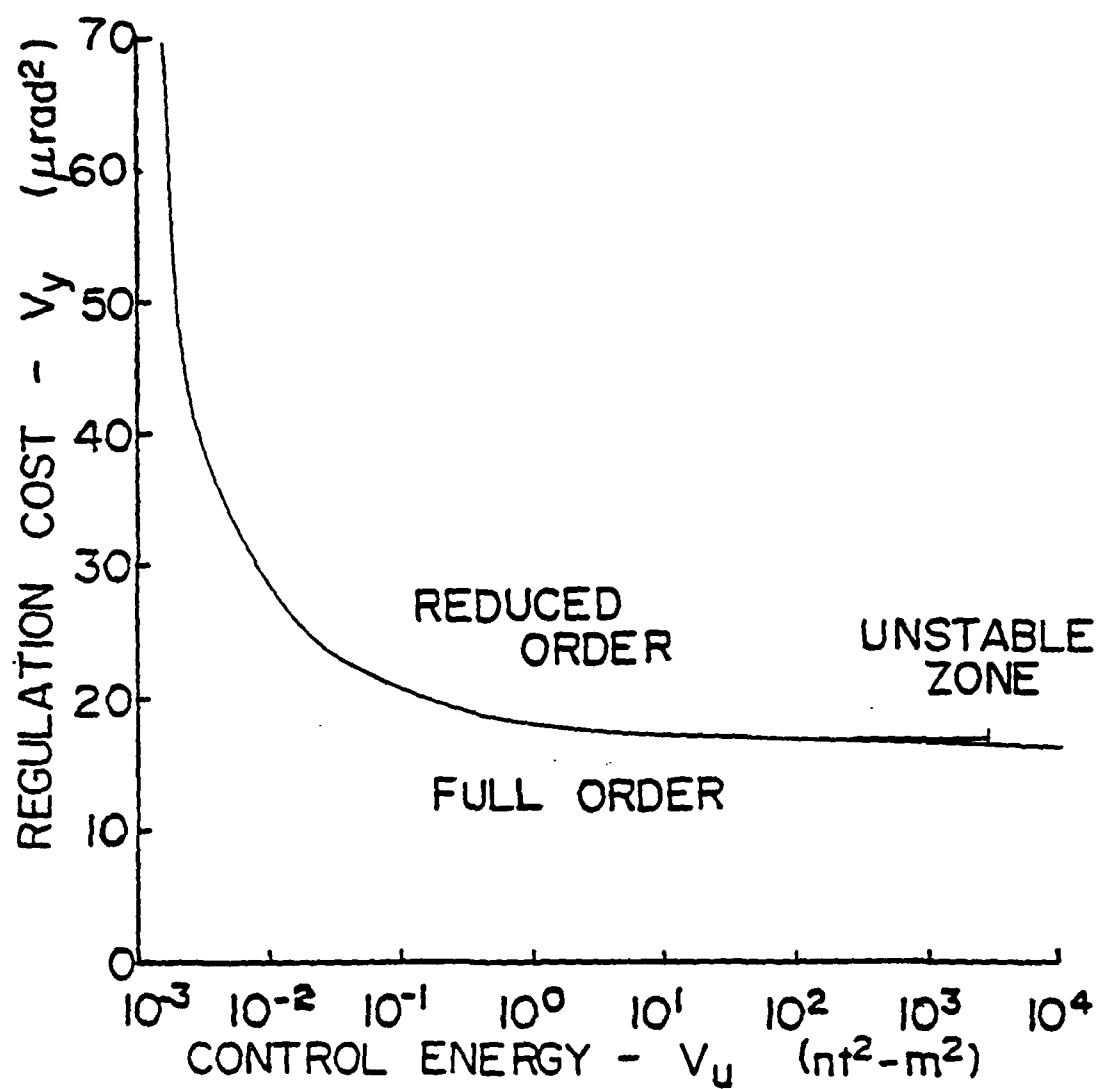
Figure B.8. System Performance Plot (h = 7.5 m).
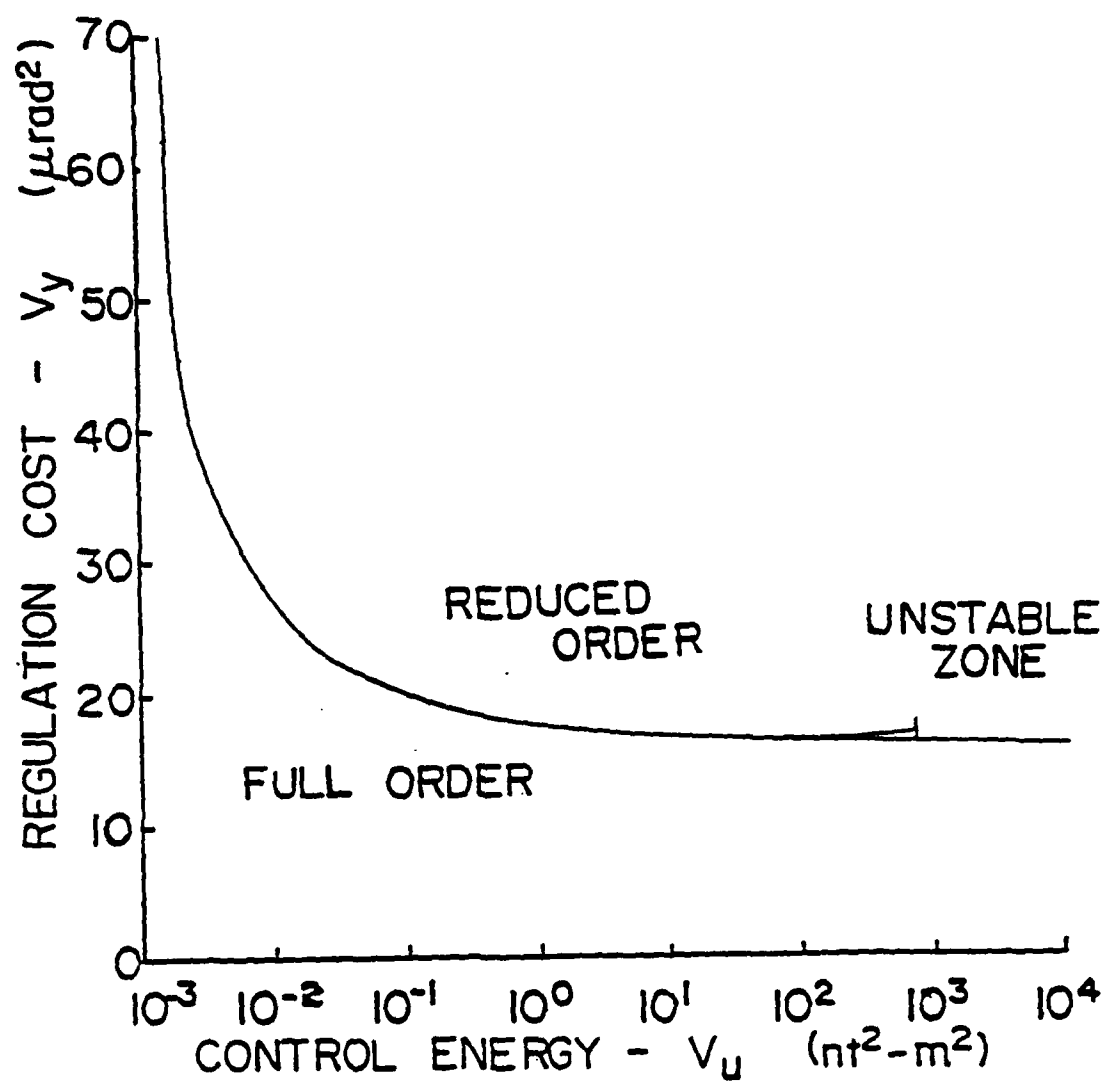
Figure B.9. System Performance Plot (h = 15.0 m).

Figure B.10. System Performance Plot (h = 22.5 m).

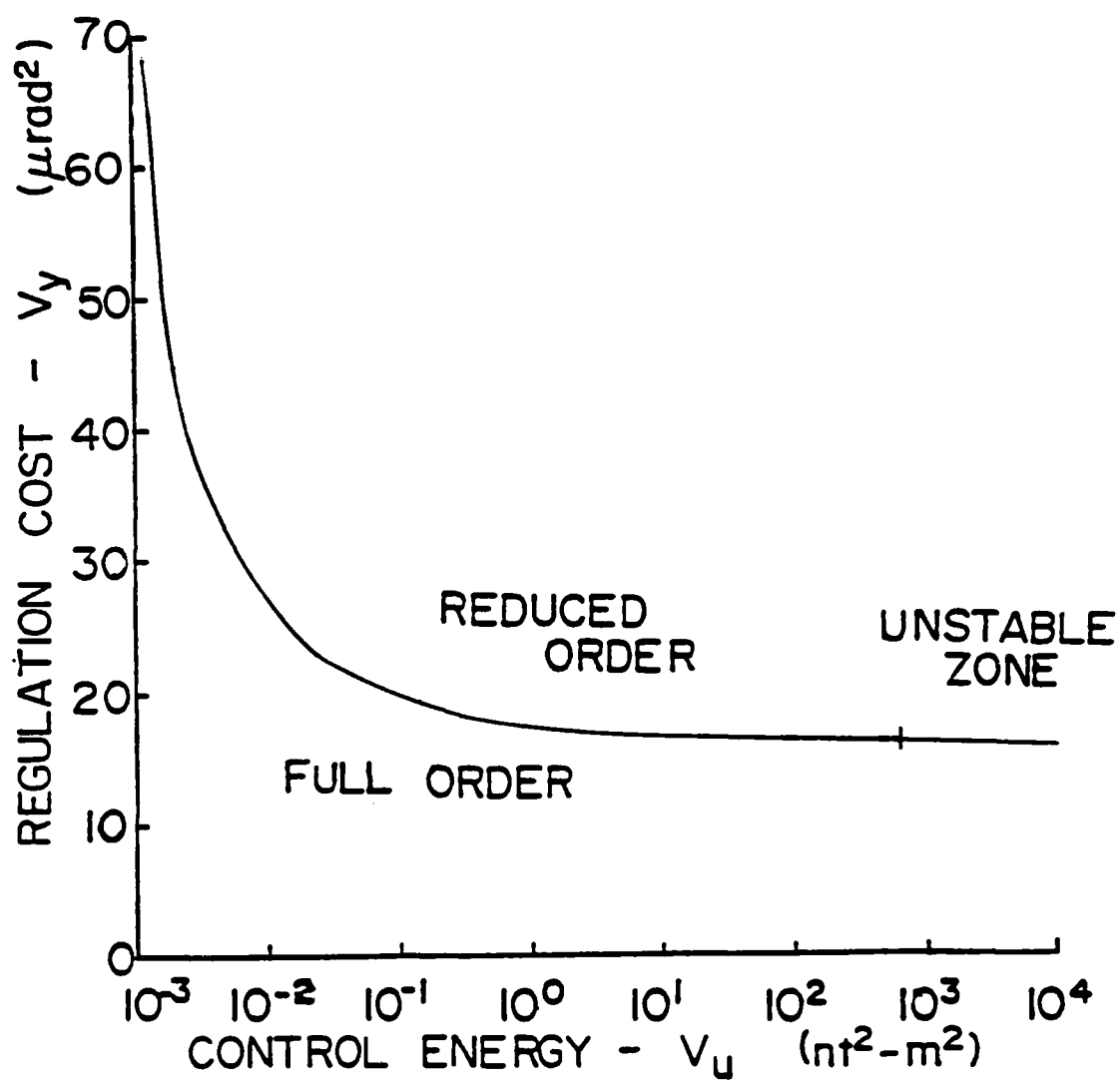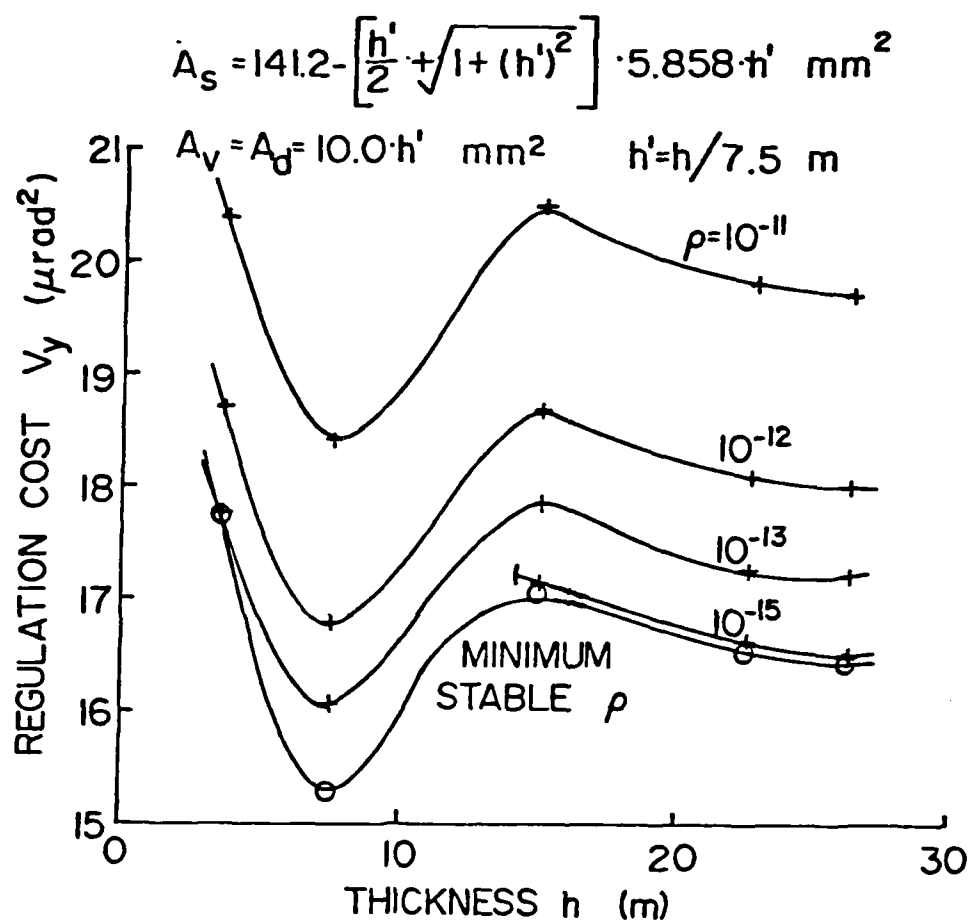Figure B.11. System Performance Plot (h = 27.5 m).

$$\dot{A}_s = 141.2 - \left[\frac{h'}{2} + \sqrt{1 + (h')^2}\right] \cdot 5.858 \cdot h' \ \ mm^2$$

$$A_v = A_d = 10.0 \cdot h' \ \ mm^2 \qquad h' = h/7.5 \ m$$

Figure B.12. System Performance vs. Thickness
(Controller Order = 8).

$$\dot{A}_s = 141.2 - \left[\frac{h'}{2} + \sqrt{1 + (h')^2}\right] \cdot 5.858 \cdot h' \text{ mm}^2$$

$$A_v = A_d = 10.0 \cdot h' \text{ mm}^2 \qquad h' = h/7.5 \text{ m}$$
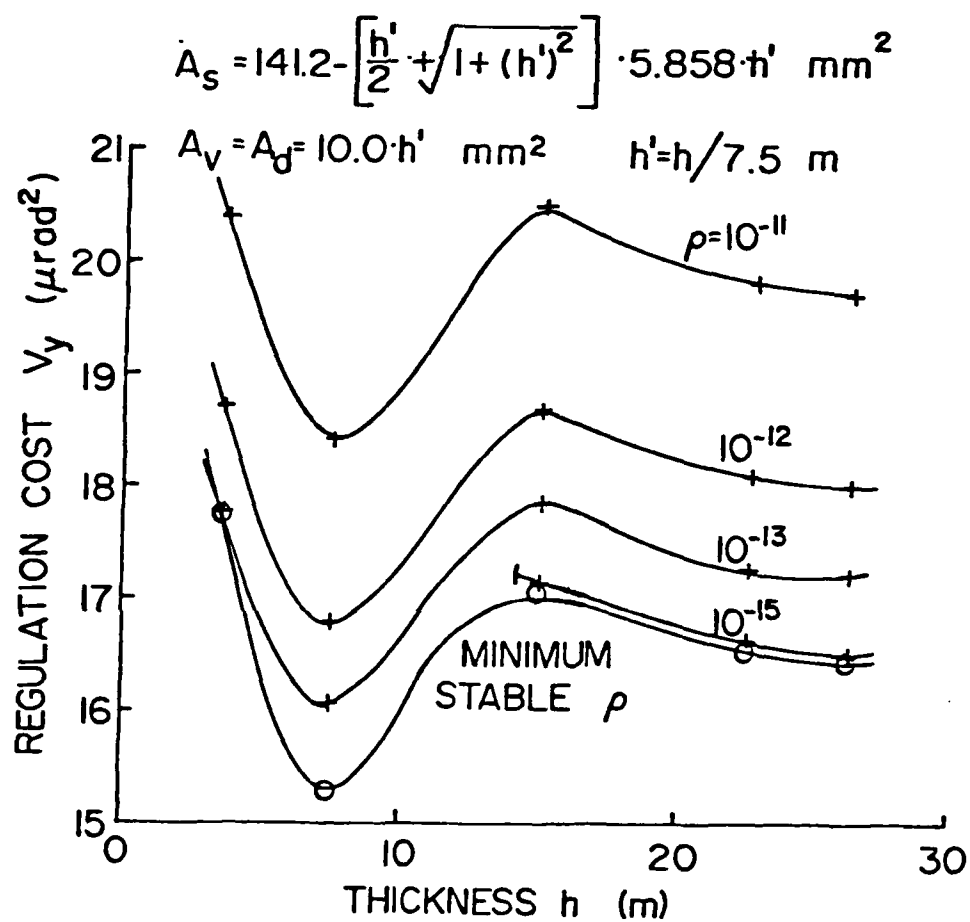
Figure B.13. System Performance vs. Thickness
(Controller Order = 12).

VITA

VITA

Steven E. Lamberson is a Captain in the United States Air Force (USAF). He received his B.S. in Engineering Sciences from Purdue University in May 1974. He received his M.S. in Engineering Sciences from Purdue University in December 1974. From July 1975 to August 1978 he was assigned to the Structures Division of the Air Force Flight Dynamics Laboratory, where he modified and used existing finite element codes to design advanced fiber reinforced composite aircraft structures. From August 1978 to August 1982 he was assigned to the Laser Division of the Air Force Weapons Laboratory where he made the structural vibration predictions for the Airborne Laser Laboratory, modelled with detailed finite element models, using both dynamic substructuring and component modal synthesis. Since August 1982 he has been a Ph.D. student in the School of Aeronautics and Astronautics at Purdue University. Steven Lamberson was born on October 13, 1952 in New Castle, Indiana.

# END

# FILMED

1-86

# DTIC